MATHEMATICAL MODELLING OF PASSIVE COOLING IN BUILDINGS

A thesis submitted to the University of Zimbabwe
in partial fulfillment of the requirements for the degree of Doctor of Philosophy
in the faculty of Science

Author:	Gerald Tendayi Marewo
Supervisor:	Dr. D. J. Henwood
Department:	Department of Mathematics
Date of Submission:	August 2004

Contents

List of Figures

List of Tables

Abstract

This thesis presents mathematical models for thermal energy storage in low energy buildings. Two different cooling systems are considered. One uses a ventilated slab, the other a packed bed.

The ventilated slab design is incorporated in a large commercial building in Harare, and uses concrete floor and ceiling slabs with an air gap in between to store coolth. The site engineer provided measured temperature data for various positions in the building, sufficient to identify the performance of the building. Because the measurements indicate an unexpected outcome, the instrumentation was carefully tested and proved to be correct. A mathematical model for the design is proposed and a comparison is made of three numerical methods in order to establish the most suitable. The computer code allows for time varying fan speeds and convective heat transfer coefficient, and slab inlet temperatures from measured data. Measured outlet temperatures are compared with the model predictions; there is good agreement between the trends but some differences. These were investigated through varying certain parameters.

The cooling system at the Harare International School uses a packed bed for storing night coolth to be used later for day-time air conditioning. This is described and a mathematical model stated which includes heat dispersion in the fluid and heat loss to the ground surrounding the bed. A numerical method of solution is outlined and the results are compared with measured data at the outlet of the bed both using the measured inlet temperature. A good agreement of trends is seen. The differences are examined through sensitivity analyses for both the convective heat transfer coefficient and air velocity. A parametric study for heat storage with materials and bed size is given.

Acknowledgements

I would like to thank my supervisors Dr David Henwood, research fellow at Brighton University and Dr Rachel Dunwell formely of the Bindura University of Science Education, and Professor James Milford of the Department of Physics at the University of Zimbabwe for the all the academic and moral support. Special thanks go to NUFU for their financial support. Without them my research would not be possible.

I would also like to thank Professor Mike Holmes of Ove Arup and Partners Ltd, London and Michael Rainbow of the Nottingham Arup office for all the useful discussions and advice.

I am grateful to my long time research colleagues and friends Dr Sandile Motsa, Dr Cloud Makasu and everyone else I brushed my shoulders with during my studies at the University of Zimbabwe.

I am greatly indebted to my family for their moral support. My late father, my mother, my three sisters and brother. To my wife, thanks for the support and giving me our lovely daughter.

Chapter 1

Introduction

1.1 The role of mass in low energy cooling systems

Several studies [28, 9, 26] indicate how much attention has been given in the last few years to the design of low energy buildings that use thermal mass and\or active thermal storage systems. Thermal mass is defined by Balaras [9] as the part of the construction mass of a building that is used to store thermal energy. There has been a growing need to reduce on energy consumption for

- supply air cooling to the internal environment of such buildings and,
- ventilation: extraction of the exhaust air from the internal environment to the outside.

Coupled with saving on energy is the need to reduce on operational and maintenance costs. A lower load on systems used for supplying air cooling and ventilation results in less frequent maintenance. It is also desirable to reduce the need to have active thermal storage systems. Chen [13] presented a predictive system for the operation of a building thermal system with thermal mass and gave results on the minimising of energy consumption and operation costs. Other studies which focus on strategies on saving energy at lower costs and maintaining a comfortable internal environment of a building include that of Chen and Liu [14] and Paul and Saini [24].

The energy technology systems used in low energy buildings may be classified as either active or passive [28]. Active thermal energy storage systems are those that require additional

devices to store or recover thermal energy or, to control the systems that provide thermal energy. A few examples are:

- variable volume pumping systems (the Eastgate building in Harare, Zimbabwe uses timed fans for this purpose) and,
- solar collectors.

The weakness with active thermal storage is that extra energy and hence costs are required to drive the system.

Passive thermal storage technologies include:

- Shading (at Eastgate this is provided by massive protruding concrete structures and plants on the exterior of the building) and,
- Natural ventilation using atria integrated in the building, for example the Eastgate building has an atrium (open space) in its core, glazed over to promote ventilation.

1.2 An overview of fabric thermal storage

The use of building fabric for storing thermal energy has been shown in several studies to be an effective way of cooling (or heating) the internal environment of buildings [8, 34]. Basically, air is drawn from outside the building via passages within the fabric to cool the inside. During the hottest part of the day (noon to mid-afternoon) the external air temperate is too high to provide a comfortable internal environment. Building fabric is used to delay the impact of the external climatic conditions on the internal environment. Heat is extracted from the passing air into the fabric before entering the interior. The stored heat is released later when the outside air temperature is lower and usually when the building is no longer occupied. Fabric thermal storage also helps in decreasing the diurnal swing of the supply air temperature and hence keeps the temperature within a comfortable range.

The design of low energy buildings that use fabric thermal storage involves implementing special features as part of the supply air passage. Two features related to the work presented in this thesis are:

- ventilated slabs and,

- packed beds.

The ventilated slabs are pre-cast concrete floor/roof slabs. One such slab was implemented in the design of the Eastgate building in Harare, Zimbabwe. Some studies have been made on thermal storage in ventilated slabs of the type at Eastagate. In 1996, Holmes and Wilson [19] gave an assessment of the thermal performance of a ventilated floor slab thermal storage system using a thermal network model. The author's Masters thesis [20] presents a numerical model for the ventilated floor slab thermal storage system used at Eastgate. Validation of the model is done against measured data. In this thesis an extension of this work is presented.

Another type of ventilated slab uses hollow cores within the slab for passing the supply air. This is based on the TermoDeck system as described by Barton *et. al* [10] in their paper on a numerical model for its thermal performance. Ren and Wright [26] gave a thermal network model for a hollow core ventilated slab. The hollow core ventilated slab thermal storage system has been implemented in several buildings across the world for example in one laboratory of the Chemical Engineering Department at the National University of Science and Technology in Bulawayo, Zimbabwe.

Contrary to ventilated slabs, packed beds are usually part of the foundation of the building as is the case for Harare International School in Zimbabwe [25]. A bed packed with solid material (rocks for the case of Harare International School) acts as the thermal storage system. Various studies have been published on heat transfer in a packed bed thermal storage system. In 2004, Chen and Liu [14] presented a study on the use of an air-based rock bed for passive heating in a cold climate. They also investigated the effect of various thermal and physical properties on the thermal performance of the bed. A similar theoretical analysis is involved for a different application of packed beds: waste heat recovery, [35]. Other recent studies on packed bed thermal storage systems include those of Al-Nimr *et. al* [7, 6] and Adebiyi *et. al* [5, 4]. Earlier studies have also been published [30, 27, 15, 3]. There are three major differences between the packed bed thermal storage model presented in this thesis and those by other authors:

- No previous report has been found referring to the application to room cooling.
- The model presented includes
  - ground coupling,
  - fluid heat dispersion and,
  - variable fluid flow rate.

- The model in this thesis is validated against measured results taken on site of a typical building design.

1.3 An overview of the current work

The work in this thesis is divided into two parts. Both parts are on regulating the air temperature in the interior of a building for a typical design

- using a ventilated slab for the Eastgate building in Harare and,
- using a packed bed for the Harare International School.

The first part is a continuation of the author's Masters thesis [20]. A mathematical model is developed for heat transfer in a ventilated slab. The slab material is coupled to the air by a convection boundary condition. Heat transfer within the slab material is modelled by the standard parabolic diffusion equation and an energy balance is used to derive the governing equation for the air. Approximation in space is by finite elements and marching in time is by an implicit finite difference scheme. The measured results that were used earlier on [20] to validate the numerical model did not seem satisfactory and so a thorough investigation of the measurements is carried out in chapter 2 of this thesis. Also given in the same chapter is a description of the supply air cooling and ventilation at Eastgate. A full description of the numerical model for Eastgate is given in chapter 3. Results are presented on a finite element approach and on two finite difference schemes: a simple lumped parameter method and another involving a modification on the boundaries. Chapter 3 ends with results on validating the numerical model against measured data.

The second part of the thesis is on packed bed thermal storage and a case study on Harare International School. Chapter 4 begins with a review of existing models. They are classified as either single or two phase depending on whether an energy equation is needed for each of the energy transporting fluid and storage material. The Schumann model [30] of 1928 is introduced as a benchmark for all other models that follow. This is followed by a description of the supply air cooling and ventilation at the Middle School part of the Harare International School. A mathematical model and two methods of solution are then presented. A code developed for the model is verified, and predicted and measured results are compared in chapter 5. The sensitivity of the model to the convective heat transfer coefficient h_c and

the fluid flow rate $\dot{V}_f$ is also investigated. The effect of ground coupling on the thermal performance of the bed and a brief parametric study conclude chapter 5.

Chapter 2

Eastgate and measurements

2.1 The building and measurements

2.1.1 Overall overview of the structure

The termitary; a model for Eastgate

The Eastgate building in Harare uses the same heating and cooling principles as the termite mound (see Figure 2.1). Deep inside the termitary, insects farm fungus which must be kept at an optimum temperature. Air is vented in at the base of the mound, down into chambers cooled by wet mud and up through a channel to the peak. Ants constantly dig new vents and plug old ones to regulate the temperature. The air from outside the termitary acts as the energy transporting medium and, the soil and the mud that make up the termite mound act as the energy storage material. Combined together they form a heat exchanger.

The Eastgate complex operates in a similar fashion. Air drawn from outside the building together with the building mass form the heat exchanger which is used to regulate the temperature in the office space.

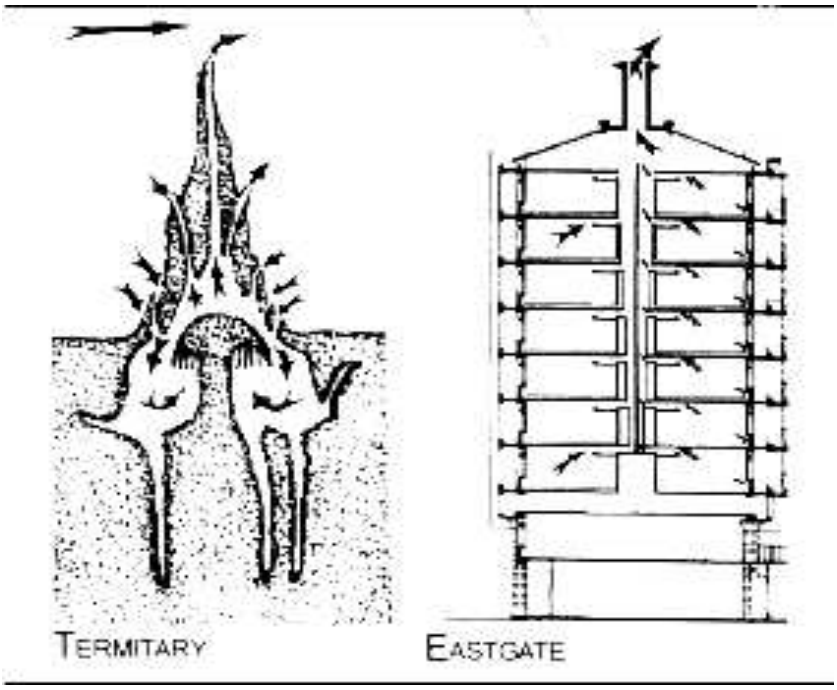

Figure 2.1: Design model

The building

The design of Eastgate, done by Mick Pearce of Pearce partnership, was motivated by the need to construct a building that is habitable with no air conditioning and almost no heating. The benefits include saving on energy consumption and maintenance costs while operating within acceptable comfort levels of the occupants.

It has been reported that the total energy consumption for Eastgate is 35% less than the average consumption of six other conventional buildings in Harare that use full high voltage air conditioning (HVAC). In the event of power cuts the Eastgate ventilation system runs by natural convection.

The Eastgate complex is made up of two buildings side by side that are separated by an atrium which is glazed over and open to the breezes, see Figure 2.3. Below the glass roof are steel bridges and lifts suspended on cables from steel lattice beams. On the second floor there is a glass sky-walk that runs the length of the atrium and connects the lifts. This sky-walk is connected to the ground floor by escalators.

The interior of the building is protected from the harsh high veld sun by the use of very

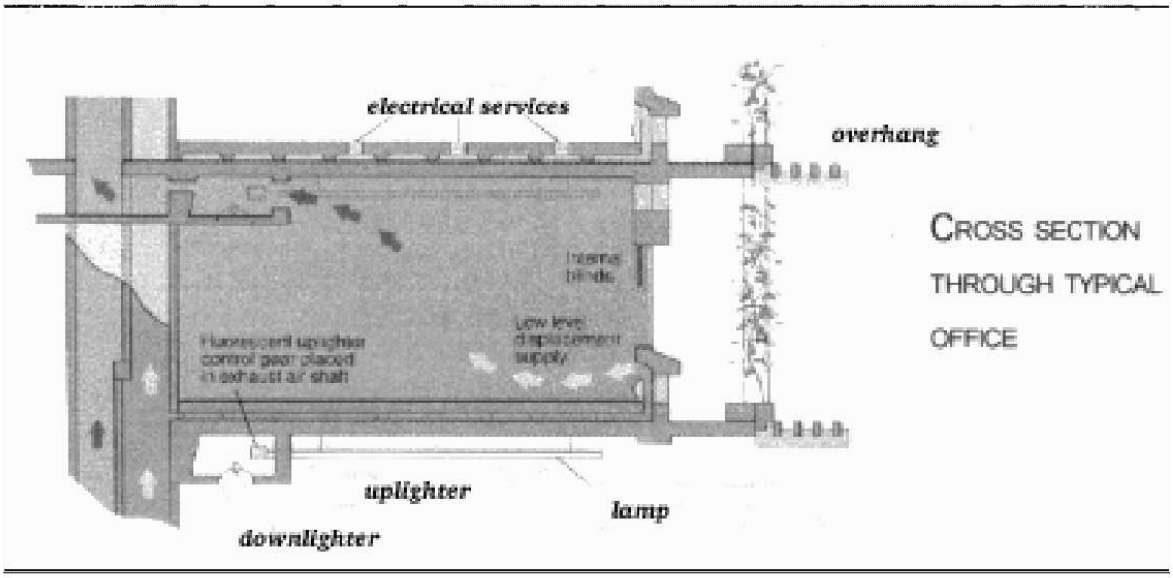

Figure 2.2: Cross-section of an office

little glass with most of the building being made up of concrete. Windows are screened by massive protruding stone elements and plants. The protruding ledges increase surface area of the building's exterior. This helps improve heat loss to space at night thereby storing more thermal energy in the slab mass mode which is used during the day to regulate the temperature of the air in the office area. This energy is sometimes referred to by the engineers as "coolth". Also, during the day heat gain is minimised.

The sandwich of the vaulted ceiling, air void and the floor above acts as a thermal store and exchanger. The air void is festooned with concrete teeth to increase surface area and augment convective heat transfer. The vaulted ceiling provides an increased surface area to enhance heat absorption from the lights which face the ceiling upwards. These are sometimes referred to as "uplighters".

Fans in the mezzanine floor below the offices suck air from the atrium and blow it up through the supply section of vertical ducts in the central spine core of each office block. The air passes through the void before entering the room above as part of a displacement ventilation system. It rises as it is warmed to the ceiling and it is sucked out through exhaust ports in the ceiling at the end of each vault to exhaust sections of the vertical ducts. See Figure (2.2). On the roof are 48 round brick chimneys which pull exhaust air out of the seven office floors below.

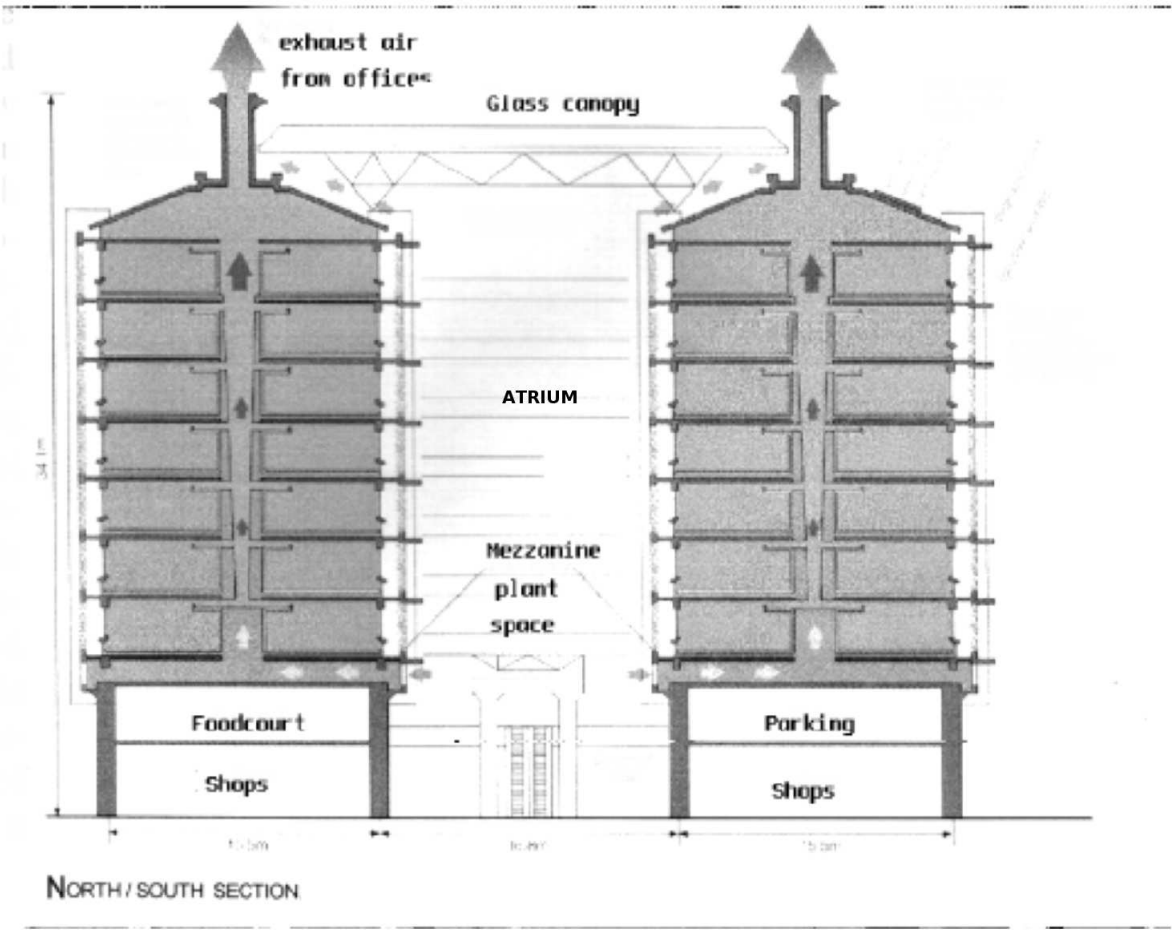

Figure 2.3: Building structure

High volume fans run at night to give ten air changes per hour and during the day low volume fans are switched on to give two air changes per hour. By timing the change over from high to low volume fans the use of the diurnal swing can be optimised.

For most countries in Europe the mean air temperature is mostly less than the mean working temperature in the office space, so the system needs to be heated to raise the mean temperature of the ventilation air. However, in Africa the mean ambient air temperature is approximately equal to the optimum office space temperature. Therefore what needs to be done is to reduce the diurnal swing of the ambient temperature.

2.1.2 On temperature monitoring at Eastgate

Introduction

To ensure that measured data for validating mathematical models that were obtained was reliable, investigations were carried out on the temperature monitoring at the Eastgate complex. For a detailed description of the models, see Chapter 3. The engineers involved, Ove Arup and Partners installed an 8-bit ACR data logger and, six external temperature sensors positioned to measure temperatures at different locations in the building:

- outside air
- diffuser supply (this is placed through a low level grille in the office space to hang at the exit of a horizontal duct. See Figure 2.4)
- riser air (this is placed at the entrance to the horizontal duct as shown in Figure 2.4)
- room medium level
- atrium air (this hangs in the atrium near the fans)
- slab

The data logger has one internal temperature sensor, used to measure the room temperature at low level.

Monitoring the temperatures at selected points in the building gave results that are not representative of what is expected. Figure 2.5 shows a sample of measured data taken for

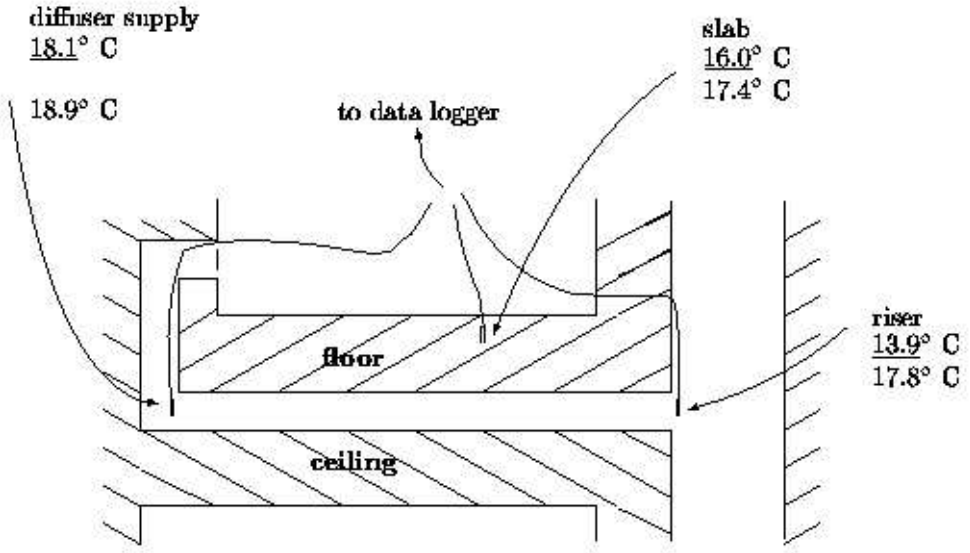

Figure 2.4: Temperatures at selected points in the building, 01-08-2000

the indicated period at the inlet to and the outlet from the ventilated floor slab. In Figure 2.4 the underlined values correspond to temperatures at the given positions at 5:24 am, which happened to be the coldest time on a typical day. The other values were taken later in the day at 6:18 pm. It is clear that the ventilation air increases in temperature by 4.2° C and 1.1° C at 5:28 am and 6:18 pm respectively through the horizontal duct. Note that in the morning, the air at the riser is cooler than the slab by about 2.1° C and so it is warmed to 18.1° C as it leaves the duct. In the afternoon, the air enters at a higher temperature than the slab but it still appears to get warmed through the duct. Furthermore, the mean temperatures for the day for the riser and diffuser supply are 16.2° C and 18.6° C respectively, showing that the air is being heated as it goes through the duct.

Consequently, two questions were considered.

1. Are the calibrations used for the temperature measurements correct?

2. Are the temperature sensors properly exposed or subject to influences which lead to temperatures which are not representative of the air stream being measured?

To answer these questions the following activities were suggested by Professor James Milford of the Physics department at the University of Zimbabwe

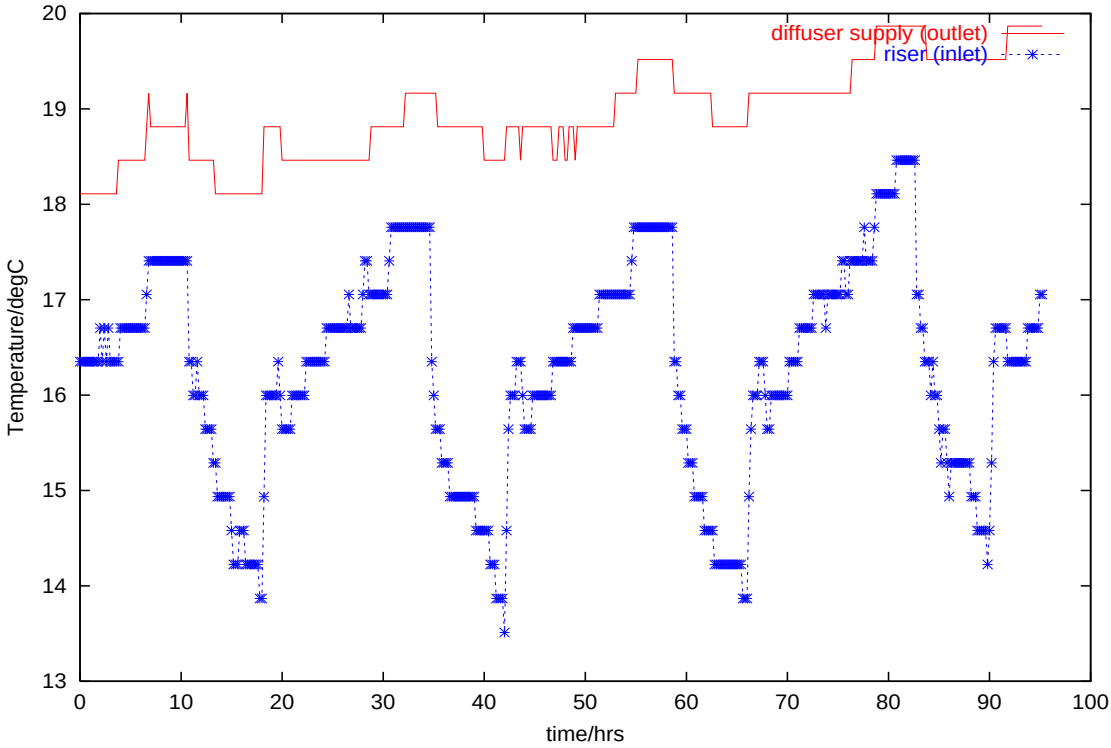

Figure 2.5: Measured results for period: 31-07-2000 to 04-08-2000

- Calibration of sensors in the laboratory
- In situ comparison of sensors
- A check on representivity

Experiments

Laboratory calibration of the sensors

Action A spare ACR data logger, with two external temperature sensors (thermistors) from Eastgate was compared with a reference thermometer in the laboratory. The two sensors and, a Mercury (Hg) bulb thermometer were bound together and used to simultaneously measure the temperature of water in a thermos flask over a range of temperatures. Since the data logger only accepts one external sensor at time, measurements were taken from the Hg bulb thermometer and only one thermistor at a time. The same experiment was conducted using a stirred water bath in place of a thermos flask to make taking of readings from the thermometer easier.

Results and Conclusion In the first experiment, Thermistor 1 gives results to within 0.1° C of the Mercury bulb thermometer on average. For thermistor 2 the absolute value of the mean of the difference of its temperature from that of the Mercury bulb thermometer is 0.3° C. Part of thermistor 2 was damaged during installation for a measurement exercise at a different site. This could account for the less accurate results obtained.

In the second experiment, the mean of the absolute values of the difference between readings from the mercury thermometer and, thermistors 1 and 2 are 0.07° C and 0.09° C respectively.

The ACR data logger used in this experiment is 8-bit and so there are only $2^8 = 256$ possible values at a time. On a temperature range of 0° C to 100° C this gives a resolution of 0.39° C. This is the minimum difference between any two consecutive readings. It can be concluded from these observations that the sensors and ACR data logger are accurate and consistent within resolution.

In situ comparison of sensors

Action The six external sensors were brought back to the data logger position and, bound together with a mercury bulb thermometer. They were immersed in well stirred water and compared over a range of temperatures. Also compared was the spare ACR logger and, two sensors that were re-calibrated at the University of Zimbabwe Physics department as described in the previous sections.

Results and conclusion Thermistor 1 and the six external sensors take a longer time to respond to sudden changes in temperature of the surroundings than the mercury thermometer. Upon taking this into account it was deduced from these results that all the sensors give results to within 0.2° C of the mercury thermometer.

A check on representivity

Introduction The riser air temperature sensor measures the temperature of the air in the supply section of the vertical ducts. It goes through a hole which is about 50mm above the floor. It then emerges in the vertical duct and hangs at the entrance to the horizontal duct. The temperature reading it gives is taken as the input temperature for the ventilated floor

slab. To check if the readings from the riser air sensor were not affected by radiation from nearby surfaces the following experiment was carried out.

Action A second hole was drilled about 200mm away from the one through which the riser sensor goes at the same height above the floor. Two sensors were inserted through this hole, one of them exposed and the other shielded from direct radiation by a louvered aluminium foil. Readings were taken from both sensors over a range of temperatures.

Results and conclusion A comparison of the readings from the exposed sensor against those from the shielded one showed that they were the same to within 0.5° C. This is of the same order of magnitude as the resolution of the sensors.

2.1.3 Discussion

From the experiments done to test the temperature sensors and the data logger, the following conclusions were made.

- Laboratory calibration and in situ comparison of the sensors showed that the instruments were accurate to within their resolution.
- The effect of radiation emitted from neighbouring surfaces on the temperature readings from the sensors is negligible.

Since the exact positioning of both the slab and the riser air sensors were uncertain, this could have resulted in error in taking temperature measurements. For example, the diffuser supply temperature sensor could have been placed closer to the grille that lets air out into the office space than to the outlet of the ventilated floor slab where it is supposed to take temperature readings. Because of this and the possibility of office air mixing with duct air near the grille temperatures recorded by the diffuser supply sensor could have been a misrepresentation of the desired temperature readings.

Although improper calibration and misplacing of temperature sensors could be possible sources of error in taking temperature readings lax monitoring of the ventilation system could have also contributed significantly. It is not surprising to go into the fan control room and find out that the system is operating in summer mode when it is actually winter. Also,

there have been reports that the air filtering system was blocked for several months without maintenance. However, the system operates successfully by natural convection during such moments. Another issue related to this is that if filters are blocked, supply air is not available from the outside to the building's interior via the ventilated floor slabs. Consequently, the impact of the external environment is not delayed as much as is required because there is no extra thermal mass to temporarily store the not needed energy during the hours of occupancy. Furthermore, there is less reduction in the diurnal swing and hence room temperature may not fall within acceptable comfort levels. In this case the measured data is not suitable for use to validate the mathematical model.

Chapter 3

On modelling supply air cooling at Eastgate

3.1 Introduction

This chapter gives a description of some models for heating and cooling in the Eastgate building. The models are derived mathematically and compared.

3.2 What is being modelled?

It was thought that most of the heat transfer in the building occurs in the horizontal ducts. (See Chapter (2) for a detailed description of the structure of the building.) As a result, the part of the structure that is modelled is the ceiling slab-air void-floor slab sandwich (sometimes referred to by engineers as a ventilated floor slab), see Figure 3.1. However, by the time the ventilation air reaches higher level floors it would have been cooled by the vertical ducts in the lower level floors. Since modelling is local, this effect cannot be exhibited by the model. The following assumptions are made in developing the mathematical model for heat exchange in the slab-air-slab sandwich.

1. The three-dimensional physical problem is reduced to a two-dimensional model. The actual physical setup is such that when ventilation air enters the horizontal void it spreads sideways as it drifts towards the exit points. See Figure 3.1. However, in this

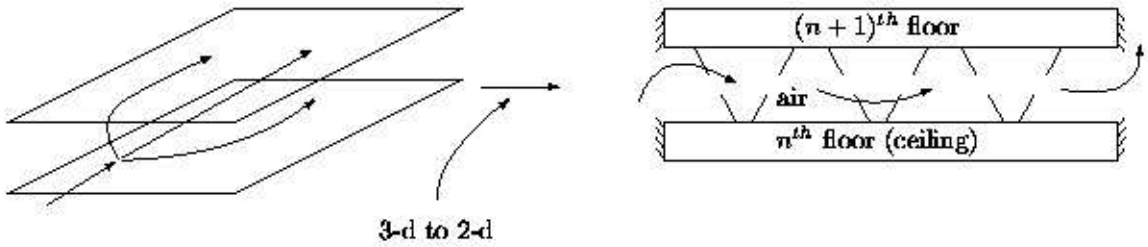

Figure 3.1: Reduction of model to 2-d

model only a vertical two-dimensional section is considered.

2. The following boundary conditions are imposed.

   (a) The floor slab is assumed to be insulated all the way round except on the surface of contact between the floor slab and the air in the void where there is convective heat transfer with the air and radiative heat transfer with ceiling slab below. This assumption is based on the fact that a carpet sits on the surface of the floor that faces the office area.

   (b) Similarly, there is a convective and radiative heat transfer boundary condition on the surface of contact between the ceiling and the air in the void. On the surface of the ceiling facing the office area below, the boundary condition is a prescribed spatially uniform heat flux. This models the heat gain from the lighting and the office equipment that emit radiation. On the rest of the boundary of the ceiling slab an insulation boundary condition is assumed.

3. The entire slab is assumed to be homogeneous. A special type of concrete called screed poured over pre-cast concrete makes the floor slab. Since the screed is much thinner than the pre-cast concrete this assumption is reasonable.

4. Thermal storage in concrete teeth is incorporated in the rest of the body of the slab. This simplifies the geometry to a rectangular cross-section. The extra thermal mass provided by the concrete teeth is assumed negligible. However, if the amount of thermal mass is considerable, it enhances thermal interaction with the supply air and hence improves the conditioning of the interior of the building.

5. A uniform convective heat transfer coefficient h_c for each period of either low or high flow along the duct is assumed. However, there is turbulent air flow due to the existence

of concrete teeth in the void. This results in a non-uniform air velocity and hence variation (which is assumed negligible here) in h_c along the duct.

6. Constant air and slab properties are assumed except for the air velocity which may vary with time to cater for different fan speeds at different times.

7. The initial temperature distribution in both the slab and the air is assumed to be uniform.

3.3 Description of the Mathematical models

3.3.1 Introduction

The following sections give a description of the full mathematical model for thermal energy storage and recovery in a ventilated floor slab. Also given are two simplified forms of the full model; test problems A and B. These are used as an alternative to using measured data to validate the full model. In both problems, an assumption of symmetry in the geometry and boundary condtions about the air flow path allows for analysis to be restricted to half the problem domain, and to neglect radiative heat transfer. Also, the air temperature at the inlet experiences a step change at initial instant. The major difference between the two problems is that one assumes a prescribed uniform air temperature and in the other the variation of air temperature is governed by a suitable energy equation. The aspect of the full model that is tested by the two simplified models is the dynamic response of the air inlet temperature to a time-wise variation. Results for the response to a step change in inlet air temperature can be used together with the principle of superposition as described in [29]. Also, an energy balance is checked to verify the energy equations.

3.3.2 The full model

A description of the full model is stated here.

The problem is to find $T(\mathbf{x}, t)$, the floor temperature, $T^{\star}(\mathbf{x}, t)$, the ceiling temperature and $T^{\infty}(x, t)$, the air temperature that satisfy the following partial differential equations subject to the given boundary and initial conditions. The problem domain concerned is shown in

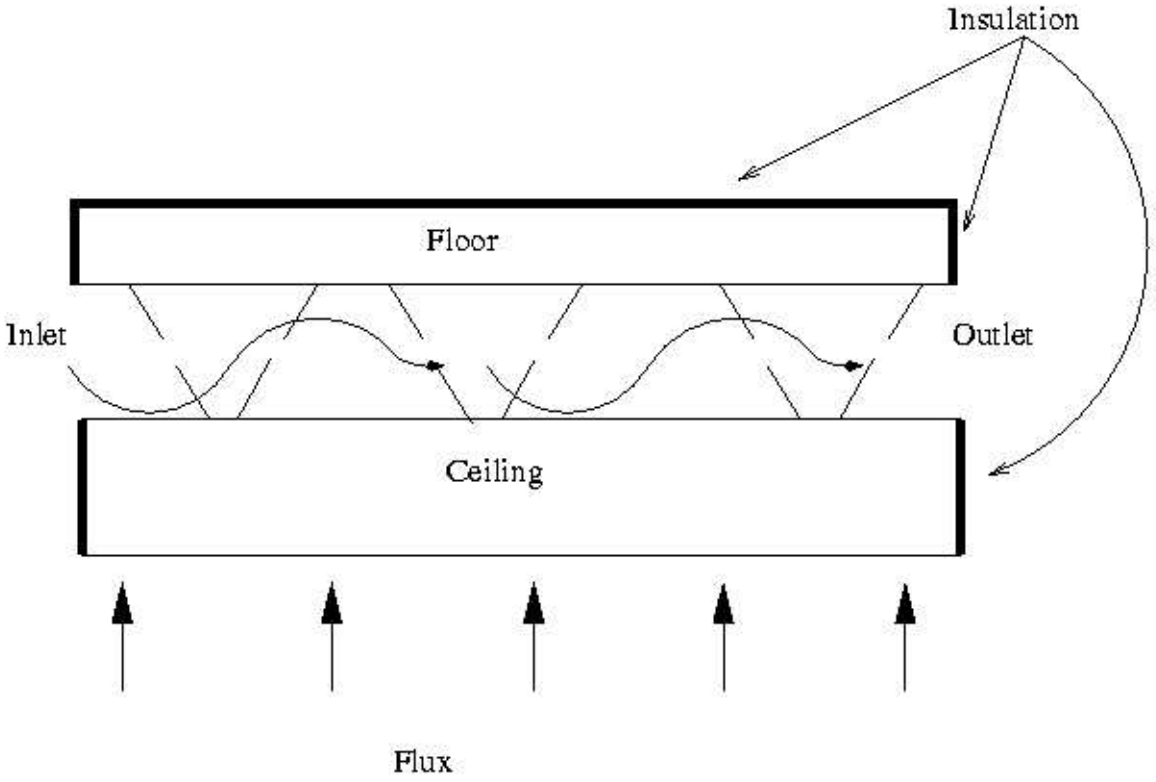

Figure 3.2: Problem domain for the full problem

Figure 3.2. The energy equations for the floor are:

$$\frac{\partial T}{\partial t} = \alpha \nabla^2 T \quad \mathbf{x} \in D \text{ and } t > 0,$$

with boundary conditions

$$-k_m \frac{\partial T(x,t)}{\partial n} = \begin{cases} h_c(T(x,t) - T^{\infty}) & \\ +h_r(T(x,t) - T^{\star}(x,t)) & \text{on } \partial D(\text{in contact with air}) \\ 0 & \text{on } \partial D(\text{the remaining part}), \end{cases}$$

and initial condition

$$T(\mathbf{x}, 0) = T_0, \quad \mathbf{x} \in D,$$

those for the ceiling are:

$$\frac{\partial T^\star}{\partial t} = \alpha \nabla^2 T^\star \quad \mathbf{x} \in D^\star \text{ and } t > 0,$$

with boundary conditions

$$-k_m \frac{\partial T^\star(x,t)}{\partial n} = \begin{cases} h_c(T^\star(x,t) - T^\infty) & \\ +h_r(T^\star(x,t) - T(x,t)) & \text{on } \partial D(\text{in contact with air}) \\ q^\star & \text{on } \partial D(\text{exposed to the room}) \\ 0 & \text{on } \partial D(\text{the remaining part}), \end{cases}$$

and initial condition

$$T^\star(\mathbf{x}, 0) = T_0^\star, \quad \mathbf{x} \in D^\star,$$

and for air they are:

$$\frac{\partial T^\infty(x,t)}{\partial t} + v_f \frac{\partial T^\infty(x,t)}{\partial x} = \beta(T(x,t) - T^\infty(x,t)) + \beta(T^\star(x,t) - T^\infty(x,t)), \ x \in G$$

with initial condition

$$T^\infty(x, 0) = T_0, \quad x \in G,$$

and boundary condition

$$T^\infty(0, t) = f(t), \quad t > 0,$$

where $\alpha = \dfrac{k_m}{\rho_m c_m}$ and $\beta = \dfrac{h_c}{\rho_f c_f g}$. D, $D^\star$ and G are the problem domains for the floor, ceiling and air respectively. $f(t)$ is an arbitrary function of time whose values are obtained from measured data.

A derivation of the standard parabolic diffusion equation is well established and may be

found in various books on heat transfer, for example on pages 7-10 of [11]. Appendix A.2 gives a brief outline of the derivation of the energy equation for the air.

3.3.3 Input data for model

Heat flux

The net heat gain on the ceiling surface facing the office below is modelled collectively as a prescribed flux. During the day, from 7am to 6pm a uniform heat flux of 17.6 Wm^{-2} is used as recommended by the engineers. Outside hours of occupancy, different small values of the heat flux can be tried out. Initially, a value of 0 Wm^{-2} was tried out for periods outside the hours of occupancy. It is worth noting that switching off of lighting and machines in the office outside working hours is not strictly monitored. Consequently, it was thought unreasonable to assume a heat flux of 0 Wm^{-2} during these times. This also applies to weekends when some offices maybe occupied.

Air velocity

In summer mode, the low volume fans run during the day and during the night the high volume fans are switched on to cool the slab for the next day. In winter mode the high volume fans are never switched on. The timing procedure used for the fan speed in the summer is as follows

$$\text{velocity }, v_f = \begin{cases} 0.25\ ms^{-1} & \text{from 7am to 6pm (low flow)} \\ 1.1\ ms^{-1} & \text{from 10pm to 5:30am (high flow)} \\ v_{f_{free}}\ ms^{-1} & \text{otherwise (natural convection)} \end{cases}$$

In the winter, the fans are never switched on between 10pm and 5:30am. The ventilation system operates by natural convection at such times during this period of the year. $v_{f_{free}}$ was initially chosen to be 0 ms^{-1} but several values were tried out later, one typical value is 0.01 ms^{-1}. It was thought that such a small value should include the effect of natural convection on the response of the ventilated floor slab.

Air temperature at the inlet

The temperature of the air at the inlet to the ventilated floor slab is taken from measured data.

Numerical values used for physical constants

k_m	=	$1.4\ W/mK$	thermal conductivity of the concrete
g	=	$.2\ m$	air gap
L	=	$6\ m$	length of each slab
B	=	$.15\ m$	thickness of each slab
c_m	=	$1000\ J/KgK$	specific heat capacity of concrete
ρ	=	$2400 Kg/m^3$	density of concrete
h_c	=	$16\frac{v^{.8}}{g^{.2}}\ W/m^2K$	convective heat transfer coefficient
h_r	=	$5.1\ W/m^2K$	radiative heat transfer coefficient
c_f	=	$1006\ J/KgK$	specific heat capacity of air
ρ_f	=	$1.177\ Kg/m^3$	density of air

3.3.4 Testing the full model on two problems, A and B

Three numerical methods for analysing the thermal performance of a ventilated floor slab, are compared. The methods are: a simple electrical analogue; an improvement through boundary modifications; and finite elements. The methods are tested against an analytic solution for accuracy and again on a more realistic problem for convergence with mesh refinement. Both problems are excited by a step temperature input. The models are discretised in space, time integration is analytic. The energy balance is checked.

The method of the electrical analogue to heat flow is commonly used among engineers. In this work this approach is called the "lumped parameter" method. A lumped parameter model of a hollow core concrete ventilated slab thermal storage system and associated zone has been presented in [26].

The lumped parameter method and a modified form are compared with finite elements. Two aspects are considered in particular:

- Are each of the methods consistent with the mathematical model? In other words, on refining the mesh will the error tend to zero?

- To examine the methods for rates of convergence on refining the mesh and for relative efficiency.

A description of the setting of the original modelling given in Section 3.3.2 indicates the type of problem to which the methods are relevant. The following sections present the two simplified problems (A and B) used to test the three numerical methods.

The first test problem is sufficiently simple to allow an analytic solution, and the second is closer to the actual problem but consequently has no analytic solution and the solution has to be judged from the convergence behaviour shown by refining the mesh of the numerical methods.

Test problem A

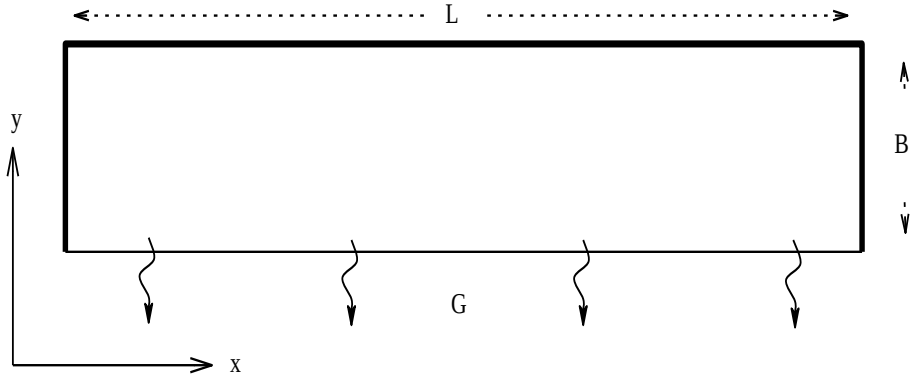

Figure 3.3: Test problem A

Consider replacing the flux boundary condition in the full model of Section (3.3.2) with an insulation boundary condition. This introduces symmetry in the boundary conditions. Furthermore, if symmetry in the geometry is incorporated, it is sufficient to consider only half the problem domain as shown in Figure 3.3 and to neglect radiative heat transfer between the floor and the ceiling surfaces facing each other. A slab is insulated on three sides, indicated in Figure 3.3 by thickened lines, and the fourth experiences convection to the outside fluid which remains at a constant temperature. The heat transfer in the slab is modelled by the

standard parabolic diffusion equation:

$$\begin{aligned}
\text{Slab: } \frac{\partial T(\mathbf{x},t)}{\partial t} &= \alpha \nabla^2 T(\mathbf{x},t) \quad \mathbf{x} \in D \quad \text{where } D = (0,L) \times (0,B) \\
\text{initial condition } \quad T(\mathbf{x},0) &= T_0, \quad \mathbf{x} \in D \\
\text{boundary conditions } \quad -k_m \frac{\partial T(x,t)}{\partial n} &= \begin{cases} h_c(T(x,t) - T^\infty) & \text{on } \partial D \text{(in contact with air)} \\ 0 & \text{on } \partial D \text{(the remaining part)} \end{cases}
\end{aligned}$$

where the fluid temperature T^∞ is constant.

The analytic solution to this problem is given in [30] on page 15 and given in appendix A.1 for convenience.

Test problem B

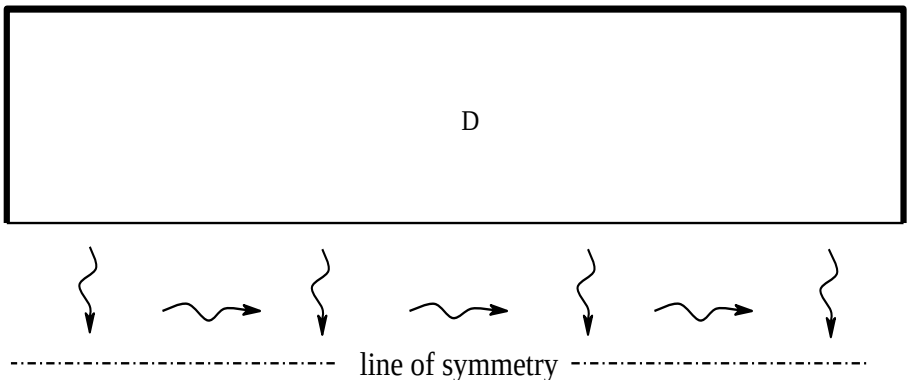

Figure 3.4: Test problem B

The ventilated slab is assumed to be insulated all round except on the slab to air interface, where heat interchange occurs by convection into the moving air. The ceiling and floor slabs are assumed to be identical thus reducing the size of the problem through symmetry and not involving radiation.

Expressed mathematically, the problem is to follow the time variation of the temperature in the slab $T(\mathbf{x},t)$ and in the air $T^\infty(x,t)$, see Figure 3.4. The energy equation for the slab is:

$$\frac{\partial T(\mathbf{x},t)}{\partial t} = \alpha \nabla^2 T(\mathbf{x},t), \ \mathbf{x} \in D, \ t > 0, \tag{3.1}$$

with initial condition:

$$T(\mathbf{x},0) = T_0, \quad \mathbf{x} \in D,$$

and boundary conditions:

$$-k_m \frac{\partial T(x,t)}{\partial n} = \begin{cases} h_c(T(x,t) - T^\infty(x,t)) & \text{on } \partial D(\text{in contact with air}) \\ 0 & \text{on } \partial D(\text{the remaining part}), \end{cases}$$

That for air is:

$$\frac{\partial T^\infty(x,t)}{\partial t} + v_f \frac{\partial T^\infty(x,t)}{\partial x} = \beta(T(x,t) - T^\infty(x,t)),\ x \in G, \tag{3.2}$$

with initial condition:

$$T^\infty(x,0) = T_0,\ x \in G,$$

and boundary condition:

$$T^\infty(0,t) = f(t),\ t > 0,$$

where $f(t)$ is the air temperature as it enters the gap. For the step problem used in the tests $f(t) = T_H$ a constant, so that the step is $T_H - T_0$.

Heat transfer in the slab is modelled by the standard parabolic diffusion equation (3.1). Equation (3.2) is a special case of the energy equation for the air for the full problem. In the derivation of the latter, given in Appendix A.2 only heat flow from one concrete slab should be considered to obtain equation (3.2). The air mass flow rate $\dot{m}_f$ and the air velocity v_f are related by $\dot{m}_f = \rho_f v_f g$, where ρ_f, ρ_f and g are the density and the average velocity of the air and, g is the air gap in the slab.

3.4 Details of the mathematical methods for test problems A and B

Three methods are considered. The first is the simplest, the heat conservation equation written in the form of the electrical analogy to heat flow. The slabs and air gap are divided into small sections. The flow in and out of a section is considered together with the rate of temperature change resulting from any imbalance - this is denoted as the simple lumped parameter method (**slp**). It can be modified by an improved modelling of the boundary effects of the slab surface and the slab/air interface, this is denoted as the modified lumped parameter method (**mlp**), and finally the finite element method (**fe**).

3.4.1 The simple lumped parameter method, slp

Introduction

Thermal network modelling has been used by other investigators as a means of analysing heat transfer processes in ventilated floor slabs [19, 26]. In the lumped capacitance model [11], it is assumed that the building fabric has a sufficiently large thermal conductivity, k_m and hence a small *Biot number*, Bi. This holds if the internal thermal resistance is negligible compared to the surface thermal resistance. Bi is defined as follows:

$$Bi = \frac{h_e l_c}{k_m} \tag{3.3}$$

where h_e is an effective heat transfer coefficient that in general takes into account heat transfer by both radiation and convection, and l_c is a characteristic length of the storage material. A derivation of this condition for applicability of the lumped capacitance model is given in [11]. Shaw [31] presented a derivation of the lumped capacitance approximation using asymptotic analysis for solid bodies that are exposed to constant property environments. If Bi is small then it may be assumed that the slab mass temperature is only a function of time and is uniform throughout the system at any instant, otherwise temperature gradients in the slab mass may not be neglected. It is then necessary to divide the slab mass into a finite number of sections. Each section behaves like a small lumped capacitance and is taken as a node which is connected to its neighbors through thermal resistances [19]. Thermal storage in the slab material and air is represented in the thermal network model by a thermal capacity.

Consider dividing the problem domain occupied by the slab into n_x, n_y rectangular sections of widths Δx and Δy each in the x-direction and y-direction respectively,

$$L = n_x \Delta x, \quad B = n_y \Delta y.$$

Since the air temperature is dependent on only one spatial coordinate x, discretisation need only be in one direction. The temperatures for the nodes in the air and floor slab are denoted by

$$T^{\infty}(P,t) \sim T_P^{\infty}(t), \quad T(P,t) \sim T_P(t),$$

and for the sake of brevity the time argument t is omitted.

Energy equations for the slab material

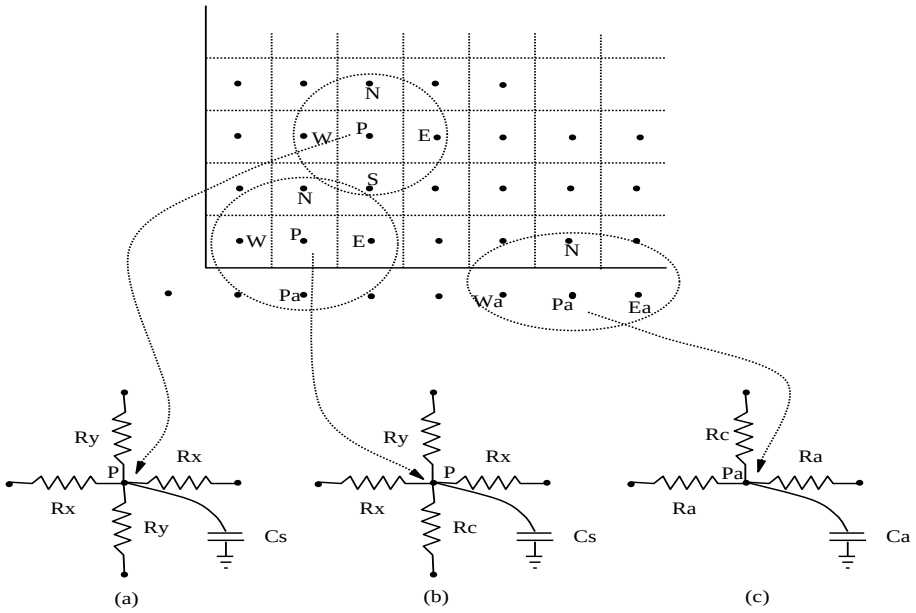

Figure 3.5: Discretisation for the slab and air nodes for the slp method, and corresponding networks. Inner node (a), boundary (with air) node (b) and air nodes (c).

For the section containing node P, see Figure 3.5 the heat flow into the section from node W across the side of width Δy is

$$\begin{aligned} \Delta y \; q_w &= \Delta y \; (-k_m \frac{\partial T}{\partial n}) \\ &\approx k_m \Delta y \frac{T_W - T_P}{\Delta x}, \end{aligned}$$

where q_w is the net heat flow rate per area of cross-section going through thermal resistance labelled R_y.

Since the rate of accumulation of energy at a node, equals the net rate of heat flowing into that node then

$$\begin{aligned} \rho_s c_s \Delta x \Delta y \frac{dT_P}{dt} &= k_m \Delta y \frac{T_W - T_P}{\Delta x} + k_m \Delta y \frac{T_E - T_P}{\Delta x} + k_m \Delta x \frac{T_S - T_P}{\Delta y} + k_m \Delta x \frac{T_N - T_P}{\Delta y} \\ \text{or} \quad C_s \frac{dT_P}{dt} &= \frac{T_W - T_P}{R_x} + \frac{T_E - T_P}{R_x} + \frac{T_S - T_P}{R_y} + \frac{T_N - T_P}{R_y}, \end{aligned} \tag{3.4}$$

where, using the electrical analogue [18], $C_s = \rho_s c_s \Delta x \Delta y$ is the thermal capacitance of the section and

$$R_x = \frac{\Delta x}{k_m \Delta y}, \quad R_y = \frac{\Delta y}{k_m \Delta x}$$

are the thermal resistances in the x and y directions.

Energy equations for the air

Consider approximating equation (3.2) by a backward difference [22] in the space derivative. We have that

$$\frac{\partial T^\infty}{\partial x}(P,t) \approx \frac{T_P^\infty - T_W^\infty}{\Delta x}$$

This discretisation in the spatial variable x reduces a partial differential equation (the energy equation for the air problem domain) to a system of ordinary differential equations for each node P in terms of an unknown (air temperature at a node) that depends on time only. The resulting approximation is:

$$\rho_f c_f g \frac{dT_P^\infty}{dt} + \dot{m}_f c_f \frac{T_P^\infty - T_W^\infty}{\Delta x} = h_c \left(T_N - T_P^\infty \right), \tag{3.5}$$

where T_P^∞ is the air temperature at node P.

Upon multiplying throughout by Δx and using an analogy between electric flow and heat flow [18] and re-arranging, equation (3.5) assumes the following form,

$$\mathcal{C}_a \frac{dT_P^\infty}{dt} = \frac{T_W^\infty - T_P^\infty}{R_a} + \frac{T_N - T_P^\infty}{R_c} \tag{3.6}$$

$\mathcal{C}_a = \rho_f c_f g \Delta x$ is the thermal capacitance of the air. Thermal resistance to heat flow along the air void R_a, and thermal resistance to convective heat flow (fluid to solid) R_c are defined

as follows

$$R_c = \frac{1}{h_c \Delta x}, \quad R_a = \frac{1}{\dot{m}_f c_f}$$

It is clear from equation (3.6) that the net heat flow into node P equals the thermal energy stored in the section of node P. A thermal network for a section in the air is shown in Figure 3.5:c.

Energy balance equations in matrix form

When the energy balance equations (3.4) and (3.6) are applied for all the nodes in the slab and air, they form a matrix equation

$$\begin{aligned} C\frac{d\mathbf{U}(t)}{dt} &= B\mathbf{U}(t) + \mathbf{v} \\ \text{where } \mathbf{U} &= [T_1^\infty, T_2^\infty, \ldots, T_m^\infty |\ T_1, T_2, \ldots, T_{mn}]^{\mathrm{T}} \\ \text{and } \mathbf{v} &= [R_a T_H, 0, 0, \ldots]^{\mathrm{T}} \end{aligned} \tag{3.7}$$

3.4.2 A modified lumped parameter method, mlp

Introduction

Nodes are introduced on the boundary in order to improve the modelling there, resulting in the sections around the boundary being either a half or quarter of the area of the internal sections.

The equations for an internal slab node and for the air nodes are the same as for the slp model and for this reason are not repeated. The new boundary forms are given below.

Heat transfer at a node on an insulated boundary

Consider the setting shown in Figure 3.6(a). If an artificial node W is introduced, the insulation boundary condition at node P may be approximated by a central difference as $T_W = T_E$. Using this result on equation (3.4) and re-arranging yields the following as the

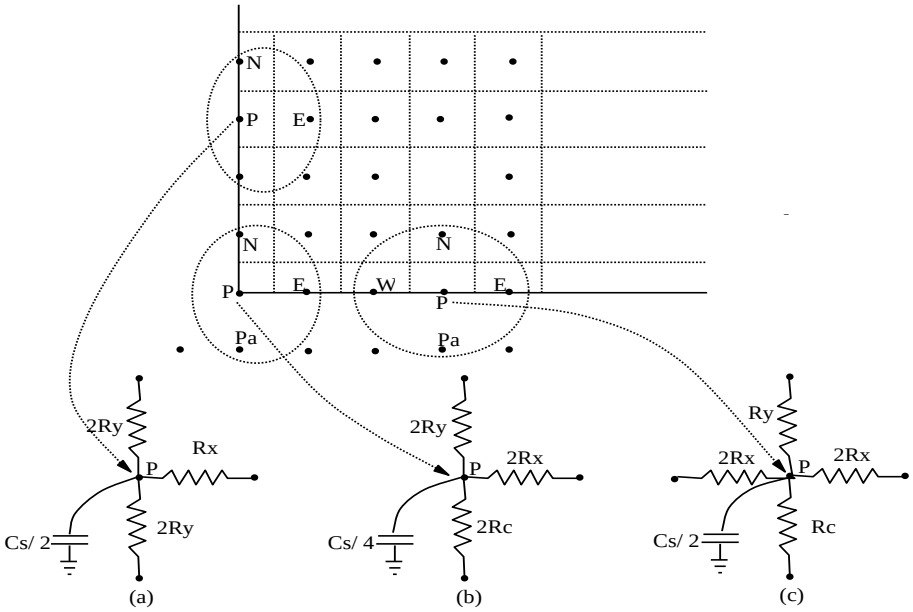

Figure 3.6: Discretisation on the boundary for mlp

thermal resistance-capacitance formulation for insulation on a plane surface.

$$\frac{\mathcal{C}_s}{2}\frac{dT_P}{dt} = \frac{T_S - T_P}{2R_x} + \frac{T_N - T_P}{2R_x} + \frac{T_E - T_P}{R_y} \tag{3.8}$$

Heat transfer at a node on an insulated boundary and with convection

On the air boundary the convection condition is approximated by

$$\frac{(T_S - T_N)}{2R_y} = \frac{(T_P^{\infty} - T_P)}{R_c}$$

which when used in equation (3.4) gives the following as the thermal resistance-capacitance formulation for a convection boundary condition at a plane surface, see Figure 3.6(c),

$$\frac{\mathcal{C}_s}{2}\frac{dT_P}{dt} = \frac{T_W - T_P}{2R_x} + \frac{T_E - T_P}{2R_x} + \frac{T_P^{\infty} - T_P}{R_c} + \frac{T_N - T_P}{R_y} \tag{3.9}$$

Heat transfer at a corner with insulation, also with convection

The section size is now a quarter of the standard giving, using a similar method, for the insulated corner

$$\frac{\mathcal{C}_s}{4}\frac{dT_P}{dt} = \frac{T_W - T_P}{2R_x} + \frac{T_N - T_P}{2R_y}, \tag{3.10}$$

and similarly with air convection, see Figure 3.6(b).

$$\frac{\mathcal{C}_s}{4}\frac{dT_P}{dt} = \frac{T_E - T_P}{2R_x} + \frac{T_N - T_P}{2R_y} + \frac{T_P^\infty - T_P}{2R_c} \tag{3.11}$$

Energy balance equations in matrix form

The equations for the mlp method combine into a global equation of the same form as the slp, equation (3.7).

3.4.3 The finite element method (fe)

Rectangular elements are used, and since no sudden temperature changes are expected it is reasonable to use a bilinear approximation on an element in the slab. See [17].

$$\phi(x, y) = a + bx + cy + dxy$$

This is linear when reduced to one dimension and so will fit with using linear approximation for the elements of the air. The nodes on the slab and air are at the same points as for the mlp method. Discretisation for the floor slab is

$$\begin{aligned} M\frac{d\mathbf{T}}{dt} &= -K\mathbf{T} + H(\mathbf{T}^\infty - \mathbf{T}) \\ \text{where } \mathbf{T} &= [T_1, T_2, \ldots, T_m|\ T_{m+1}, \ldots, T_{mn}]^{\mathrm{T}} \\ \mathbf{T}^\infty &= [T_1^\infty, T_2^\infty, \ldots, T_m^\infty|\ 0, \ldots, 0]^{\mathrm{T}} \end{aligned} \tag{3.12}$$

m and n are the number of nodes along the air void (which is the same as along the length of the floor slab), and along the thickness of each slab, respectively. The terms of the matrices

are given in terms of the basis functions as

$$\begin{aligned} M_{rc} &= \rho_m c_m \int_D \phi_r(\mathbf{x})\phi_c(\mathbf{x})dA \\ H_{rc} &= h_c \int_{\partial D} \phi_r(x)\phi_c(x)dx \\ K_{rc} &= k_m \int_D \nabla\phi_r(\mathbf{x}) \cdot \nabla\phi_c(\mathbf{x})dA. \end{aligned}$$

The space discretisation for the air void is

$$\begin{aligned} P\frac{d\mathbf{t}^\infty}{dt} &= -Q\mathbf{t}^\infty - R(\mathbf{t}^s - \mathbf{t}^\infty) \\ \text{where } P_{rc} &= \int_G \phi_r(x)\phi_c(x)dx \ , \\ Q_{rc} &= v_f \int_G \phi_r(x)\frac{d\phi_c(x)}{dx}dx \\ \text{and } R_{rc} &= \beta P_{rc} \\ \text{and } \mathbf{t}^\infty &= [T_1^\infty, T_2^\infty, \ldots, T_m^\infty]^{\mathrm{T}}, \\ \mathbf{t}^s &= [T_1, T2, \ldots, T_m]^{\mathrm{T}}, \end{aligned} \tag{3.13}$$

The coupled equations (3.12), (3.13) may be combined into a single matrix system

$$\begin{aligned} F\frac{d\mathbf{U}(t)}{dt} &= G\mathbf{U}(t) + \mathbf{y} \\ \text{where } \mathbf{U} &= [\mathbf{t}^\infty|\ \mathbf{T}]^{\mathrm{T}} \\ \mathbf{y} &= [H(1,1)T_H, 0, 0, \ldots, 0]^{\mathrm{T}}. \end{aligned} \tag{3.14}$$

Note that from the boundary conditions $T_0^\infty \equiv$ constant, T_H.

3.4.4 An analytic method for solving in the time domain

The finite element equations (3.14) and the energy balance equations for the thermal resistance-capacitance formulation, equations (3.7), all have the same form and may be written as

$$\dot{\mathbf{x}}(t) = E\mathbf{x}(t) + \mathbf{w}(t), \tag{3.15}$$

after multiplying throughout by the inverse of the first coefficient matrix.

If, as is the case with the test problems, the source function $\mathbf{w}(t)$ can be expressed in terms of

elementary functions (it is a constant here) this system of equations can be solved analytically rather than numerically. Usually in the time domain some form of finite difference time stepping is needed, say the explicit method or Crank-Nicolson, which would introduce it's own error. The advantage with an analytic method in comparing the different models is that it would introduce only a very small rounding error, so that the error which is present in the final results comes from the modelling equations themselves. An outline of the uncoupling of the equations is given below; in a different context the method is described in [23].

Suppose the matrix E satisfies the following eigenvalue properties

$$EX = XD, \text{ where } D = \text{diag}\{\lambda_1, \lambda_2, \ldots, \lambda_s\} \tag{3.16}$$

and $\lambda_i,\ i = 1, 2, \ldots, s$ are its eigenvalues and, the columns of X are the corresponding eigenvectors. Upon inserting $\mathbf{x}(t) = X\mathbf{z}(t)$ into equation (3.15) and using equation (3.16) the following uncoupled system is obtained

$$\dot{\mathbf{z}}(t) - D\mathbf{z}(t) = X^{-1}\mathbf{w}(t) \tag{3.17}$$

Equation (3.17) may be solved by standard techniques (Laplace transforms were chosen in this case) to yield $\mathbf{z}(t)$ and hence the required solution $\mathbf{x}(t) = X\mathbf{z}(t)$.

For the case of a nearly singular capacitance matrix (which may arise for an inhomogeneous slab due to varying physical properties), the generalized eigenvalue problem may be considered instead. The resulting eigensystem is solved by the qz algorithm (see [21]).

3.5 Results on test problems, A and B

3.5.1 Data used for the test problems

The dimensions and physical parameters chosen for the test problems are,

Slab dimensions:	$L = 6.00\,m, \quad B = 0.15\,m$
Slab parameters:	$k = 1.40\,W/mK, \quad \rho_m = 2400\,kg/m^3, \quad c_s = 1000\,J/kg\ ^\circ C$
Air gap:	$g = 0.20\,m$
Air parameters:	$v_f = 0.25\,m/s, \quad \rho_f = 1.177\,kg/m^3, \quad c_f = 1006\,J/kg\ ^\circ C$
Convective heat transfer coefficient:	$h_c = 2.00\,W/m^2\ ^\circ C$

The slabs and the air were assumed to be initially at a uniform temperature of $20°C$, then the input air temperature was given a step increase to $30°C$. The models estimate the rise of slab and air temperatures to the same value. The actual data from the Eastgate building was numerical and roughly periodic and sinusoidal, however since any arbitrary function of time can be approximated to a required accuracy as a linear combination of step functions, the present test is sufficient to validate the models, see pages 86–88 of [30].

3.5.2 Accuracy and energy conservation

Testing accuracy with problem A

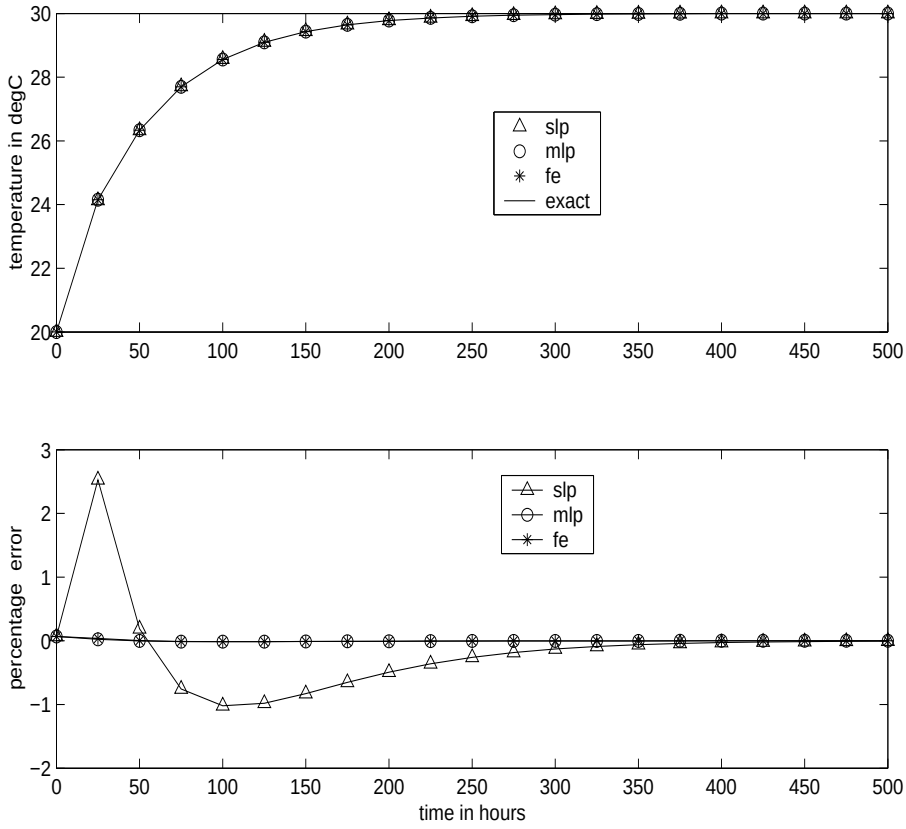

Figure 3.7: Comparison of methods against the exact solution to test problem A

The upper half of Figure (3.7) shows the analytic solution at the slab boundary as it experiences convection over 500 hours. The three methods which are compared use the mesh $m = 5$ and $n = 12$ which, judging from the later tables from the test problem B, will give

a good representation for the methods. The symbols for the methods over-lay showing the errors to be small. The graph below shows how the errors relate to each other in detail; only slp has a significant error and this is less than 3% throughout the time period.

Checking on the overall energy balance

As a check on the computer code, it should predict the balance between the input energy i.e. the heat lost by the air as it passes along the gap, and the heat stored in the floor and ceiling slabs.

An outline of the computation follows.

$$\begin{aligned} \frac{d}{dt}[e(t)] &= \dot{m}_f c_f T^{\infty}(0,t) - \dot{m}_f c_f T^{\infty}(L,t) \\ \text{where } e(t) &= E_a(t) + E_{s,f}(t) + E_{s,c}(t) \end{aligned} \tag{3.18}$$

Here, $E_a(t)$, $E_{s,f}(t)$ and $E_{s,c}(t)$ denote the total energy content of the air, floor and ceiling slab respectively and hence $e(t)$ is the total energy. The finite element and lumped parameter equivalents of the energy terms are found by using the nodal temperatures that are obtained from code. Each node is either associated with a part of the slab or the air. The solution to equation (3.18) is obtained as

$$e(t) - e(0) = \dot{m}_f c_f \left[t\, T^{\infty}(0,t) - \int_0^t T^{\infty}(L,\tau) d\tau \right] \tag{3.19}$$

Since $T^{\infty}(L,t)$ is known from section (3.4.4), equation (3.19) can be evaluated explicitly and can be used to check an energy balance for the slab-air-slab sandwich. The integration for the finite element calculation is analytic and can be obtained for any time. For the simple lumped parameter method this proved difficult and the trapezoidal rule was used for the integration. The Trapezoidal rule has truncation error $O(h^2)$ and the Simpson's rule $O(h^5)$ hence more accurate, where h is the spacing between neighbouring points used in the numerical integration. However, no sudden changes in air outlet temperature $T^{\infty}(L,t)$ after the initial instant are expected. This is evident from Figure (3.8) which shows very little change in temperature between neighbouring points. Hence the Trapezoidal rule is adequate to demonstrate conservation of energy. Moreover, Simpson's rule is more computationally intensive and hence compromises the storage requirement of Matlab, [1] since the time over which the temperature is integrated is relatively long.

It is clear from the tables 3.2 and 3.1 that there is good agreement and that the codes do

time(mins)	energy(kJ) stored	lost	(stored-lost)/stored
4.00	54.2450	54.2446	8.3e-06
8.00	99.6295	99.6290	4.5e-06
12.00	144.9237	144.9233	3.1e-06
16.00	190.1300	190.1296	2.4e-06
20.00	235.2506	235.2501	1.9e-06
24.00	280.2874	280.2869	1.6e-06
28.00	325.2424	325.2420	1.4e-06
32.00	370.1176	370.1171	1.2e-06
36.00	414.9146	414.9141	1.1e-06
40.00	459.6351	459.6346	9.8e-07
44.00	504.2808	504.2803	8.9e-07
48.00	548.8531	548.8526	8.2e-07
52.00	593.3536	593.3531	7.6e-07
56.00	637.7835	637.7831	7.0e-07
60.00	682.1443	682.1438	6.6e-07

Table 3.1: Energy balance for the slp method applied to test problem B

time(hrs)	energy(kJ) stored	lost	(stored-lost)/stored
5	3274.55	3272.28	0.00069
10	6273.36	6268.99	0.0007
15	9049.2	9043.28	0.00065
20	11618.5	11611.5	0.0006
50	23474.8	23466.6	0.00035
100	34243.3	34238.6	0.00014
150	39157.8	39155.5	5.9×10^{-5}
200	41387.7	41386.3	3.4×10^{-5}

Table 3.2: Energy balance for the fe method applied to test problem B

have the energy balance built into them. The mlp code was not tested because the values given were very close to those of the fe method which was known to be satisfactory.

3.5.3 On the minimum mesh size with slp for test problem B

It became evident while making the various tests that for the slp method two sections in the breadth gave a significant improvement in accuracy compared with using only one. This is shown in the two Figures 3.8 and 3.9, which give the results of comparing the slp method with one and two sections, i.e. one or two nodes in the breadth of the slab. The test problem B was used and Figure 3.8 gives the air temperature at the outlet and 8 records the temperature of the slab nearest to the air outlet. Note that with the slp method the

nodes are at the centre of the sections, so that for the 2×1 and 2×2 meshes the outlet air node position is in fact three-quarters of the way down the gap for both, whereas the slab positions differ slightly (by a quarter of the thickness). The fe results used as the base values to compare against are the *converged* values with a 23×7 mesh (the values have not formally converged, it is that they have stabilised to 3 decimal places with mesh refinement).

Figure 3.8 shows the outlet air temperature with an initial sharp rise. The rise occurs because of the step input temperature of $30°C$ from the starting value of 20, which at $2.5m/s$ takes 2.4 seconds to travel the $6m$ length of the air gap. Thereafter the rate of increase is relatively small. The important feature is that the 2×1 mesh predicts a temperature about $1.5°C$ too high whereas the 2×2 estimate is reasonable with an error of around 0.2. The corresponding

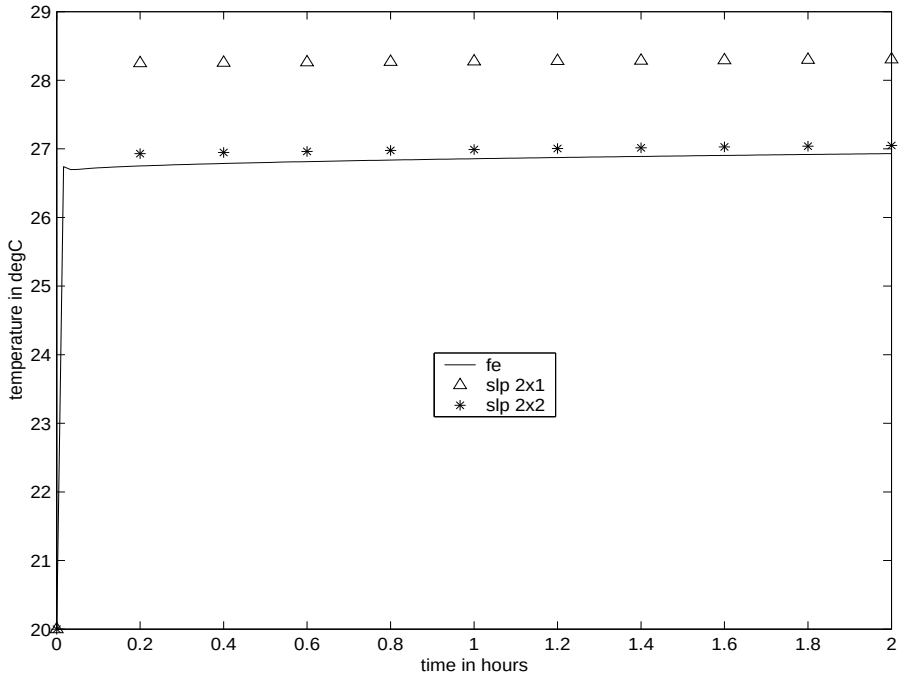

Figure 3.8: Comparison of slp method between a 2×1 and 2×2 mesh with the *converged* solution at the air outlet, using problem B

results over 360 hours for the slab temperature at the node nearest the outlet are shown in Figure (3.9). The error for the 2×1 mesh is again considerably more than for the 2×2 mesh although generally the slab errors are less than the errors at the air outlet. The discrepancy between the results of the two meshes comes from the form of the heat-flow through the slab thickness. This will be exponential rather than linear and thus will need at least two nodes to adequately represent the behaviour. Hence in the tables below at least 2 nodes or elements were used in the thickness.

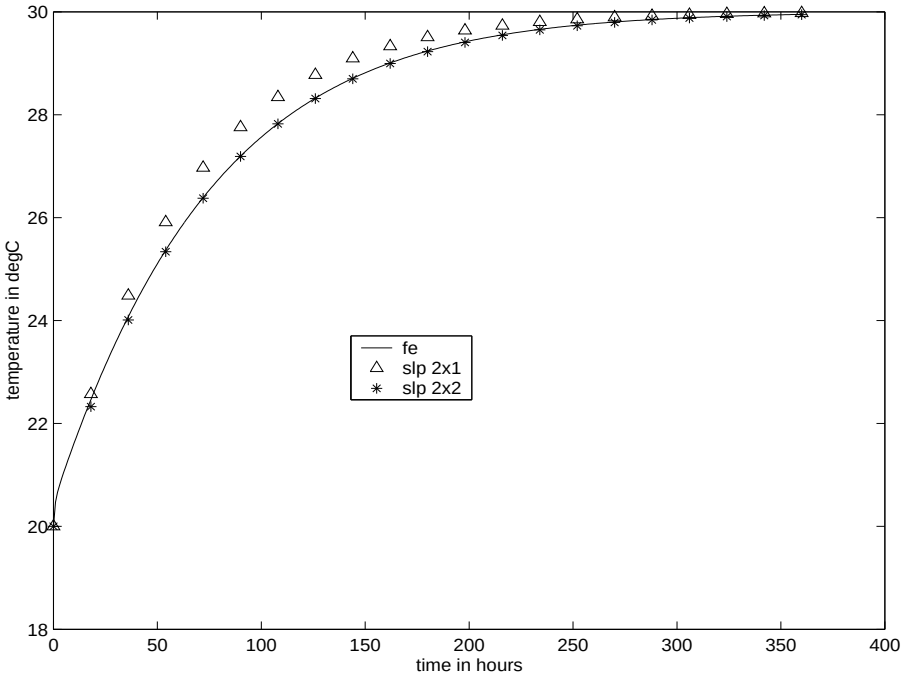

Figure 3.9: Comparison against an exact solution to problem A

3.5.4 Convergence and accuracy with test problem B

The variance of the errors with time are shown in the previous section. In the tables below, which look at the convergence rates of the three methods and their relative efficiency, the temperatures are considered at a particular time. This has been chosen at 45 hours after the start, being a reasonable compromise considering the different error behaviour of the air and slab.

The aim of the gap between floor and ceiling is to cool the air as it passes through. The cooling gain is measured by the difference between the input air temperature of $30°C$ and the temperature as it leaves i.e. at the node closest to the outlet. Table 3.3 below shows the values given as the mesh is refined, with m and n being the number of nodes in the length and breadth respectively.

Clearly the system converges very early in the refinement judged by the consistency of the prediction. The convergent process of refinement is shown more clearly by the differences between this converged value and the estimates of the refining process, see table 3.4. These differences show that even for the simplest mesh, 3×2, the error is only 0.007 which would not be noticeable (and also hardly measurable).

n\ m	3	7	11	15	19	23	27	31
2	28.421	28.421	28.421	28.421	28.421	28.421	28.421	28.421
3	28.426	28.427	28.427	28.426	28.426	28.426	28.426	28.426
4	28.427	28.427	28.427	28.427	28.427	28.427	28.427	28.427
5	28.427	28.428	28.428	28.428	28.428	28.428	28.428	28.428
7	28.428	28.428	28.428	28.428	28.428	28.428	28.428	28.428
11	28.428	28.428	28.428	28.428	28.428	28.428	28.428	28.428

Table 3.3: Indication of convergence for the fe scheme: temperature of air at the duct outlet, at time = 45 hours

n\ m	3	7	11	15	19	23	27	31
2	0.007	0.007	0.007	0.007	0.007	0.007	0.007	0.007
3	0.002	0.001	0.001	0.002	0.002	0.002	0.002	0.002
4	0.001	0.001	0.001	0.001	0.001	0.001	0.001	0.001
5	0.001	0.000	0.000	0.000	0.000	0.000	0.000	0.000
7	0.000	0.000	0.000	0.000	0.000	0.000	0.000	0.000
11	0.000	0.000	0.000	0.000	0.000	0.000	0.000	0.000

Table 3.4: Progress towards convergence of the fe scheme with mesh refinement: air temperature at the duct outlet, at time = 45 hours. *Converged* temperature (28.428) - estimate

The corresponding differenced values given by the modified lp scheme are similar and show convergence to a similar value $28.431°C$.

The values shown in table 3.5 are very slightly less accurate than the fe, with the worst result only in error by $0.037°C$ which may not change the first decimal place in the recorded temperature. Note that the lp method over-estimates the temperature (slightly) whereas fe under-estimates. The values change with both m and n for the lumped parameter methods, whereas very little change is observed to three decimal places as n varies in the fe method. This is because the section size, and hence the node position which is best considered as being at the centre of the section, varies with m and n for the lumped parameter methods. The mathematical construction of the fe method ensures that the node values are estimated at the vertices of the (rectangular) elements.

The simple lp results show the greatest variation and the slowest convergence with refinement, as would be expected. If we take the temperature $28.430°C$ (as being the *converged* value) from the two previous methods then the differences are given in table (3.6).

n\ m	3	7	11	15	19	23	27	31
3	-0.037	-0.010	-0.005	-0.002	-0.001	0.000	0.000	0.000
4	-0.037	-0.011	-0.005	-0.003	-0.002	-0.001	0.000	0.000
5	-0.037	-0.011	-0.005	-0.003	-0.002	-0.001	0.000	0.000
7	-0.038	-0.011	-0.006	-0.003	-0.002	-0.001	-0.001	0.000
11	-0.038	-0.011	-0.006	-0.003	-0.002	-0.001	-0.001	0.000

Table 3.5: Progress towards convergence of the mlp scheme with mesh refinement: air temperature at the duct outlet, at time = 45 hours. *Converged* temperature (28.431) - estimate

n\ m	2	6	10	14	18	22	26	30
2	-0.777	-0.247	-0.140	-0.095	-0.069	-0.053	-0.042	-0.032
3	-0.779	-0.251	-0.145	-0.099	-0.074	-0.058	-0.047	-0.039
4	-0.781	-0.253	-0.147	-0.102	-0.077	-0.061	-0.050	-0.041
6	-0.782	-0.255	-0.150	-0.105	-0.079	-0.063	-0.052	-0.044
10	-0.783	-0.257	-0.152	-0.107	-0.082	-0.066	-0.055	-0.047

Table 3.6: Progress towards convergence of the slp scheme with mesh refinement: air temperature at the duct outlet, at time = 45 hours. *Converged* temperature (28.430) - estimate

It is clear that the results indicate a convergent process but not exactly to the value 28.430. In addition to the position of the nodes varying with refinement mentioned above, the value can also be influenced by the modelling of the time change: the model is not as accurate as the other two in both space and time, so that the "45 hours" may not be as precise.

However with these reservations the method is still quite accurate and with a mesh of 6×2 the error is less than a quarter of a degree.

The temperature values in the slab are also available, and in order to show how they behave for the three schemes the set of tables 3.3 through 3.6 corresponding to the set above is given. The temperature is estimated at the node in the slab nearest to the outlet; this point exhibits behaviour similar to the air outlet, but reacts more slowly to the step input.

In table 3.7 for the simple lp scheme the *converged* value is taken to be the average of the two other, more accurate schemes i.e. 24.759. This *converged* value is not the temperature the slp scheme is converging to, which explains partly the residual differences. As mentioned before when explaining the behaviour of the air estimates, another cause of the erratic behaviour is that the central node of each section varies in position as the dimensions, m, n change. Also the previous comments on the accuracy of the time modelling hold. Having made these

n\ m	2	6	10	14	18	22	26	30
2	0.044	0.079	0.082	0.082	0.081	0.079	0.078	0.077
3	0.025	0.059	0.062	0.062	0.061	0.060	0.058	0.057
4	0.014	0.048	0.051	0.051	0.050	0.049	0.047	0.046
6	0.003	0.036	0.040	0.040	0.038	0.037	0.036	0.035
10	-0.007	0.027	0.030	0.030	0.029	0.027	0.026	0.025

Table 3.7: Progress towards convergence of the slp scheme with mesh refinement: temperature of slab nearest to the duct outlet, at time = 45 hours. *Converged* temperature (24.760) - estimate

allowances the estimates are quite accurate.

Efficiency

n\ m	3	7	11	15	19	23	27	31
2	0.007	0.007	0.007	0.007	0.007	0.007	0.007	0.007
3	0.002	0.001	0.001	0.002	0.002	0.002	0.002	0.002
4	0.001	0.001	0.001	0.001	0.001	0.001	0.001	0.001
5	0.001	0.000	0.000	0.000	0.000	0.000	0.000	0.000
7	0.000	0.000	0.000	0.000	0.000	0.000	0.000	0.000
11	0.000	0.000	0.000	0.000	0.000	0.000	0.000	0.000

Table 3.8: Progress towards convergence of the fe scheme with mesh refinement: air temperature at the duct outlet, at time = 45 hours. *Converged* temperature (28.428) - estimate

The form of the data displayed in the tables with the inconsistent numbers chosen for m and n makes it difficult to make a detailed analysis, however the general indication is clear.

The mlp and fe methods have a similar behaviour with fe being more accurate for the same mesh, but both give acceptable accuracy for the simplest mesh.

To compare slp with, say, the fe method for the air temperature, see tables 3.8 and 3.9. Suppose we wish to achieve a prescribed accuracy and record the smallest number of degrees of freedom needed. If say an error less than 0.1 is required, the slp requires $s = m \times n$ to be at least $14 \times 2 = 28$ whereas fe needs only $3 \times 2 = 6$. In fact this simple mesh gives an error of less than 0.01; it appears that fe (and mlp) is, on the basis of the size of matrices required to solve the problem, more efficient.

n\ m	2	6	10	14	18	22	26	30
2	-0.777	-0.247	-0.140	-0.095	-0.069	-0.053	-0.042	-0.032
3	-0.779	-0.251	-0.145	-0.099	-0.074	-0.058	-0.047	-0.039
4	-0.781	-0.253	-0.147	-0.102	-0.077	-0.061	-0.050	-0.041
6	-0.782	-0.255	-0.150	-0.105	-0.079	-0.063	-0.052	-0.044
10	-0.783	-0.257	-0.152	-0.107	-0.082	-0.066	-0.055	-0.047

Table 3.9: Progress towards convergence of the slp scheme with mesh refinement: air temperature at the duct outlet, at time = 45 hours. *Converged* temperature (28.430) - estimate

3.5.5 Discussion

A comparison is made of three mathematical methods for modelling, in space and time, the thermal storage in a ventilated floor slab. The problem to be solved involves the coupling of slab heat flow with ventilating air. Two of the methods, slp and mlp have a direct derivation in terms of heat flow and so may be more intuitive and, especially slp, easy to code. The other, fe, has a more mathematical explanation and may not be so readily available for someone not familiar with the technique. All three methods are briefly described and judged on a simple problem with an analytic solution, and to conserve energy. When examined on a problem having the essential features of the ventilated slab, the slp method is shown to require at least two sections in the slab thickness to give reasonable results. The mlp and fe methods were roughly comparable with each other, with the fe being slightly more accurate. Both were more efficient than slp when judged by the number of degrees of freedom required for a particular accuracy.

The accuracy requirement in a method is not easily stated; some of the problem parameters themselves are not known precisely, for example the convective heat transfer coefficient, and even the physical model has questionable assumptions built into it. However assuming that the smallest contribution to the overall error from the solution method for a given computational cost is required, the results given in this chapter indicate that the fe method should be seriously considered.

The model has some inadequacies which could be addressed in future work and hence modification in code. Perhaps a comparison of CPU times could be more useful then. Also, the programming language used `Matlab` is interpreted and generally slow. A compiled language like `C` could be considered in the future since it is faster and more extensible (for those intending to apply the model).

3.6 Results on the full model with measured air inlet temperature

3.6.1 Comparing measured with predicted air outlet temperature

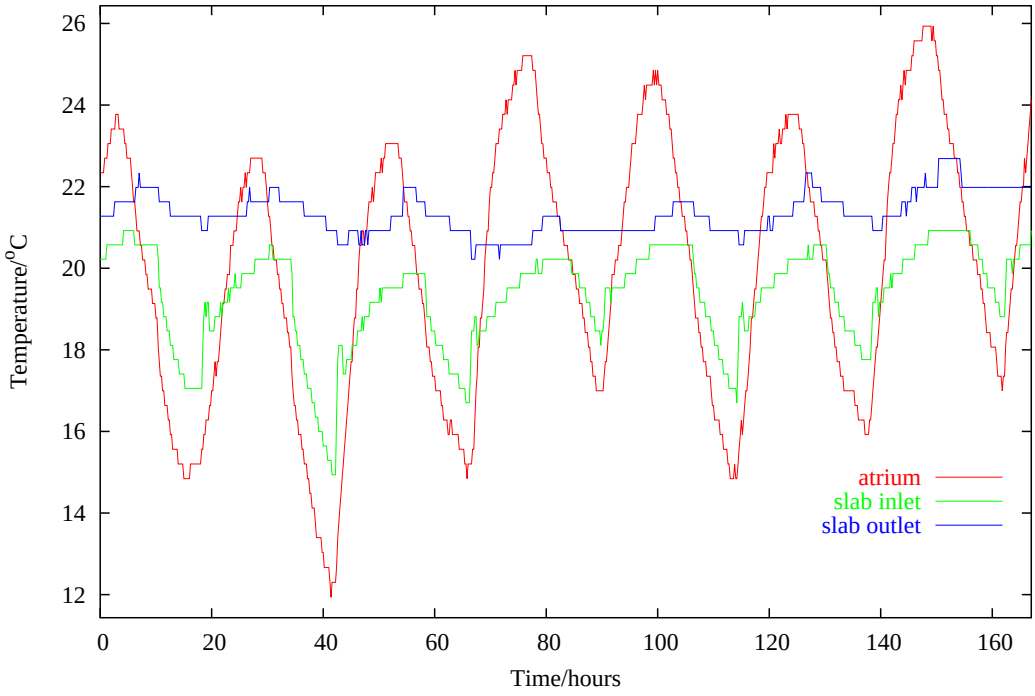

Figure 3.10: Effect of thermal mass between fans (in the atrium) and slab inlet on supply air cooling

In this section a comparison is made between measured and predicted air outlet temperatures. The transient response of a ventilated slab to a time-wise variation in air inlet temperature is considered. Use is made of measured air inlet temperature. Figure 3.10 shows the measured air temperature given by three three sensors at three different positions: the atrium temperature sensor is situated near the fans on the ground floor, the other two sensors are situated at the inlet and outlet of a slab on the fifth floor of the building. The model is local to the slab and it does not include the effect of the thermal mass between the atrium and the inlet to the slab. The bulk of heat transfer seems to occur between the atrium and the slab inlet as indicated in Figure 3.10 for a week of operating the slab. The figure shows the damping and the delay in the peaking of the supply air temperature between the fans in the atrium and the slab inlet.

Concrete	c_m	=	1000	$J/kg\,^oC$
	ρ_m	=	2400	kg/m^3
	k_m	=	1.4	$W/m\,^oC$
Air	c_f	=	1006	$J/kg\,^oC$
	ρ_f	=	1.177	kg/m^3
Other parameters	L	=	6	m
	d	=	0.15	m
	g	=	0.2	m
	ϵ'	=	0.94	
	σ	=	5.7×10^{-8}	$W/m\,^oC^4$
	T_{mean}	=	20	$^\circ$ C
	h_r	=	$\frac{4\sigma T_{mean}^3}{\frac{2}{\epsilon'} - 1}$	$W/m^2\,^\circ C$

Table 3.10: Input parameters

Table (3.10) shows values used for the basic input parameters to generate the results presented in this section.

The correlation between h_c and the air velocity v_f used, 3.20 is that recommended by Holmes and Wilson [19].

$$h_c = 16\frac{v_f^{0.8}}{g^{0.2}} \tag{3.20}$$

where

$$v_f = \begin{cases} 0.25\,m/s & \text{for low flow} \\ 1.1\,m/s & \text{for high flow} \\ 0.01\,m/s & \text{fan off} \end{cases}$$

The velocity repeats the same cycle every week and similarly the heat source to the ceiling slab. Figures 3.11 and 3.12 show the variation with time of the velocity and heat source profiles used for obtaining results in this section. The shown profiles are for a week beginning on a Friday at midnight and they clearly indicate (virtually) no air flow and no heat source during the weekend. A zero heat source corresponds to periods outside occupancy of the building.

Shown in Figure 3.13 is a comparison of measured with predicted outlet air temperature. Also shown is the air velocity to indicate how it affects the outlet air temperature. The heat source profile was left out for clarity but a profile corresponding to the air velocity can

be deduced from the weekly cycle of the heat source given in Figure 3.12. A time scale of two weeks was chosen to make sure that the numerical system has settled down since it was assumed that the ventilated slab is initially at a constant temperature throughout.

The predicted outlet air temperature underestimates the measured outlet air temperature. This could be due to the following limitations in the model:

- It is assumed that the carpet sitting on the floor slab provides insulation and hence there is no thermal interaction with room above.
- Thermal interaction with the room below the slab is modelled as a heat source. A value of $17.59\,W/m^2\,^\circ C$ was used during hours of occupancy. This was advised by the site engineer but was uncertain.

Also, an average air velocity v_f and hence constant h_c is assumed along the slab. This is not the case since air spreads sideways as it moves from the inlet of the slab to its outlet resulting in a variation of the velocity with the length of the slab.

There is a prolonged absence of forced air flow during the weekend since the fans are off then. This results in very little variation in the outlet air temperature. The predicted air outlet temperature does not pick up the decay in the air inlet temperature at these times.

One weekness of the comparison between predicted and measured data is that measured surface temperatures were not available to help identify discrepancies. The measured surface temperatures are essential in determining a reasonable value for h_c since convective heat transfer on the conrete-air interface is given by

$$q_c = h_c A\left(T_s - T_\infty\right) \Rightarrow h_c = \frac{q_c}{A\left(T_s - T_\infty\right)}$$

where T_s is the surface temperature and T_∞ is the air bulk temperature.

3.6.2 Sensitivity tests

Effect of heat source

Due to the uncertainty of the value used for the heat source to the slab from the room below, changes in the value used are considered. The objective is to investigate how sensitive the

numerical model is to these changes and whether or not the comparison given in section 3.6.1 improves. The heat source value of $17.59\,W/m^2\,°C$ was doubled and trebled as shown in Figure 3.14.

The results show that raising the heat source value raises the predicted outlet air temperature and brings it closer to the measured outlet air temperature. However, the swing of the predicted outlet temperature is increased and hence overestimated in the process. Trebling the heat source value is unreasonably high for a single source. Another possible heat source not included in the model is through the floor. This is assumed to be insulated but the floor will most probably receive heat through the carpert.

Effect of the convective heat transfer coefficient

When the fans are off the system is driven by free convection and a velocity of $0.01m/s$ was chosen at these times to try and account for the slight motion in the supply air. The correlation for h_c given by equation (3.20) gives a value of $h_c = 0.6\,W/m^2\,°C$. This value was thought to be too low and so it was increased to $4\,W/m^2\,°C$. The latter value seems reasonable as it is of the same order of magnitude as those suggested by other authors, for example [11] on page 24 indicates values of h_c for gases for natural convection in the range of about $5 - 50\,W/m^2\,°C$.

Now, for the standard specification for the numerical model the following should be noted:

- The fans are either
  - *on* and blowing the supply air at low and high velocities of $0.25m/s$ and $1.1m/s$ respectively, or
  - they are *off* and an air velocity of $0.01m/s$ is assumed.
- Convection is either
  - *forced* and h_c is given by 3.20 for both low and high air flow, or
  - it is *free* and $h_c = 4\,W/m^2\,°C$.

For the same velocity profile $v_f(t)$, two variations of the standard specification are introduced: the heat transfer coefficient profile $h_c(t)$ is either halved or doubled. Figure 3.15 gives a comparison of the outlet air temperature for the three different cases. The period of

operation of the slab is two weeks but, only about two days in the middle of the week are shown to get a closer look at the results.

The results show that:

- The higher the heat transfer coefficient the more the damping there is in the outlet air temperature. A higher h_c results in increased convective heat transfer on the slab - air interface and hence the supply air loses more heat to the slab.
- Increasing h_c also results in an increase in the phase change of the supply air temperature. Thus the peaking of the supply air temperature is delayed more by a bigger h_c.

While values of h_c were thought to be uncertain as indicated by the need to do sensitivity tests, experimental determination together with statistical analysis could improve the model. However, this involves working with surface temperatures and these were not available.

Effect of the air velocity when the fans are off

The value used for the air velocity when the fans are off, $v_{f_{free}} = 0.01m/s$ is very uncertain. It seems too low to pick up the decay in the supply air temperature during weekends. In this section slight changes in this value are made and their effect on the numerical model is considered. The heat transfer coefficient profile $h_c(t)$ is the same as for the standard specification for the numerical model and it is computed from equation (3.20) for both forced and free convection. During the periods when the fans are off two different values for the air velocity: $0.05m/s$ and $0.10m/s$ are used. Figure 3.16 shows the air outlet temperature for the three different cases. The slab was operated for a fortnight but, the figure only shows Saturday and Sunday to indicate the prolonged absence of forced air flow.

The results show the following.

- Increasing $v_{f_{free}}$ reduces the thermal resistance to heat flow in the supply air through the slab. This results indicate:
  - a closer match in the decay of the air outlet temperature between the predicted and measured values and,
  - the swing of the supply air temperature increases and gets the predicted closer to the measured values.

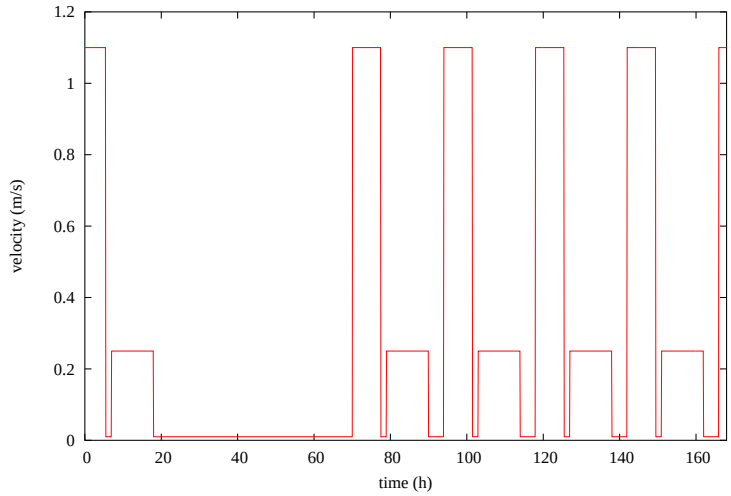

Figure 3.11: Weekly cycle (starting Friday at midnight) of the velocity profile for Eastgate

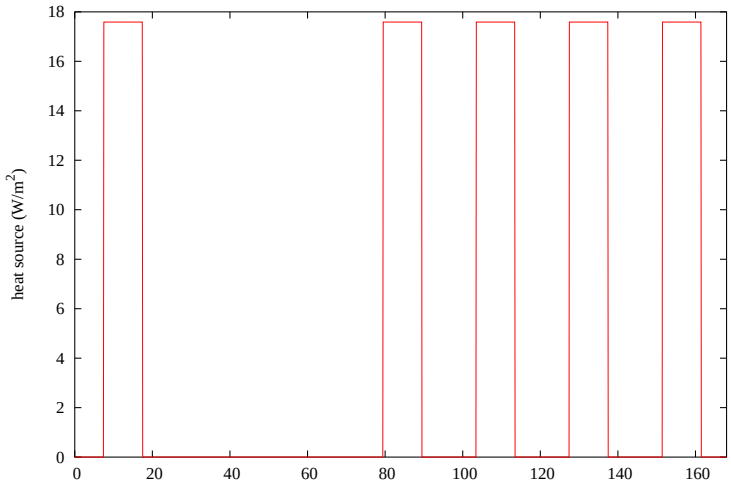

Figure 3.12: Weekly cycle (starting Friday at midnight) of the heat source profile for Eastgate

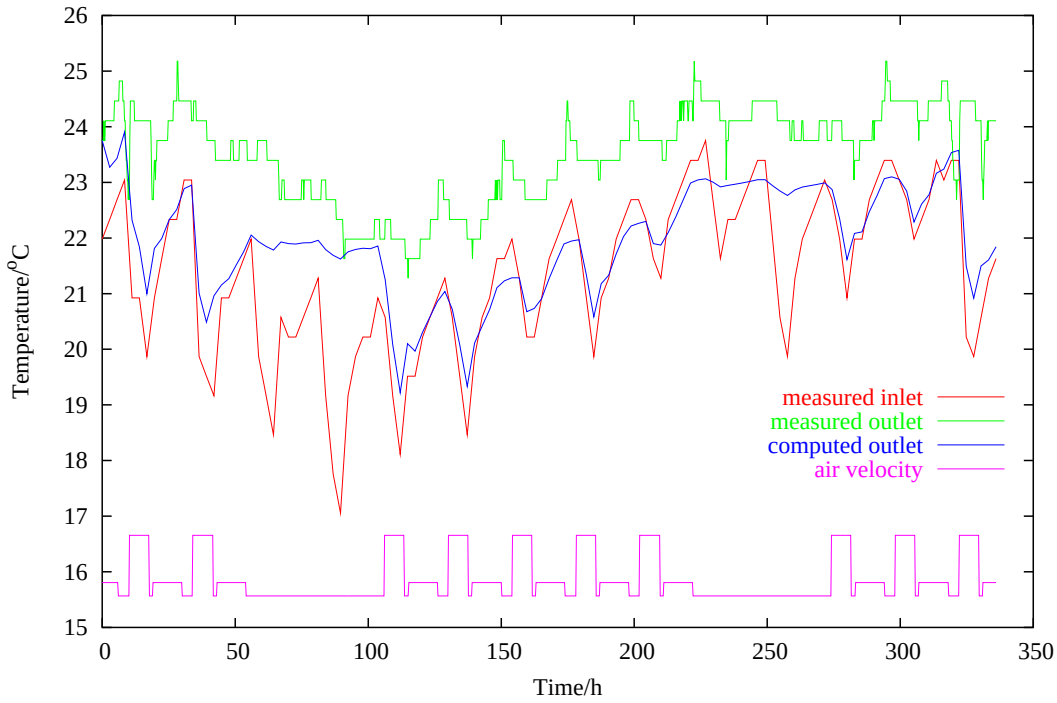

Figure 3.13: Comparing measured with predicted outlet air temperature for Eastgate

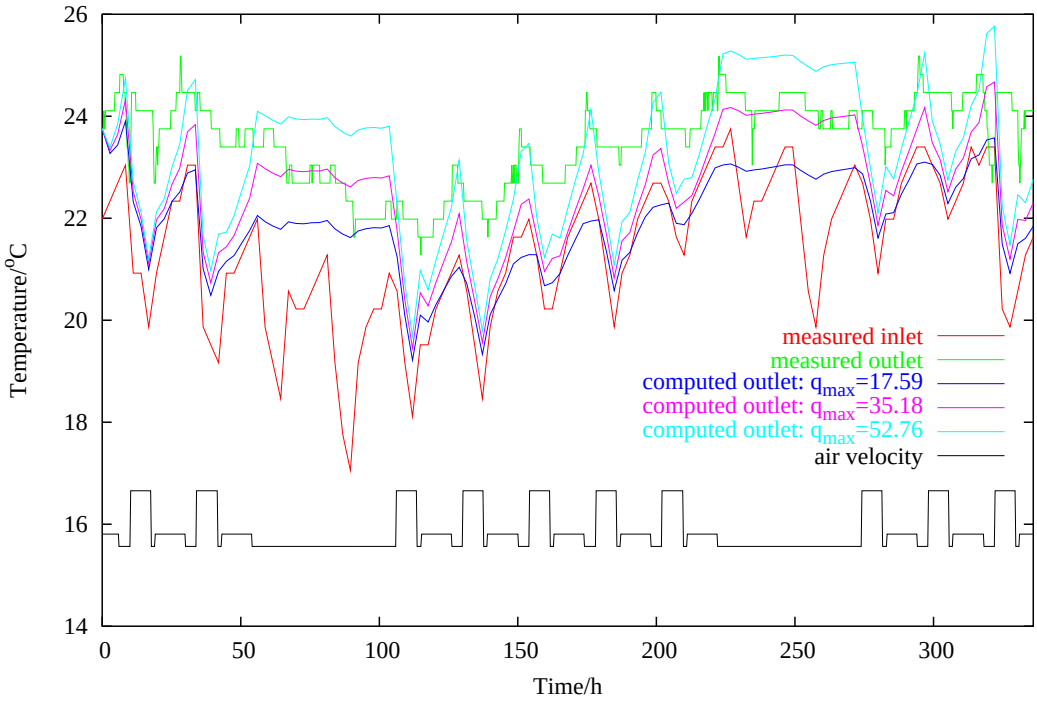

Figure 3.14: Sensitivity of numerical model to heat source

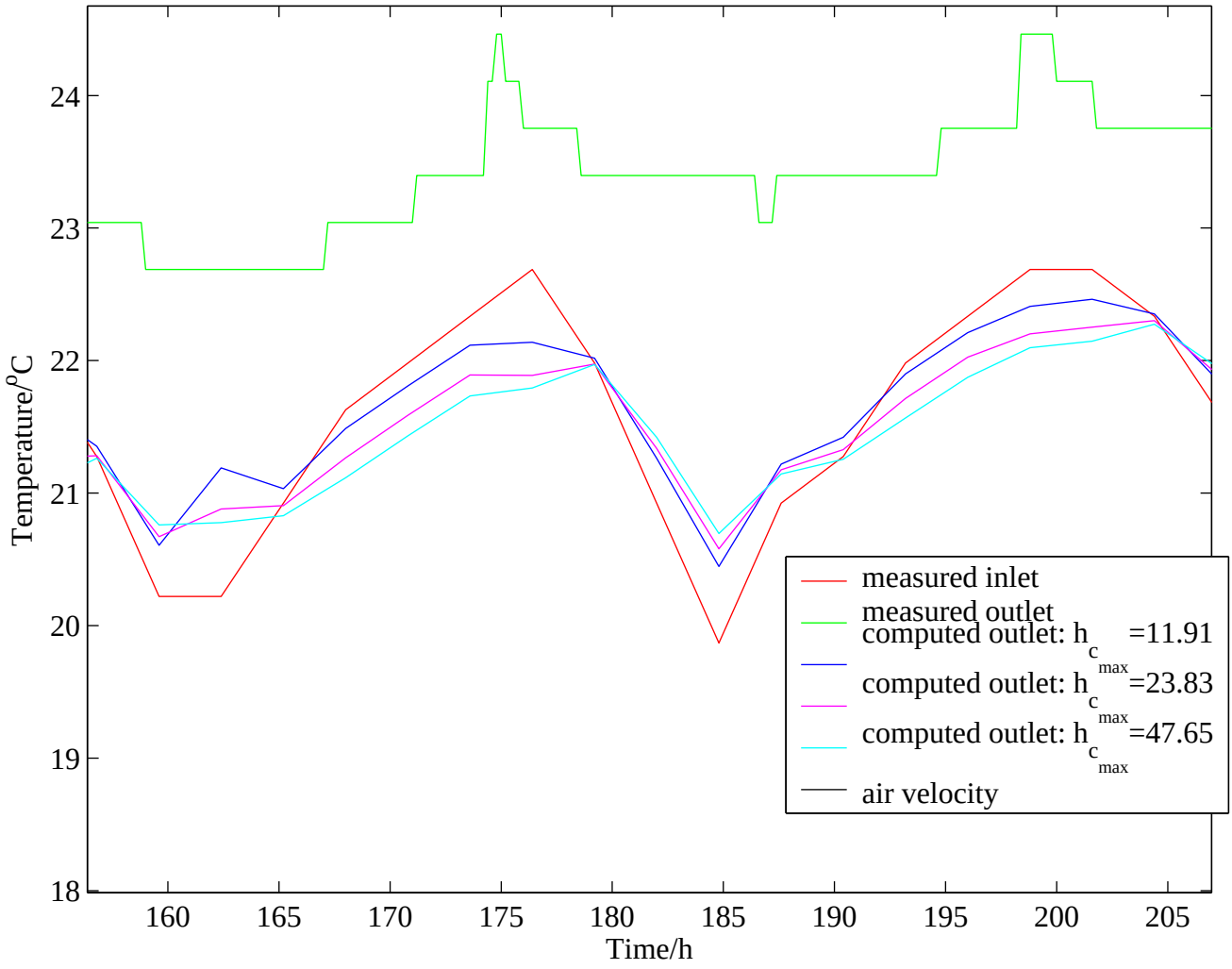

Figure 3.15: Sensitivity of numerical model to the convective heat transfer coefficient

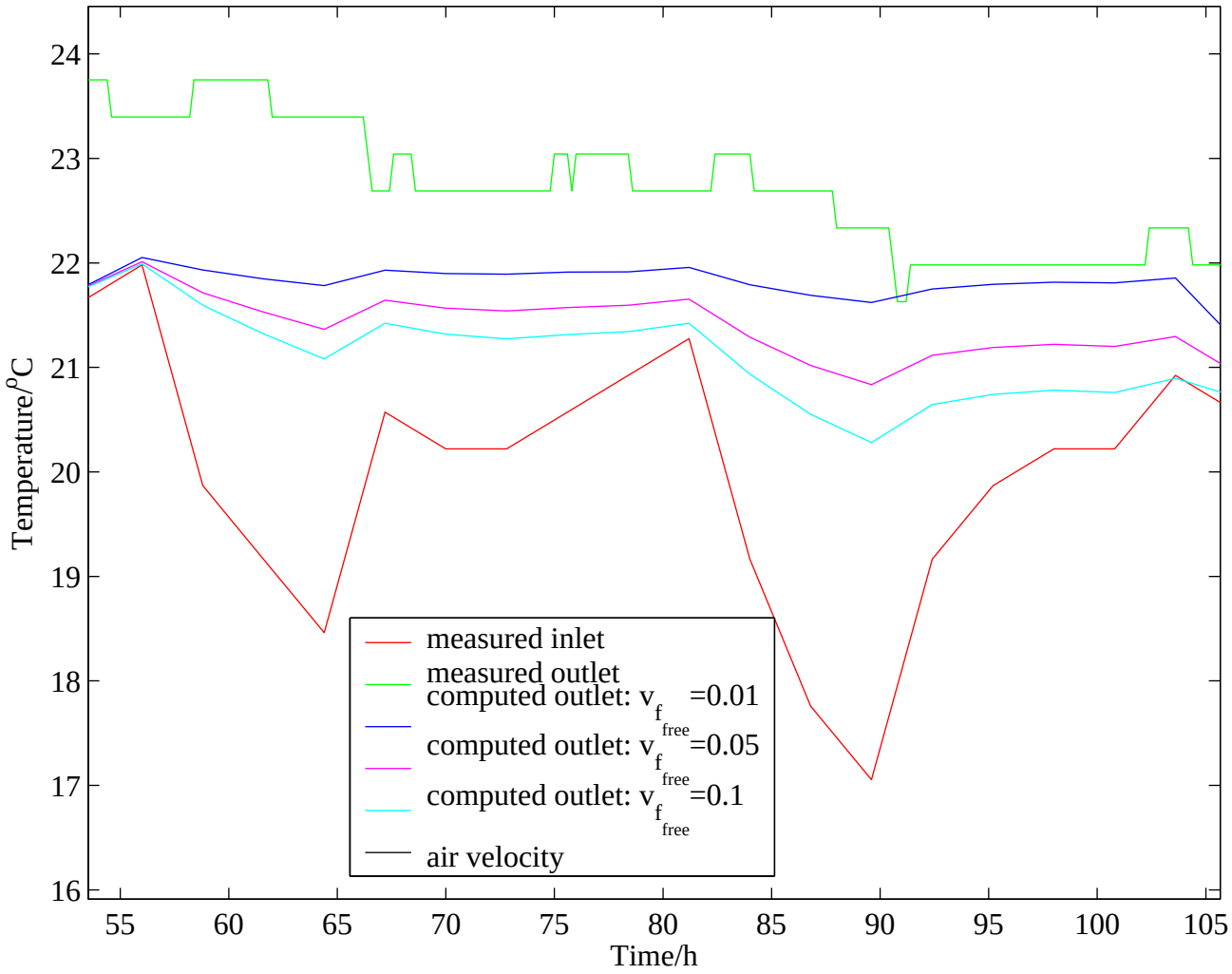

Figure 3.16: Sensitivity of numerical model to the air velocity when the fans are off

Chapter 4

On modelling space cooling with packed beds and Harare International School

4.1 Introduction

The problem considered here is that of mathematically modelling the transient response of a packed bed to a varying fluid inlet temperature. The bed is used as a thermal storage system to regulate temperature in the room space environment for a typical building design; Harare International School [25]. The energy transporting fluid and the energy storage medium are air and rock respectively. The results from the developed model are compared with measured data and the model is used to do a parametric study in chapter 5.

The method of solution uses a finite difference approximation for discretising space in the solid problem domain. A finite element approximation is used in the fluid problem domain. Time stepping is done by finite differences.

4.2 A general review of models for thermal storage in packed beds

4.2.1 Introduction

This section gives a review of models for thermal energy storage in packed beds. Perhaps the most important of these models is the Schumann model [30]. It is the first known model for thermal energy storage in packed beds. The other models are modifications in one way or another. It is for this reason that this benchmark model is presented in its own section.

The next two sections describe with examples single-phase and two-phase models. The former model assumes that the solid and fluid phases have the same temperature on any cross-section of the bed perpendicular to the direction of the fluid flow. This allows for a single energy equation to model heat transfer for both phases. The latter model allows for separation of the fluid and solid phases and derivation of an energy equation for each phase. The use of the phrase *two-phase model* is according to [12]. It indicates the use of two energy equations: each for the solid and the air, contrary to either two-phase heat transfer or change of state from solid to liquid.

The last section gives a few examples to highlight the current state of research on thermal energy storage in packed beds and their applications.

4.2.2 The benchmark model (Schumann)

The benchmark model for thermal energy storage in packed beds was done by Schumann in 1928. The following assumptions were made to derive the energy balance equations for both the storage material and the energy transporting fluid.

- Dispersion effects and intra-particle conduction are negligible.
- Thermal conductivity in the transverse direction is infinite and hence there is no temperature variation in this direction.
- There is zero thermal conductivity in the direction of flow.
- Wall containers are perfectly insulated.

- Physical and thermal properties are constant. This is valid for small temperature ranges.
- The convective heat transfer coefficient h_c is uniform.
- Fluid flow is one-dimensional and the velocity of the fluid is constant.
- The bed is initially at constant temperature.
- Radiation effects are negligible. This is reasonable for packed beds operating under moderate temperature conditions.
- Rate of accumulation of energy by the fluid in the bed is negligible. This is true for most practical purposes, see page 18 of [29]. Furthermore, according to Adebiyi [2], this is true provided the thermal capacity of the fluid is much smaller than that of the bed material. That is

$$\frac{\varepsilon \rho_f c_f}{(1-\varepsilon)\rho_m c_m} \ll 1 \tag{4.1}$$

- There is no internal heat generation.
- There is no mass transfer. What flows into the bed flows out of it. Generally, mass transfer tends to increase the thermal storage capacity of the solid material. However, there is experimental evidence that the absorbing nature of solid materials like gravel does not significantly improve the performance of the packed bed system hence mass transfer is neglected [15].

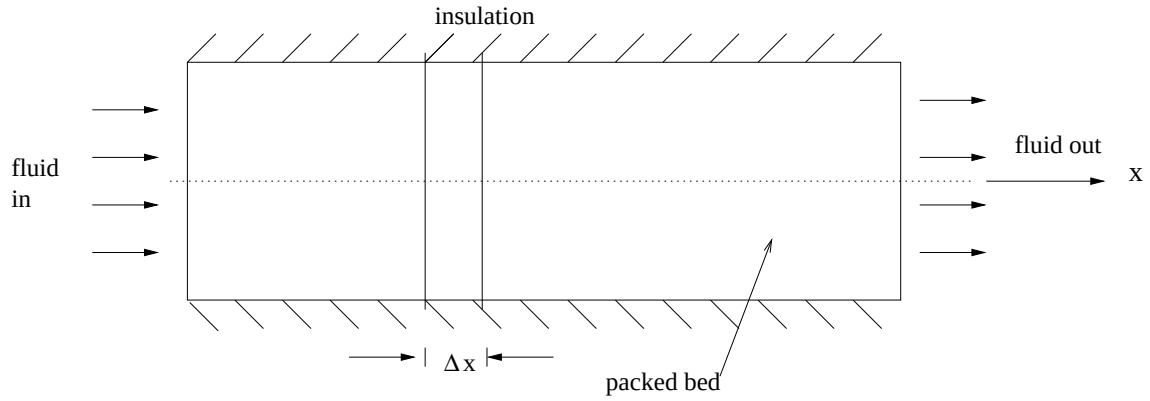

Figure 4.1: Control volume

By doing an energy balance on a control volume across the bed (see Figure 4.1), the following equations can be derived for the fluid and the solid material respectively [29] for $0 < x \leq L$ and $t > 0$.

In the fluid

$$\dot{m}_f c_f L \frac{\partial T_f}{\partial x} = h_c A \left(T_m - T_f\right)$$

and in the solid

$$S_{fr}(1-\varepsilon) L \rho_m c_m \frac{\partial T_m}{\partial t} = h_c A \left(T_f - T_m\right). \tag{4.2}$$

For this and subsequent notation in this chapter see the nomenclature (Appendix B). Dimensionless distance, time and temperature are introduced.

$$\xi = \frac{h_c A x}{\dot{m}_f c_f L},\ \tau = \frac{h_c A t}{S_{fr}(1-\varepsilon) L \rho_m c_m},\ \theta_f = \frac{T_f - T_0}{T_{fi} - T_0} \text{ and } \theta_m = \frac{T_m - T_0}{T_{fi} - T_0}.$$

Consequently, the energy equations for the fluid and the solid respectively assume the following form.

$$\begin{aligned} \frac{\partial \theta_f}{\partial \xi} &= \theta_m - \theta_f \\ \frac{\partial \theta_m}{\partial \tau} &= \theta_f - \theta_m \end{aligned} \tag{4.3}$$

where

$$0 < \xi \leq 1 \text{ and } \tau > 0$$

The bed is initially at a constant temperature throughout and it suddenly experiences a step change in the fluid inlet temperature. This mode of operation is called single-blow [29] and the associated boundary condition is

$$\text{at } \xi = 0,\ \theta_f = 1,$$

and the initial condition is

$$\text{at } \tau = 0,\ \theta_m = 0.$$

It follows from these two conditions and the energy equation for the bed material that

$$\text{at } \xi = 0,\ \theta_m = 1 - e^{-\tau}$$

Schumann transformed the energy equations (4.3) into a special case of the the *Bessel* differential equation and derived an analytic solution to this problem in the form of infinite series for the case of a semi-infinite bed. The solution follows.

$$\begin{aligned}
\theta_m(\xi,\tau) &= 1 - e^{-(\tau+\xi)} \sum_{n=0}^{\infty} \xi^n M_0^{(n)}(\xi\tau) \\
\theta_f(\xi,\tau) &= 1 - e^{-(\tau+\xi)} \sum_{n=1}^{\infty} \xi^n M_0^{(n)}(\xi\tau) \\
\text{where } M_0(\xi\tau) &= J_0(2i\sqrt{\xi\tau}) \text{ and } M_0^{(n)}(\zeta) = \frac{d^n M_0(\zeta)}{d\zeta^n};\ i = \sqrt{-1}
\end{aligned}$$

J_0 is the Bessel function of the first kind and of order 0. For a detailed derivation of this solution see [29].

4.2.3 Single-phase models

Negligible thermal resistance model

Contrary to the Schumann model, it is assumed here that there is intra-particle conduction. Furthermore, if both the thermal conductivity of the bed material k_m and the convective heat transfer coefficient h_c are assumed to be large, thermal resistance to heat transfer between the bed material and the fluid is negligible. A sufficiently large k_m ensures negligible internal thermal resistance and similarly a sufficiently large h_c ensures negligible surface thermal resistance. This follows from the following formulae for thermal resistance to internal thermal conduction and to heat transfer at the surface of contact respectively:

$$R_{internal} = \frac{L}{k_m A},\ R_{surface} = \frac{1}{h_c A}\,.$$

The consequence is that the fluid and bed temperatures are equal on any cross-section of the bed perpendicular to the direction of flow. Hence only one energy equation is needed for heat transfer in the packed bed. The rest of the assumptions are the same as those for the Schumann model.

Since the net accumulation of energy in the bed material must equal the energy lost by the fluid through the bed together with the energy transferred from the surface to the interior

of the bed material, the energy equation is

$$v_f \rho_f c_f \frac{\partial T}{\partial x} + \rho_m c_m (1-\varepsilon)\frac{\partial T}{\partial t} = k_m \frac{\partial^2 T}{\partial x^2}$$

The boundary condition at the bed's inlet is of *Danckwert* type [27] and, at distances sufficiently large from the inlet it is assumed that temperature gradients vanish:

$$\begin{aligned} \text{at } x = 0,\ -k_m \frac{\partial T}{\partial x} &= v_f \rho_f c_f (T_{fi} - T) \\ \frac{\partial T}{\partial x} &\rightarrow 0 \text{ as } x \rightarrow \infty \end{aligned}$$

If the following non-dimensional quantities are introduced,

$$\xi = \frac{v_f \rho_f c_f x}{k_m},\ \theta = \frac{T - T_0}{T_{fi} - T_0},\ \tau = \frac{(v_f \rho_f c_f)^2 t}{k_m \rho_m c_m (1-\varepsilon)}$$

the mathematical model may be written as follows

$$\frac{\partial \theta}{\partial \xi} + \frac{\partial \theta}{\partial \tau} = \frac{\partial^2 \theta}{\partial \xi^2}$$

with boundary conditions

$$\begin{aligned} \text{at } \xi = 0,\ \frac{\partial \theta}{\partial \xi} &= \theta - \theta_{fi} \\ \frac{\partial \theta}{\partial \xi} &\rightarrow 0 \text{ as } \xi \rightarrow \infty \end{aligned}$$

An analytic solution to this problem, obtained by the use of *Laplace transforms* was presented by Riaz [27] as

$$\begin{aligned} \theta(\xi,\tau) &= \frac{1}{2}\text{erfc}\left(\frac{\xi - \tau}{2\sqrt{\tau}}\right) + \sqrt{\frac{\tau}{\pi}}\exp\left[\frac{-(\xi-\tau)^2}{4\tau}\right] \\ &\quad -\frac{1}{2}(1 + \xi + \tau)\exp(\xi)\text{erfc}\left[\frac{\xi + \tau}{2\sqrt{\tau}}\right] \end{aligned}$$

Infinite NTU model

Let the non-dimensional distance and time for the Schumann model be re-defined as follows

$$\xi = \frac{x}{L},\ \tau = \frac{\dot{m}_f c_f t}{S_{fr}\rho_m c_m (1-\varepsilon) L}\,.$$

The volumetric heat transfer coefficient h_v is defined in terms of h_c by the following relation.

$$h_v = \frac{h_c A}{L\, S_{fr}}\,.$$

If we introduce the number of transfer units NTU which is defined as

$$NTU = \frac{h_v S_{fr} L}{\dot{m}_f c_f}\,,$$

and add a term that accounts for the heat loss from the fluid to the environment, then the energy equations for the Schumann model (4.2) assume the following form.

$$\begin{aligned} \frac{\partial \theta_f}{\partial \xi} &= NTU(\theta_m - \theta_f) + \frac{U\,P\,L}{\dot{m}_f c_f}(\theta_{env} - \theta) \\ \frac{\partial \theta_m}{\partial \tau} &= NTU(\theta_f - \theta_m) \end{aligned} \tag{4.4}$$

where $\dfrac{U\,P\,L}{\dot{m}_f c_f}(\theta_{env} - \theta_f)$ represents energy loss to the environment. It follows from equations (4.4) that

$$\theta_f \equiv \theta_s \sim \theta \tag{4.5}$$

is the limiting case for an infinitely large NTU (this is the case for infinitely large h_v). If these equations are added and we use identity (4.5), the following is obtained as the energy equation for the infinite NTU model [12].

$$\frac{\partial \theta}{\partial \tau} + \frac{\partial \theta}{\partial \xi} = \frac{U\,P\,L}{\dot{m}_f c_f}(\theta_{env} - \theta),\ \theta = \theta(\xi, \tau) \tag{4.6}$$

Appropriate initial and boundary conditions for a particular physical setup should be prescribed. For a packed bed operating in single-blow mode these are $\theta(\xi, \tau = 0) = 0$ and $\theta(\xi = 0, \tau) = 1$. θ_{env} is a given function of time.

4.2.4 Two-phase models

Modified Schumann model

Energy balance equations for the Schumann model, equations (4.4) may be modified to include

- the effect of large Biot numbers Bi hence accounting for large temperature gradients in the solid particles,

- the effect of large Peclet numbers Pe hence accounting for axial conduction and dispersion.

Bi represents the ratio of internal thermal resistance to surface thermal resistance. The closer it is to zero the smaller the temperature gradients in the solid material. It is given by the following formula

$$Bi = \frac{h_c L_c}{k} .$$

Pe is proportional to the ratio of the bulk heat transfer to conductive heat transfer. It is given by the following formula [30]

$$Pe = \frac{(\rho_f c_f v_f)^2 S_{fr} L \varepsilon}{k_f A} .$$

To include the effects of large Bi and large Pe the modified NTU, NTU_c, a quantity which depends on the volumetric heat transfer coefficient h_v is introduced. NTU_c is related to NTU by the following formula [12].

$$\frac{1}{NTU_c} = \frac{D}{L\ Pe} + \frac{1 + 0.2Bi}{NTU} \tag{4.7}$$

The energy equations for the modified Schumann model [12] are:

$$\begin{aligned} \frac{\partial \theta_f}{\partial \xi} &= NTU_c(\theta_m - \theta_f) + \frac{U\ P\ L}{\dot{m}_f c_f}(\theta_{env} - \theta_f) \\ \frac{\partial \theta_m}{\partial \tau} &= NTU_c(\theta_f - \theta_m) . \end{aligned} \tag{4.8}$$

Intra-particle conduction and dispersion model

In this model both the effect of intra-particle conduction and dispersion on the performance of the packed bed are taken into account. Provided the thermal capacity of the fluid is negligible compared to that of the solid, the energy equations for solid particles of spherical shape and the energy transporting fluid are as follows [30]

fluid:

$$0 = -\dot{m}_f c_f \frac{\partial T_f}{\partial x} + k_f S_{fr} \varepsilon \frac{\partial^2 T_f}{\partial x^2} + \frac{h_c A}{L}(T_{m_s} - T_f)$$

solid:

$$\rho_m c_m \frac{\partial T_m}{\partial t} = k_m \frac{1}{r^2} \frac{\partial}{\partial r}\left(r^2 \frac{\partial T_m}{\partial r}\right)$$

with a convective heat transfer boundary condition on the surface of a sphere and an additional boundary condition at the centre (zero first order derivative of the solid material temperature):

$$\begin{aligned} -k_m \frac{\partial T_m}{\partial r} &= h_c(T_{m_s} - T_f) \text{ when } r = R \\ \frac{\partial T_m}{\partial r} &= 0 \text{ when } r = 0 \end{aligned}$$

where

$$T_{m_s}(x,t) = T_m(r = R, x, t) \text{ and } T_f = T_f(x,t).$$

4.2.5 Some recent studies

In 1996, Al-nimr *et al.* [6] developed an analytical model that predicts the dynamic response of a packed bed (cylindrical) column to a variable inlet fluid temperature. The energy equation for the fluid includes heat loss to the environment:

$$\varepsilon \rho_f c_f S_{fr} L \frac{\partial T_f}{\partial t} + G c_f S_{fr} L \frac{\partial T_f}{\partial z} = h_v S_{fr} L(T_m - T_f) + U\, P\, L(T_{env} - T_f) \qquad (4.9)$$

where $G = \dfrac{\dot{m}_f}{S_{fr}}$ and the energy equation for the solid is

$$(1-\varepsilon)\rho_m c_m S_{fr} L \frac{\partial T_m}{\partial t} = h_v S_{fr} L (T_f - T_m)\,. \tag{4.10}$$

By introducing the following dimensionless quantities

$$\theta_f = \frac{T_f - T_{env}}{T_{fi} - T_{env}},\ \theta_m = \frac{T_m - T_{env}}{T_{fi} - T_{env}}, \tau = \frac{h_v t}{\rho_f c_f \varepsilon},\ Z = \frac{h_v z}{G c_f}$$

the energy equations for the solid and the fluid phases assume the following forms.

$$\frac{\partial \theta_f}{\partial \tau} + \frac{\partial \theta_f}{\partial Z} + (1 + M_1)\theta_f + \theta_m = 0 \tag{4.11}$$

$$\frac{\partial \theta_m}{\partial \tau} - M_2(\theta_f - \theta_m) = 0 \tag{4.12}$$

where

$$M_1 = \frac{UP}{h_v S_{fr}} \text{ and } M_2 = \frac{\rho_f c_f \varepsilon}{\rho_m c_m (1-\varepsilon)}\,.$$

The problem considered in this paper is of heat transfer (in the packed bed column) governed by equations (4.11) and (4.12) subject to a constant temperature profile at initial instant and a given temperature of the fluid at the inlet. A solution to this problem was developed using Laplace transforms. The predicted results were validated against experimental results.

In 1998, Ziada and Abdel Rehim [36] presented a thermal analysis of energy storage in a cylindrical packed bed made up of three layers of different materials, equal in length, that are used as thermal energy storage media with air as the energy transporting medium. The bed is packed with spheres of equal diameter. For a schematic view of the bed considered see Figure (4.2). In this study, the thermal behaviour of the bed is described by a *transient* one-dimensional model. The model allows for the energy equations to be derived separately for the air and bed material. The energy equation for air is 4.9 without the heat loss term and, the energy equation for the bed material is

$$(1-\varepsilon)\rho_m c_m \frac{\partial T_m}{\partial t} = \frac{\partial}{\partial z}\left(k_m \frac{\partial T_m}{\partial z}\right) + h_v (T_f - T_m)\,,\ 0 < z < L,\ t \geq 0 \tag{4.13}$$

The last term on the right hand side of equation (4.13) represents the thermal interaction between the air and the bed material. Thermal dispersion is neglected and air flows in the

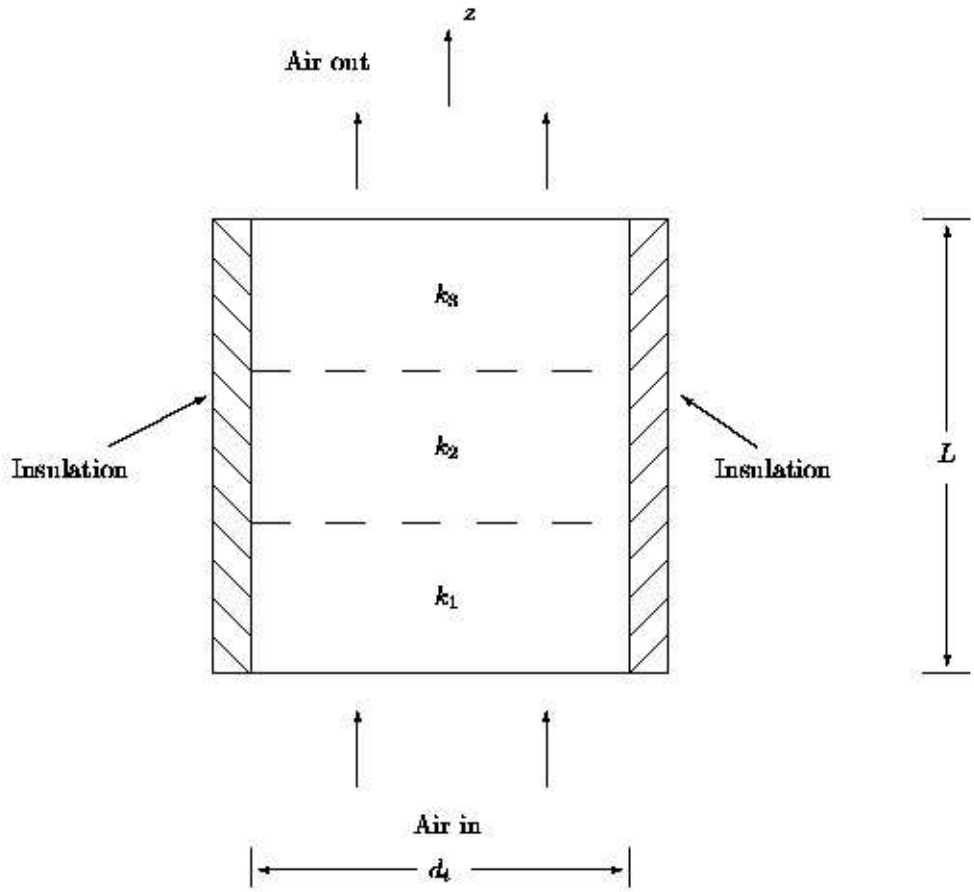

Figure 4.2: Multi-layer cylindrical packed bed

axial direction. At initial instant, the temperature throughout the bed is T_0 except at the inlet where it is the same as the fluid temperature there, that is T_{fi}.

It was intended in this model to find $T_f(z,t)$ and $T_m(z,t)$ subject to the following boundary conditions for all times $t \geq 0$:

$$\begin{aligned} T_f(0,t) &= T_{fi} \\ (1-\varepsilon)\rho_{m_1} c_{m_1} \frac{\partial T_m(0,t)}{\partial t} &= k_1 \frac{\partial^2 T_m(0,t)}{\partial z^2} + h_v(T_{fi} - T_m(0,t)) \end{aligned}$$

and

$$(1-\varepsilon)\rho_{m_3}c_{m_3}\frac{\partial T_m(L,t)}{\partial t} = k_3\frac{\partial^2 T_m(L,t)}{\partial z^2} + h_v(T_f(L,t) - T_m(L,t))$$

k_1, k_2 and k_3 are thermal conductivities of the first, second and third layers in the bed respectively and similarly for the storage material densities and heat capacities. The numerical solution considered in this model uses an upwind finite difference scheme to approximate the space derivative appearing in the energy equation for the air to ensure stability [22, 36]. Central differencing is used to approximate the space derivative that appears in the energy balance for the storage material and, marching in time uses an implicit difference scheme. Using this mathematical model Ziada and Abdel Rehim could predict

- the transient one-dimensional temperature distribution in the bed,
- variation of this temperature distribution with time,
- variation of energy stored in the bed material with time and,
- variation of storage capacities for various groups of layers with time.

In 2004, Zarrinehkafsh and Sadrameli [35] presented a numerical model for heat transfer in a fixed bed regenerative heat exchanger that is used for flue gas heat recovery. Although the application of packed beds considered is different, the same thermal analysis is applicable to the use of packed beds for space cooling as considered in this work. In the model of Zarrinehkafsh and Sadrameli, the following assumptions made for the mathematical model differ from those for the work presented in this thesis.

- The heat transfer coefficient h_c is constant during each of the charging (heating) and discharging (cooling) periods.
- The fluid mass flow rate $\dot{m}_f$ is constant.
- There is no fluid heat dispersion.
- There is no heat loss to the environment.

The thermal storage unit considered by Zarrinehkafsh and Sadrameli is made up of spheres of ceramic material to withstand the high operating temperature conditions, typically around 1400° C. Their mathematical model has the same energy equations for the both the fluid

and the solid phases as that used in analysing the cooling example which follows in the next sections except that the terms for heat loss to the environment and fluid dispersion are added. Also, the mass flow rate is assumed to vary with time in a step-wise manner.

4.3 Space cooling at Harare International School

Figure 4.3: Aerial view: (H. I. S)

Harare International School (H. I. S) is situated in Harare, the capital city of Zimbabwe with a temperate climate and experiences temperatures as high as 33° C in the summer and as low as 3° C in the winter. The school hosts 400 pupils from about 50 countries around the world.

The basic operation of space (room environment) cooling at the school is in two parts [25]:

- supply air cooling is done by using rock-store compartments, and
- exhaust air is extracted by wind driven fans that are mounted on the roofs of the buildings. See Figure (4.3) for an aerial view of the school.

The first implementation of rock-store cooling was on a part of the school, the Middle School. A typical compartment for the Middle School is divided into two units by a wall as shown in Figure (4.4). Each compartment lies beneath a veranda in front of a classroom as shown

Figure 4.4: Rock-store compartments during construction of the Middle School

in the same Figure. A unit in the rock-store compartment is packed with granite rocks and shall be referred to as a packed bed unit. The energy transporting fluid is air and the rocks in the bed act as the storage material.

Figure (4.5) shows the path taken by the air as it is drawn from the outside. It is blown by fans, one for each packed unit, via ducts which are surrounded by concrete walls. It enters a packed bed unit on one end and leaves at the other end before it enters a classroom as part of a displacement ventilation system.

The air is forced through the two units in a compartment depending on which fan is acting and the time of the day. The fan operation is either in auto or test mode. The test mode was provided for helping with experiments and monitoring of the system. Since the system normally operates in auto mode, only this mode shall be considered in the thesis. In the auto mode, a specific fan timing scheme is followed which is described in detail in chapter 5.

To monitor the cooling system at the school, a data logger connected to at least five sensors was set up. The sensors measure air temperature at different positions in the flow path, namely

- outside,
- entrance to the morning unit,
- entrance to the afternoon unit,

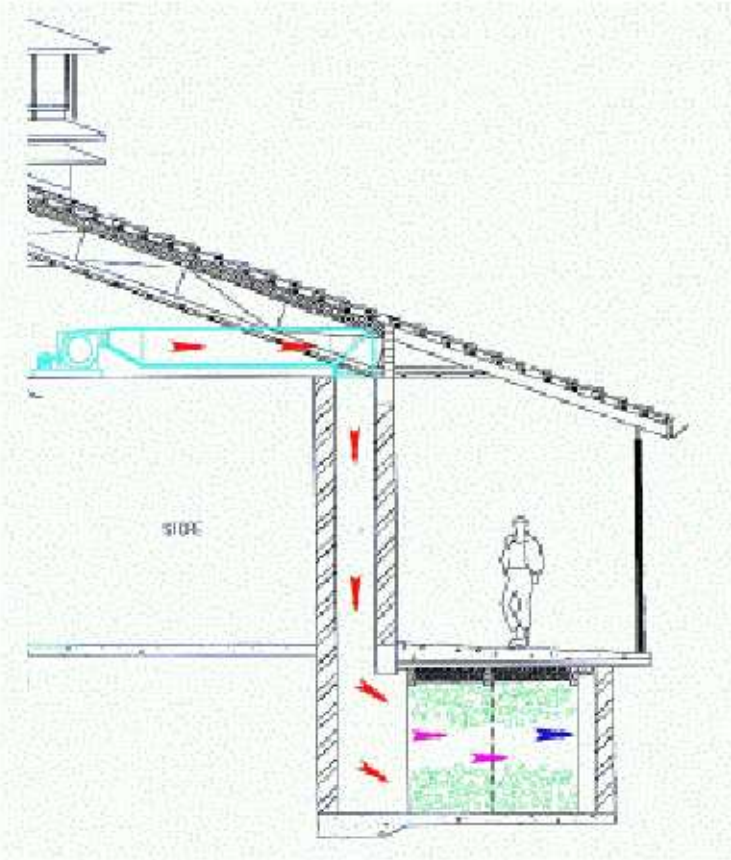

Figure 4.5: Air flow path

- exit from the rock-store compartment, and

- classroom.

The model presented in this thesis is a mathematical representation of heat transfer in each of the morning and afternoon packed bed units for the Middle School. It predicts the transient response of each unit separately, to a time-wise varying fluid inlet temperature.

4.4 A mathematical model

4.4.1 Assumptions

The underlying assumptions for the mathematical model are basically the same as for the Schumann model with the following differences.

- There is a step-wise change in the fluid flow rate. Fans blowing air through the bed are either on or off at given times of the day. It is during each of these periods that the fluid flow rate is constant: $0\,m^3/s$ for no flow and $0.6\,m^3/s$ otherwise.
- Each rock is a sphere of fixed radius R.
- Thermal conduction between neighbouring rocks is neglected. This is reasonable since the area of contact is much smaller than the surface area of a typical rock.
- The model includes the effect of fluid heat dispersion (axial conduction), intra-particle conduction and heat loss to the ground (environment). Since the ground could provide a significant amount of thermal mass and hence contribute a significant amount of thermal storage to a neighbouring packed bed unit, it is reasonable to take thermal interaction with the ground (ground coupling) into account.

4.4.2 Problem description

The problem is to find $T_m(r, x, t)$, the bed material temperature satisfying the one-dimensional parabolic diffusion equation (4.14) for $0 \leq x \leq L$,

$$\rho_m c_m \frac{\partial T_m}{\partial t} = k_m \frac{1}{r^2} \frac{\partial}{\partial r} \left(r^2 \frac{\partial T_m}{\partial r} \right),\ 0 < r < R,\ t > 0, \tag{4.14}$$

with boundary conditions:

$$-k_m \frac{\partial T_m}{\partial r}(r = R, x, t) = h_c(T_{m_s}(x, t) - T_f(x, t)),\ t > 0, \tag{4.15}$$

$$\frac{\partial T_m}{\partial r}(r = 0, x, t) = 0,\ t > 0, \tag{4.16}$$

and initial conditions:

$$T_{m_s}(x, t = 0) = T_m(r, x, t = 0) = T_o,\ 0 < x < L,\ 0 < r < R \tag{4.17}$$

and to find $T_f(x, t)$, the fluid temperature satisfying

$$\dot{m}_f c_f L \frac{\partial T_f}{\partial x} = k_f S_{fr} \epsilon L \frac{\partial^2 T_f}{\partial x^2} + h_c A \left(T_{m_s} - T_f\right) + U\, P\, L \left(T_{env} - T_f\right),\ t > 0, \tag{4.18}$$

subject to the boundary conditions:

$$T_f(x = 0, t) = T_{fi}(t),\ t \geq 0, \tag{4.19}$$

and

$$\frac{\partial T_f}{\partial x}(x = L, t) = 0,\ t \geq 0. \tag{4.20}$$

Equations (4.14) through (4.20) constitute a mathematical model for the problem. Note that since equation (4.18) is stationary, no initial condition is required for the fluid energy equation. However, the fluid temperature depends on the environment and solid temperatures at initial instant. These are assumed to be constant then. Consequently, it may be reasonable to assume a uniform fluid temperature at initial instant. This is common practise and simplifies the coding of the numerical solution.

The term on the left hand side of equation (4.18) represents an energy rate associated with the motion of the fluid through the bed. On the right hand side, the first term represents fluid heat dispersion and, the second and third terms represent convective heat transfer on the fluid-solid interface and, thermal interaction with the environment respectively. If heat loss to the environment is neglected in the energy equation for the fluid, the resulting form is as given in [29] on page 291. It is worth noting that only simplified versions of this equation without the heat loss to the environment term are solved by other authors as indicated on page 292 of [29]. Recent studies exist on similar energy equations. For example, in 2004 Rupali Shukla *et. al* [32] considered heat and fluid flow in a packed bed of spheres. Although fluid flow analysis is more thorough, the model considered here in this thesis is sufficient to give a good understanding of how the supply air conditioning system at the Harare International School works, and to explore ways of improving it as shown later in the chapter on results. Also, the model is simpler, and contrary to [32] it includes ground coupling to account for the extra thermal mass provided by the surrounding ground.

Another recent study is that by Zarrinehkafsh and Sadrameli in 2004, [35]. This study does not also include ground coupling. Furthermore, these studies have different applications of packed beds to the one considered in this thesis: supply air conditioning. For example, the application for [35] is flue gas heat recovery, and that for [32] is food processing.

4.5 Solution by a finite element - finite difference numerical scheme

4.5.1 Introduction

The finite element method has several advantages over the finite difference method. These include a better ability to handle general boundary conditions, complex geometries, variable or non-linear material properties and the ease with which general purpose software may be created. The finite element method shall be used for the fluid problem domain and in the solid problem domain we shall use a finite difference method.

A change of notation is introduced for the sake of clarity. $v(x,t)$ and $u(r,x,t)$ are substituted for the fluid and solid temperatures $T_f(x,t)$ and $T_m(r,x,t)$ respectively. Consequently, the solid surface temperature becomes $u_s(x,t) = u(r = R, x, t)$. Also, $v_{env}(x,t)$ shall substituted for the ground temperature $T_{env}(x,t)$.

4.5.2 Formulation of the problem for the fluid problem domain

Differential form

The problem is to find $v(x,t)$ satisfying

$$\dot{m}_f c_f L \frac{\partial v}{\partial x} = k_f S_{fr} \epsilon L \frac{\partial^2 v}{\partial x^2} + h_c A\,(u_s - v) + U\,P\,L\,(v_{env} - v),\ 0 < x < L$$

subject to the boundary conditions:

$$v(x = 0, t) = v_i(t),\ t \geq 0,$$

and

$$\frac{\partial v}{\partial x}(x = L, t) = 0,\ t \geq 0,$$

and initial condition:

$$v(x, t = 0) = v_o,\ 0 < x \leq L.$$

Integral form

If we form the residual for a trial function $v(x,t)$ such that $v(x = 0, t) = v_i(t)$

$$S(x,t) = \dot{m}_f c_f L \frac{\partial v(x,t)}{\partial x} - k_f S_{fr} \epsilon L \frac{\partial^2 v(x,t)}{\partial x^2} - h_c A \left(u_s(x,t) - v(x,t)\right) - U\ P\ L \left(v_{env}(x,t) - v(x,t)\right)$$

then

$$\int_0^L z(x) S(x,t) dx = 0$$

or

$$\int_0^L z \left(\dot{m}_f c_f L \frac{\partial v}{\partial x} - k_f S_{fr} \epsilon L \frac{\partial^2 v}{\partial x^2} - h_c A \left(u_s - v\right) - U\ P\ L \left(v_{env} - v\right) \right) dx = 0 \tag{4.21}$$

for all weighting functions $z(x)$ such that $z(x = 0) = 0$.

The use of integration by parts in the second part of the integral in equation (4.21) together with the boundary condition at $x = L$, and that $z(x = 0) = 0$ gives the following:

$$\begin{aligned} \int_0^L -k_f S_{fr} \epsilon L\, z \frac{\partial^2 v}{\partial x^2}\, dx &= \left[-k_f S_{fr} \epsilon L\, z \frac{\partial v}{\partial x} \right]_{x=0}^{x=L} + \int_0^L k_f S_{fr} \epsilon L\, z' \frac{\partial v}{\partial x}\, dx \\ &= \int_0^L k_f S_{fr} \epsilon L\, z' \frac{\partial v}{\partial x}\, dx \end{aligned}$$

which if substituted in equation (4.21) yields the following:

$$\int_0^L \left(\dot{m}_f c_f L\, z \frac{\partial v}{\partial x} + k_f S_{fr} \epsilon L\, z' \frac{\partial v}{\partial x} - h_c A\, z \left(u_s - v\right) - U\ P\ L\, z \left(v_{env} - v\right) \right) dx = 0 \tag{4.22}$$

Finally, the integral form of the problem is to find $v(x,t)$ satisfying equation (4.22) for all weighting functions $z(x)$ such that $z(x=0)=0$.

4.5.3 Discretisation in space for the fluid problem domain

If the solution space for $v(x,t)$ is spanned by the basis $\{\psi_1, \psi_2, \ldots, \psi_{N'}\}$, each associated with a node in the problem domain, then its approximation is

$$v(x,t) \approx \sum_{l=1}^{N'} \psi_l(x) v_l(t) \sim \sum_l \psi_l v_l$$

where v_l is the value of v at node l in the fluid problem domain $0 \leq x \leq L$. Upon substituting the approximation for v in equation (4.22) and setting N' different values for z, it assumes the following form:

$$\begin{aligned}
&\sum_l v_l \int_0^L \dot{m}_f c_f L\, z_n\, \psi_l'\, dx + \sum_l v_l \int_0^L k_f S_{fr} \epsilon L\, z_n' \psi_l'\, dx \\
&\qquad - \int_0^L h_c A\, z_n u_s\, dx + \sum_l v_l \int_0^L h_c A z_n \psi_l\, dx \\
&- \int_0^L U\, P\, L\, z_n v_{env}\, dx + \sum_l v_l \int_0^L U\, P\, L\, z_n \psi_l\, dx = 0
\end{aligned} \tag{4.23}$$

where

$$n = 1, 2, \ldots, N'$$

Now, if the same basis used for v is also used to express both u_s and v_{env} in its discrete form then equation (4.23) assumes the following form:

$$\begin{aligned}
&\sum_l v_l \int_0^L \dot{m}_f c_f L\, z_n\, \psi_l'\, dx + \sum_l v_l \int_0^L k_f S_{fr} \epsilon L\, z_n' \psi_l'\, dx \\
&\qquad - \sum_l u_{s_l} \int_0^L h_c A\, z_n \psi_l\, dx + \sum_l v_l \int_0^L h_c A z_n \psi_l\, dx \\
&- \sum_l v_{env_l} \int_0^L U\, P\, L\, z_n \psi_l\, dx + \sum_l v_l \int_0^L U\, P\, L\, z_n \psi_l\, dx = 0
\end{aligned} \tag{4.24}$$

where

$$n = 1, 2, \ldots, N'$$

4.5.4 The Galerkin method for the fluid problem domain

By the Galerkin method [17], we shall choose $z_n \equiv \psi_n$ so that equation (4.24) assumes the following form after re-arranging.

$$\begin{aligned}
&\sum_l v_l \int_0^L \dot{m}_f c_f L\, \psi_n\, \psi_l'\, dx + \sum_l v_l \int_0^L k_f S_{fr} \epsilon L\, \psi_n' \psi_l'\, dx \\
&\quad - \sum_l u_{s_l} \int_0^L h_c A\, \psi_n \psi_l\, dx + \sum_l v_l \int_0^L h_c A \psi_n \psi_l\, dx \\
&- \sum_l v_{env_l} \int_0^L U\, P\, L\, \psi_n \psi_l\, dx + \sum_l v_l \int_0^L U\, P\, L\, \psi_n \psi_l\, dx = 0
\end{aligned} \tag{4.25}$$

where

$$n = 1, 2, \ldots, N'$$

4.5.5 Finite element equations for the fluid problem domain

Global equations

System (4.25) is made up of N' equations. These are the finite element equations for the fluid problem domain. They may be written in the general matrix form

$$\mathrm{K}\mathbf{v} - \mathbf{f} = \mathbf{0} \tag{4.26}$$

where

$$\begin{aligned}
\mathbf{v} &= [v_1, v_2, \ldots, v_{N'}]' \\
\mathrm{K}_{nl} &= \int_0^L \left(\dot{m}_f c_f L\, \psi_n\, \psi_l' + k_f S_{fr} \epsilon L\, \psi_n' \psi_l' + h_c A\, \psi_n\, \psi_l + U\, P\, L\, \psi_n\, \psi_l\right) dx
\end{aligned}$$

and

$$\mathbf{f}_n = \sum_l u_{s_l} \int_0^L h_c A\, \psi_n \psi_l \, dx + \sum_l v_{env_l} \int_0^L U\, P\, L\, \psi_n \psi_l \, dx$$

However, vector $\mathbf{f}$ may be written in a more convenient way:

$$\mathbf{f} = \mathrm{F}\mathbf{u}_s + \mathrm{G}\mathbf{v}_{env}$$

where

$$\mathrm{F}_{nl} = \int_0^L h_c A\, \psi_n \psi_l \, dx, \quad \mathrm{G}_{nl} = \int_0^L U\, P\, L\, \psi_n \psi_l \, dx$$
$$\mathbf{u}_s = [u_{s_1}, u_{s_2}, \ldots, u_{s_{N'}}]' \text{ and } \mathbf{v}_{env} = [u_{env_1}, u_{env_2}, \ldots, u_{env_{N'}}]'$$

Element contributions

It follows from a property of integrals that the matrices in the global equations may be obtained by considering the sum of the contributions to these matrices over the elements. For example, the global stiffness matrix K equals the sum of the element mass matrices K^e, that is

$$K_{nl} = \sum_e K_{nl}^e$$

where

$$K_{nl}^e = \int_{x_i}^{x_j} (\dot{m}_f c_f L\, N_n\, N_l + k_f S_{fr} \epsilon L\, N_n' N_l' + h_c A\, N_n\, N_l + U\, P\, L\, N_n\, N_l)\, dx$$

since a global basis function ψ reduces to an element shape function N on an element (e) with end points x_i and x_j corresponding to nodes i and j in the problem domain. Both subscripts n and l are either i or j on (e). The element stiffness mass matrix in condensed form is given by:

$$K_c^e = \begin{array}{c} \begin{matrix} i & j \end{matrix} \\ \begin{bmatrix} K_{ii}^e & K_{ij}^e \\ K_{ij}^e & K_{jj}^e \end{bmatrix} \end{array} \begin{matrix} i \\ j \end{matrix}$$

where

$$
\begin{aligned}
K^e_{ii} &= \int_{x_i}^{x_j} \left(\dot{m}_f c_f L\, N_i N_i' + k_f S_{fr} \epsilon L\, N_i'^2 + h_c A\, N_i^2 + U\, P\, L\, N_i^2 \right) dx \\
&= -\dot{m}_f c_f L \frac{1}{2} + k_f S_{fr} \epsilon L \frac{1}{g} + h_c A \frac{g}{3} + U\, P\, L \frac{g}{3} \\
K^e_{ij} &= \int_{x_i}^{x_j} \left(\dot{m}_f c_f L\, N_i N_j' + k_f S_{fr} \epsilon L\, N_i' N_j' + h_c A\, N_i N_j + U\, P\, L\, N_i N_j \right) dx \\
&= \dot{m}_f c_f L \frac{1}{2} - k_f S_{fr} \epsilon L \frac{1}{g} + h_c A \frac{g}{6} + U\, P\, L \frac{g}{6} \\
K^e_{ji} &= \int_{x_i}^{x_j} \left(\dot{m}_f c_f L\, N_j N_i' + k_f S_{fr} \epsilon L\, N_j' N_i' + h_c A\, N_j N_i + U\, P\, L\, N_j N_i \right) dx \\
&= -\dot{m}_f c_f L \frac{1}{2} - k_f S_{fr} \epsilon L \frac{1}{g} + h_c A \frac{g}{6} + U\, P\, L \frac{g}{6}
\end{aligned}
$$

and

$$
\begin{aligned}
K^e_{jj} &= \int_{x_i}^{x_j} \left(\dot{m}_f c_f L\, N_j N_j' + k_f S_{fr} \epsilon L\, N_j'^2 + h_c A\, N_j^2 + U\, P\, L\, N_j^2 \right) dx \\
&= \dot{m}_f c_f L \frac{1}{2} + k_f S_{fr} \epsilon L \frac{1}{g} + h_c A \frac{g}{3} + U\, P\, L \frac{g}{3}
\end{aligned}
$$

Here, integration details have been left out and, $x_j - x_i = g$. Similarly

$$
F^e_c = h_c A \frac{g}{6} \begin{bmatrix} 2 & 1 \\ 1 & 2 \end{bmatrix} \begin{matrix} i \\ j \end{matrix} \quad \text{and} \quad G^e_c = U\, P\, L \frac{g}{6} \begin{bmatrix} 2 & 1 \\ 1 & 2 \end{bmatrix} \begin{matrix} i \\ j \end{matrix}
$$

Here, we have used the fact that the physical properties for the problem are constant on (e), that the element shape functions are linear and hence the global basis functions are piecewise linear and continuous. The choice of linear shape functions is reasonable since we do not expect any sudden changes in temperature.

If the nodes in the fluid problem domain are numbered 0 through N' and the corresponding elements 1 through $E(= N')$ then the condensed stiffness matrices for the elements are

$$
K^1_c = \begin{bmatrix} K^1_{ii} & K^1_{ij} \\ K^1_{ij} & K^1_{jj} \end{bmatrix} \begin{matrix} 0 \\ 1 \end{matrix} \begin{matrix} 0 & 1 \\ & \end{matrix}, \cdots, K^e_c = \begin{bmatrix} K^e_{ii} & K^e_{ij} \\ K^e_{ij} & K^e_{jj} \end{bmatrix} \begin{matrix} i \\ j \end{matrix} \begin{matrix} i & j \\ & \end{matrix}, \cdots, K^E_c = \begin{bmatrix} K^E_{ii} & K^E_{ij} \\ K^E_{ij} & K^E_{jj} \end{bmatrix} \begin{matrix} N'-1 \\ N' \end{matrix} \begin{matrix} N'-1 & N' \\ & \end{matrix}
$$

and similarly for F_c^e, G_c^e, $\mathbf{v}_c^e$ and hence $\mathbf{f}_c^e$. This results in a system of $N'+1$ equations in $N'+1$ unknowns for the fluid problem domain which may be written in the same matrix form as (4.26).

4.5.6 Finite difference approximation in space for the solid phase

If we let $u^{(i,j)}$ (time argument left out for clarity) denote $u(i\Delta r, j\Delta x, t)$ where Δr and Δx are distances between neighbouring nodes in the radial direction and along the direction of fluid flow then, a second order central difference approximation in the space derivative in 4.14 results in the following finite difference equations for the solid problem domain.

$$\dot{u}^{(i,j)} = \frac{\alpha_m}{i(\Delta r)^2}\left[(i-1)u^{(i-1,j)} - 2\,i\,u^{(i,j)} + (i+1)u^{(i+1,j)}\right];\ i = 1, 2, \ldots, I-2$$

and on the fluid-solid interface

$$\begin{aligned}\dot{u}^{(I-1,j)} =& \frac{\alpha_m}{(I-1)(\Delta r)^2}\left[(I-2)u^{(I-2,j)} - 2\,(I-1)\,u^{(I-1,j)}\right.\\ &\left. + I\left(u^{(I-2,j)} + 2\check{\mathrm{Bi}}\left(v_j - u_{s_j}\right)\right)\right]\\ =& \frac{\alpha_m}{(I-1)(\Delta r)^2}\left[2(I-1)u^{(I-2,j)} + \left(-2(I-1) - 2\,I\,\check{\mathrm{Bi}}\right)u_{s_j}\right]\\ &+ \frac{\alpha_m}{(I-1)(\Delta r)^2}\,2\,I\,\check{\mathrm{Bi}}\,v_j\end{aligned}$$

where

$$u_{s_j} = u^{(I-1,j)},\ \alpha_m = \frac{k_m}{\rho_m c_m}$$

is the thermal diffusivity,

$$\check{\mathrm{Bi}} = \frac{h_c \Delta r}{k_m}$$

is the Biot number per unit subdivision and $u^{(I,j)}$, the unknown at an artificial node, is eliminated by use of a central difference approximation for the boundary condition:

$$k_m \frac{u^{(I,j)} - u^{(I-2,j)}}{2\Delta r} = h_c(-u_{s_j} + v_j)$$

The finite difference equations for the solid may be written in matrix form as follows

$$\dot{\mathbf{u}}_j = A\mathbf{u}_j + v_j\mathbf{b};\ j = 0, 1, 2, \ldots, J = N' = E$$

where

$$\dot{\mathbf{u}}_j = \left[u^{(1,j)}, u^{(2,j)}, \cdots, u^{(I-2,j)}, u_{s_j}\right]',\ u_{s_j} = u^{(I-1,j)}$$
$$\mathbf{b} = \left[0, 0, \cdots, 0, \frac{\alpha_m}{(I-1)(\Delta r)^2}\, 2\, I\, \check{\mathrm{B}}\mathrm{i}\right]'$$

and the matrix A is defined as follows.

$$A = \begin{bmatrix} 2\lambda_1 & 2\lambda_1 & & & & & & \\ \lambda_2 & -4\lambda_2 & 3\lambda_2 & & & & & \\ & \ddots & & & & & & \\ & & (i-1)\lambda_i & -2i\lambda_i & (i+1)\lambda_i & & & \\ & & & \ddots & & & & \\ & & & & (I-3)\lambda_{I-2} & 2(2-I)\lambda_{I-2} & (I-1)\lambda_{I-2} & \\ & & & & & 2(I-1)\lambda_{I-1} & \left(-2(I-1) - 2\, I\, \check{\mathrm{B}}\mathrm{i}\right) \frac{\alpha_m}{(I-1)\,(\Delta r)^2} \end{bmatrix} \tag{4.27}$$

The finite difference equations for the solid problem domain may be written as single matrix structure, that is

$$\dot{\mathbf{u}} = \check{A}\mathbf{u} + \check{\mathbf{b}} \tag{4.28}$$

where

$$\mathbf{u} = \begin{bmatrix} \mathbf{u}_0 \\ \mathbf{u}_1 \\ \vdots \\ \mathbf{u}_j \\ \vdots \\ \mathbf{u}_{N'} \end{bmatrix}',\ \check{\mathbf{b}} = \begin{bmatrix} v_0\mathbf{b} \\ v_1\mathbf{b} \\ \vdots \\ v_j\mathbf{b} \\ \vdots \\ v_{N'}\mathbf{b} \end{bmatrix}'$$

and the matrix $\check{A}$ is a block diagonal matrix with matrices A on its main diagonal. (4.28) constitutes a system of $I-1$ by $N'+1$ equations in the same number of unknowns for the solid problem domain.

4.5.7 Applying the boundary condition for the fluid problem domain

Before applying boundary conditions, the finite element equations for the fluid may be written as

$$\check{\mathrm{K}}\mathbf{v} = \check{\mathrm{F}}\mathbf{u}_s + \check{\mathrm{G}}\mathbf{v}_{env} \tag{4.29}$$

where

$$\begin{aligned}\mathbf{v} &= [v_0, v_1, \ldots, v_{N'}]' \\ \mathbf{v}_{env} &= [v_{env_0}, v_{env_1}, \ldots, v_{env_{N'}}]' \\ \mathbf{u}_s &= [u_{s_0}, u_{s_1}, \ldots, u_{s'_N}]'\end{aligned}$$

Substituting the boundary condition $v_0 \equiv T_{fi}(t)$ (older notation is used here to clearly point out the fluid inlet temperature) for the first equation transforms (4.29) to the following form

$$\left[\begin{array}{c|c} 1 \quad 0 \quad \cdots \quad 0 & \\ \hline & \\ \check{\mathrm{K}} & \\ & \end{array}\right] \begin{bmatrix} v_0 \\ v_1 \\ \vdots \\ v_{N'} \end{bmatrix} = \left[\begin{array}{c|c} 0 \quad 0 \quad \cdots \quad 0 & \\ \hline & \\ \check{\mathrm{F}} & \\ & \end{array}\right] \begin{bmatrix} u_{s_0} \\ u_{s_1} \\ \vdots \\ u_{s_{N'}} \end{bmatrix} + \left[\begin{array}{c|c} 0 \quad 0 \quad \cdots \quad 0 & \\ \hline & \\ \check{\mathrm{G}} & \\ & \end{array}\right] \begin{bmatrix} v_{env_0} \\ v_{env_1} \\ \vdots \\ v_{env_{N'}} \end{bmatrix} + \begin{bmatrix} T_{fi}(t) \\ 0 \\ \vdots \\ 0 \end{bmatrix}$$

or in a more compact form

$$\mathrm{K}\mathbf{v}(t) = \mathrm{F}\mathbf{u}_s(t) + \mathrm{G}\mathbf{v}_{env}(t) + T_{fi}(t)\mathbf{f}$$

which upon re-arranging becomes

$$\mathbf{v}(t) = \hat{\mathrm{L}}\mathbf{u}_s(t) + \mathrm{Q}\mathbf{v}_{env}(t) + T_{fi}(t)\mathbf{g} \tag{4.30}$$

where

$$\hat{\mathrm{L}} = \mathrm{K}^{-1}\mathrm{F},\ \mathrm{Q} = \mathrm{K}^{-1}\mathrm{G},\ \mathbf{f} = \begin{bmatrix} 1 \\ 0 \\ \vdots \\ 0 \end{bmatrix},\ \mathbf{g} = \mathrm{K}^{-1}\mathbf{f},\ \mathrm{K} = \left[\begin{array}{cccc} 1 & 0 & \cdots & 0 \\ \hline & & & \\ & \check{\mathrm{K}} & & \\ & & & \end{array}\right]$$

$$\mathrm{F} = \left[\begin{array}{cccc} 0 & 0 & \cdots & 0 \\ \hline & & & \\ & \check{\mathrm{F}} & & \\ & & & \end{array}\right] \text{ and } \mathrm{G} = \left[\begin{array}{cccc} 0 & 0 & \cdots & 0 \\ \hline & & & \\ & \check{\mathrm{G}} & & \\ & & & \end{array}\right].$$

Expanding (4.30) to the same size as the solid equations' matrix structure gives the following results:

$$\mathrm{L}\mathbf{u}_s(t) = \begin{bmatrix} \hat{L}_{11} & \hat{L}_{12} & \dots & \hat{L}_{1,N'+1} \\ \hat{L}_{21} & \hat{L}_{22} & \dots & \hat{L}_{2,N'+1} \\ \vdots & & & \\ \hat{L}_{N'+1,1} & \hat{L}_{N'+1,2} & \dots & \hat{L}_{N'+1,N'+1} \end{bmatrix} \begin{bmatrix} u_{s_0}(t) \\ u_{s_1}(t) \\ \vdots \\ u_{s_{N'}}(t) \end{bmatrix}$$

becomes

$$\left[\begin{array}{cccc} & & & \\ & & & \\ & & & \\ \hat{L}_{11} & \hat{L}_{12} & \dots & \hat{L}_{1,N'+1} \\ \hline & & & \\ & & & \\ & & & \\ \hat{L}_{21} & \hat{L}_{22} & \dots & \hat{L}_{2,N'+1} \\ \hline \vdots & & & \\ & & & \\ & & & \\ & & & \\ \hat{L}_{N'+1,1} & \hat{L}_{N'+1,2} & \dots & \hat{L}_{N'+1,N'+1} \end{array}\right] \left[\begin{array}{c} u^{(1,0)}(t) \\ \vdots \\ u^{(I-2,0)}(t) \\ u_{s_0}(t) \\ \hline u^{(1,1)}(t) \\ \vdots \\ u^{(I-2,1)}(t) \\ u_{s_1} \\ \hline \vdots \\ \hline u^{(1,N')}(t) \\ \vdots \\ u^{(I-2,N')}(t) \\ u_{s_{N'}}(t) \end{array}\right]$$

and similarly

$$\mathrm{Q}\mathbf{v}_{env} = \begin{bmatrix} Q_{11} & Q_{12} & \dots & Q_{1,N'+1} \\ Q_{21} & Q_{22} & \dots & Q_{2,N'+1} \\ \vdots & & & \\ Q_{N'+1,1} & Q_{N'+1,2} & \dots & Q_{N'+1,N'+1} \end{bmatrix} \begin{bmatrix} v_{env_0}(t) \\ v_{env_1}(t) \\ \vdots \\ v_{env_{N'}}(t) \end{bmatrix}$$

becomes

$$\left[\begin{array}{cccc} & & & \\ & & & \\ & & & \\ Q_{11} & Q_{12} & \dots & Q_{1,N'+1} \\ \hline & & & \\ & & & \\ & & & \\ Q_{21} & Q_{22} & \dots & Q_{2,N'+1} \\ \hline \vdots & & & \\ \hline & & & \\ & & & \\ & & & \\ Q_{N'+1,1} & Q_{N'+1,2} & \dots & Q_{N'+1,N'+1} \end{array}\right] \left[\begin{array}{c} 0 \\ \vdots \\ 0 \\ v_{env_0}(t) \\ \hline 0 \\ \vdots \\ 0 \\ v_{env_1}(t) \\ \hline \vdots \\ \hline 0 \\ \vdots \\ 0 \\ v_{env_{N'}}(t) \end{array}\right]$$

and,

$$\mathbf{g}\, T_{fi}(t) = \mathrm{K}^{-1}\mathbf{f}\, T_{fi}(t) = \mathrm{M}\,\mathbf{f}\, T_{fi}(t) = \mathrm{M} \begin{bmatrix} 1 \\ 0 \\ \vdots \\ 0 \end{bmatrix} T_{fi}(t) = \begin{bmatrix} M_{11} \\ M_{21} \\ \vdots \\ M_{N'1} \end{bmatrix} T_{fi}(t)$$

expands to

$$[0, \dots, 0, M_{11} | 0, \dots, 0, M_{21} | \dots | 0, \dots, 0, M_{N'1}]'\, T_{fi}(t)$$

and finally $\mathbf{v}(t)$ expands to

$$[0,\ldots,0,v_0(t)|0,\ldots,0,v_1(t)|\ldots|0,\ldots,0,v_{N'}(t)]'.$$

4.5.8 A brief description of the energy equations in matrix form

The energy equations for the solid phase may be written as follows.

$$\dot{\mathbf{u}}(t) = \check{\mathrm{A}}\mathbf{u}(t) + \check{\mathbf{b}}(t) \tag{4.31}$$

where

$$\check{\mathbf{b}}(t) = \frac{\alpha_m\, 2\, I\, \mathrm{Bi}}{(I-1)(\Delta r)^2}[0,\ldots,0,v_0(t)|0,\ldots,0,v_1(t)|\ldots|0,\ldots,0,v_{N'}(t)]'$$

and $\check{A}$ is a block diagonal matrix with matrices A on its main diagonal. The matrix A is defined in (4.27).

The energy equations for the fluid phase may be written as follows.

$$\mathbf{v}(t) = \hat{\mathrm{L}}\mathbf{u}(t) + \mathrm{Q}\mathbf{v}_{env}(t) + T_{fi}(t)\mathbf{g} \tag{4.32}$$

(4.32) is the expanded form of (4.30).

4.5.9 Time stepping

Upon writing $\check{\mathbf{b}}(t)$ in terms of the expanded form of $\mathbf{v}(t)$, (4.31) assumes the following form.

$$\dot{\mathbf{u}}(t) = \check{\mathrm{A}}\mathbf{u}(t) + \frac{\alpha_m\, 2\, I\, \mathrm{Bi}}{(I-1)(\Delta r)^2}\mathbf{v}(t) \tag{4.33}$$

Substituting the right hand side of (4.32) for $\mathbf{v}(t)$ in (4.33) eliminates nodal values for the fluid temperature away from the inlet of the bed and gives the following matrix equation.

$$\dot{\mathbf{u}}(t) = B\mathbf{u}(t) + \hat{\mathrm{Q}}\mathbf{v}_{env}(t) + T_{fi}(t)\check{\mathbf{d}} \tag{4.34}$$

where

$$\check{\mathbf{d}} = \frac{\alpha_m \, 2 \, I \, \mathrm{Bi}}{(I-1)(\Delta r)^2}[0, \ldots, 0, M_{11}|0, \ldots, 0, M_{21}| \ldots |0, \ldots, 0, M_{N'1}]'$$

$$B = \check{\mathrm{A}} + \frac{\alpha_m \, 2 \, I \, \mathrm{Bi}}{(I-1)(\Delta r)^2}\hat{\mathrm{L}} \text{ and } \hat{\mathrm{Q}} = \frac{\alpha_m \, 2 \, I \, \mathrm{Bi}}{(I-1)(\Delta r)^2}\mathrm{Q}$$

The Crank-Nicolson method is chosen to ensure stability [33] for reasonably big time steps. The equation of concern is approximated at mid-points between time levels $n\Delta t, n = 0, 1, 2, \cdots$, and an unknown at these mid-points is replaced by an average of two nodal values immediately above and below it in the time domain. For (4.34) this gives the following implicit finite difference scheme:

$$\left(\mathrm{I} - \frac{\Delta t}{2}B\right)\mathbf{u}_{n+1} = \left(\mathrm{I} + \frac{\Delta t}{2}B\right)\mathbf{u}_n + \frac{\Delta t}{2}\hat{\mathrm{Q}}\left(\mathbf{v}_{env_{n+1}} + \mathbf{v}_{env_n}\right) + \frac{\Delta t}{2}\left(T_{fi}^{n+1} + T_{fi}^{n}\right)\check{\mathbf{d}} \quad (4.35)$$

The iterative scheme (4.35) is for computing $\mathbf{u}$ at all time levels and, the corresponding values of $\mathbf{v}$ are computed using equation (4.32).

Chapter 5

Numerical predictions

5.1 Introduction

In this chapter, the mathematical model for heat transfer in packed beds that was developed in chapter 4 is used to give numerical predictions. Code in the *Octave* programming language was written for the numerical computations. To check this code, different code in *Matlab* was written by my supervisor Dr. David Henwood. The numerical results from the two distinct codes are compared.

The mathematical model is validated against measured data and used in a parametric study. The results from the parametric study can be used to optimise design and operational parameters for a typical packed bed unit. Owing to the level of uncertainty in the values used for the convective heat transfer coefficient h_c and the fluid mass flow rate $\dot{m}_f$, tests are carried out to see how sensitive the model is to slight changes in these two parameters. Also presented is the effect of ground coupling on the model.

5.2 On checking the numerical solution

Considered here is the transient response of a packed bed to a step change in the inlet fluid temperature in the absence of thermal interaction with the surroundings of the bed. The bed is initially at a constant temperature T_0 throughout, taken at 0° C. It then experiences a sudden change in the fluid inlet temperature to T_{fi} taken at 20° C. The fluid inlet temperature

is maintained at T_{fi}, a constant temperature for all times $t \geq 0$ since the occurrence of the step change. The fluid outlet temperature $T_f(x = L, t)$ is observed as it rises exponentially with time towards its maximum possible value T_{fi} and observation stops at 90 %.

The method used for generating the *Matlab* code uses finite differences with 4 nodes in space for the rocks. 3 quadratic finite elements with 7 nodes are used for the fluid problem domain. The solution in time is analytic. An iterative process is used to solve the fluid and solid energy equations uncoupled. For each time step t_1 to t_2:

1. Estimate $\mathbf{T}_f(t_2)$ the fluid temperatures at time t_2 using $\mathbf{T}_m(t_1)$ the solid temperatures at time t_1, $T_{fi}(t_2)$ the fluid inlet temperature at time t_2 and the fluid energy equation. That is
$$\mathbf{T}_f(t_2) = \hat{\mathrm{L}}\mathbf{T}_m(t_1) + T_{fi}(t_2)\mathbf{g}$$

2. Solve the solid energy equations analytically in time
$$\dot{\mathbf{T}}_m(t) = B\mathbf{T}_m(t) + b\mathbf{T}_f(t)$$
assuming a linear variation in the fluid temperatures in the interval $t_1 < t < t_2$, that is
$$\mathbf{T}_f(t) = \mathbf{T}_f(t_2) + \frac{t - t_1}{t_2 - t_1}\left(\mathbf{T}_f(t_2) - \mathbf{T}_f(t_1)\right)$$
and compute an estimate of $\mathbf{T}_m(t_2)$.

3. Repeat stages 1 and 2 using $\mathbf{T}_m(t_2)$ instead of $\mathbf{T}_m(t_1)$.

The method for generating the *Octave* code uses finite differences with the same number of nodes in space for the rocks as the *Matlab* code. 5 linear finite elements with 6 nodes are used for the fluid problem domain. The solution in time uses an implicit Crank-Nicolson finite difference method with a constant time step of 30 seconds.

Figure (5.1) shows a comparison of the fluid outlet temperature produced by the two different codes. The results from the *Octave* code are represented by the blue circles, the green solid line represents results from the *Matlab* code and the inlet fluid temperature is the red solid level line. The fluid outlet temperature rises to 90 % of the maximum possible value in 12.812 hours for the *Octave* code and in 12.805 hours for the *Matlab* code showing a good agreement between the two different codes.

To measure the gain in the fluid outlet temperature and the associated phase change it is

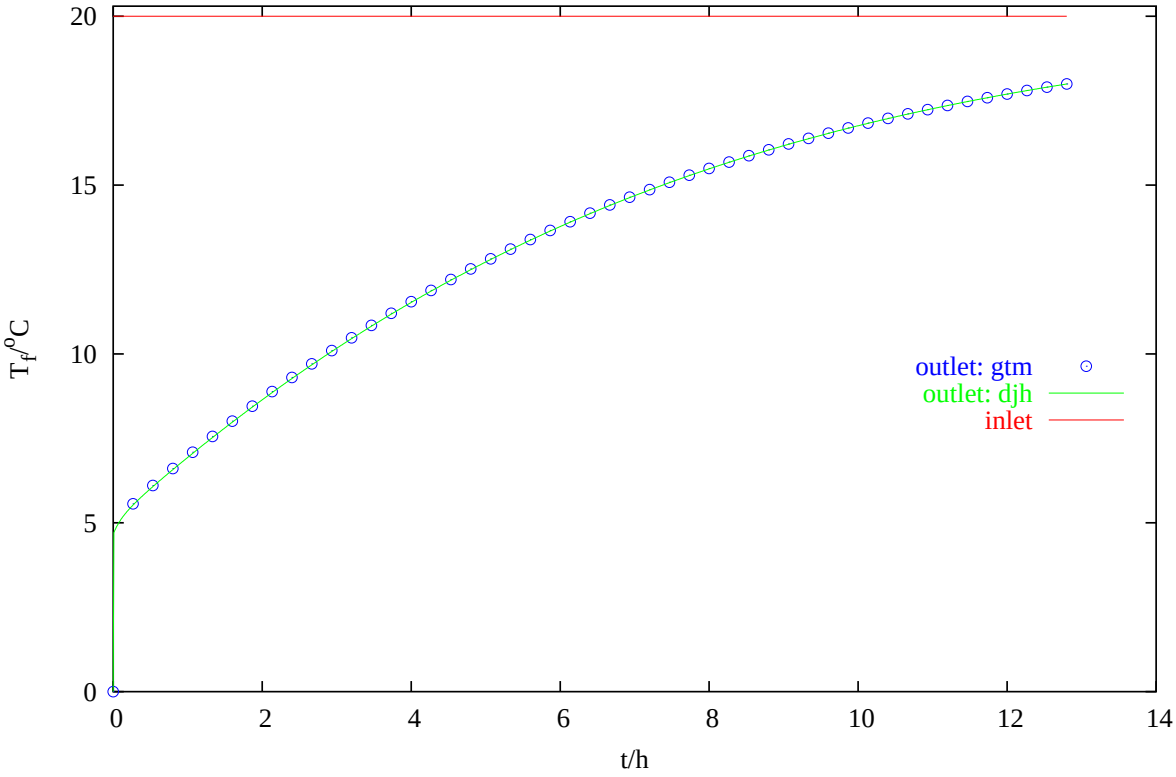

Figure 5.1: On checking the code

more appropriate to consider the transient response of the bed to a sinusoidal variation in the fluid inlet temperature. Figure (5.2) shows the numerical predictions made using the *Octave* code for a time scale of 36 hours. The difference between the temperature at the second peak of the fluid inlet and outlet temperatures gives the gain. Similarly, the difference between the corresponding times gives phase change. As previously, a comparison is made with the *Matlab* code. The gain is 3.733° C and 3.739° C for the *Octave* and *Matlab* codes respectively. Similarly, the phase changes are 2.600 hours and 2.613 hours respectively again showing how well the two different codes agree.

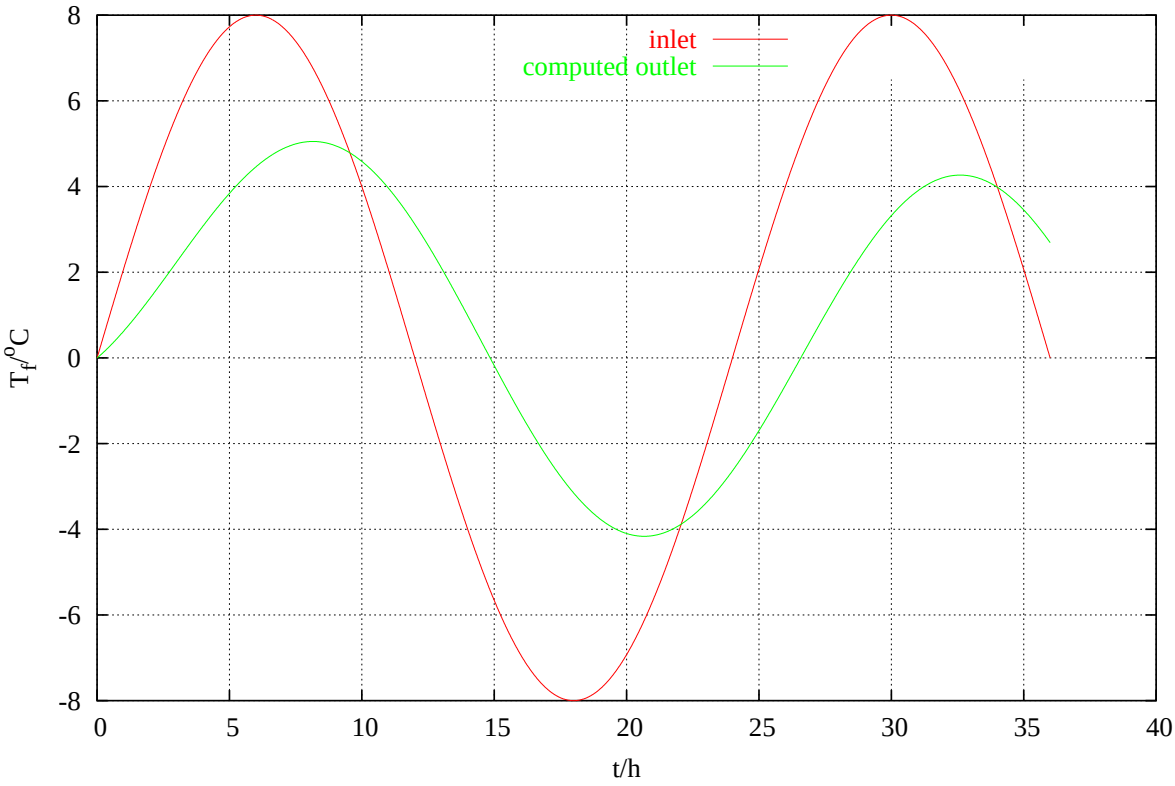

Figure 5.2: On fluid temperature gain and phase change

5.3 Comparing measured and predicted fluid outlet temperatures

5.3.1 Introduction

As described in section 4.3, a packed bed unit is one of two halves that make a rock-store compartment. One is the *morning unit* and the other the *afternoon unit* depending on whether it is supplied air by the *am* or *pm fan*. Each fan is switched on and off depending on the time of the day, and day of the week.

The am fan timing is as follows.

$$\text{AM fan status} = \begin{cases} \text{ON} & \text{from 10 pm to 6 am (Sunday to Thursday only)} \\ \text{ON} & \text{from 8 am to 12 pm (Monday to Friday only)} \\ \text{OFF} & \text{at any other times (and any other day)} \end{cases}$$

Similarly, the pm fan timing is as follows.

$$\text{PM fan status} = \begin{cases} \text{ON} & \text{from 10 pm to 6 am (Sunday to Thursday only)} \\ \text{ON} & \text{from 12 pm to 3:30 pm (Monday to Friday only)} \\ \text{OFF} & \text{at any other times (and any other day)} \end{cases}$$

To summarise, both fans are switched on at 10 pm at night till 6 am in the morning when they both are switched off for the next 2 hours. At 8 am the am fan is switched on and it runs till 12 pm when it is switched off and at the same time the pm fan is switched on and it runs till 3:30 pm. Both fans are off then till 10 pm and the cycle is repeated for the week. However, the weekend is an exception. Both fans are not switched on at 10 pm on Friday. They stay off throughout Saturday, Sunday morning and afternoon and, both of them are only switched on Sunday at 10 pm for the next weekly cycle.

In this section, the mathematical model is compared with measured data for the purpose of validation, for both the morning and the afternoon unit. Use is made here of measured fluid inlet and outlet temperatures. These readings were taken off a data logger as described in section 4.3. Two different sensors are used to measure the fluid inlet temperature for each of the morning and the afternoon units. They are positioned after the am and pm fans respectively. Consequently, a different fluid inlet temperature is used depending on which unit (morning or afternoon) is being considered.

Granite rocks	c_m	=	800	$J/kg\,^o$C
	ρ_m	=	2700	kg/m^3
	k_m	=	2.1	$W/m\,^o$C
	R	=	0.1	m
Air	c_f	=	1007	$J/kg\,^o$C
	ρ_f	=	1.106	kg/m^3
	k_f	=	0.25	$W/m\,^o$C
Other parameters	h_c	=	6	$W/m^2\,^o$C
	ϵ	=	.5	
	L	=	2	m
	S_{fr}	=	5.4	m^2
	A	=	$3\frac{(1-\epsilon)}{R}S_{fr}L$	m^2

Table 5.1: Input parameters

Table (5.1) shows values used for the basic parameters to generate the results presented in this section. The flow rates for the am and pm fans used are shown in Figure (5.3). The time scale of interest is one week beginning on a Monday. The figure clearly indicates when

the fans are off for the weekend.

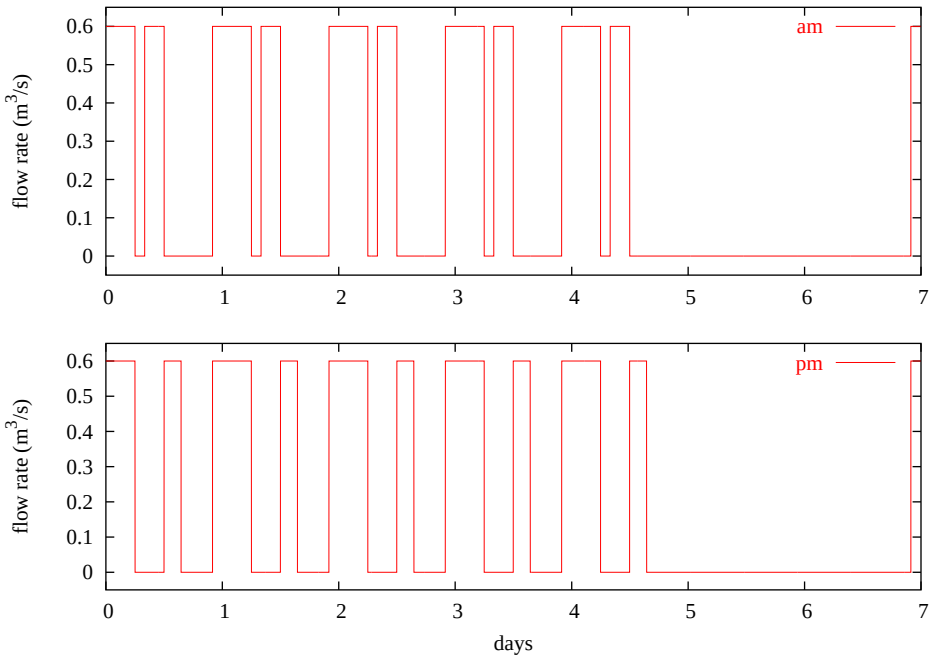

Figure 5.3: Volume flow rates for the am and pm fans

5.3.2 Performance of the morning unit

In this section, a comparison is made of the predicted with the measured outlet fluid temperature for the morning packed bed unit. The measured data used was taken in October, one of the hottest months of the year in Harare. A constant heat transfer coefficient h_c is assumed. Values for this and other parameters used are given in Table (5.1).

Figure (5.4) shows the transient response of the morning packed bed unit to ambient air temperature. A time scale of two weeks was chosen to make sure that the numerical system has settled down since it was assumed that the packed bed unit is initially at a constant temperature throughout. The predicted and measured fluid outlet temperatures are shown in the figure. Also shown is the variation of the volume flow rate $\dot{V}_f$ throughout the fortnight to indicate how the fluid outlet temperature is affected by changes in the fluid flow rate.

Generally, the agreement between predicted and measured fluid outlet temperatures is satisfactory especially for the night cooling periods. However, the morning cooling is underestimated. This may be due to an incorrect value for either h_c or $\dot{V}_f$. Tests are carried out

later in the chapter to see how the agreement is sensitive to slight changes in the values of h_c and $\dot{V}_f$. During the weekend there is a prolonged absence of forced fluid flow. The agreement between predicted and measured results then is better for the second week since the numerical system has settled down.

5.3.3 Performance of the afternoon unit

The predicted and measured fluid outlet temperatures for the afternoon packed bed unit are compared in this section. The material and fluid parameters used are the same as in the previous section and they are shown in Table (5.1). The fluid volume flow rate varies as shown in Figure (5.3).

Shown in Figure (5.5) is a comparison of the predicted with the measured fluid outlet temperature for the afternoon unit responding to a measured fluid inlet temperature and a given fluid flow variation over a period of two weeks.

The predicted fluid outlet temperature follows the trends of the measured fluid outlet temperature. However, it is uniformly higher, even for the weekend. The results are worse in this respect than those for the morning unit. There are several possible explanations for this difference. Amongst them are the following.

- Two different sensors measure the fluid inlet temperature for each of the morning and afternoon packed bed unit. They may either be non-uniformly calibrated or not equally shielded from thermal radiation. Physical damage on one of the sensors could also contribute.

- They are located at different physical positions. Improper placement of sensors could give wrong temperature readings as was the case for a different building, Eastgate: due to lack of strict monitoring, a sensor that was supposed to measure air temperature at the exit of a ventilated floor slab was actually measuring room air temperature.

Possible reasons for differences between measured and computed results which are valid for both the morning and the afternoon units include the following:

- The thermal mass between the fans and bed inlet along the air flow path is not included in the model. The walls surrounding theses channels are made up of concrete. This

will add to the thermal capacity of the bed and delay its reaction to changes in the ambient air temperature.

- There is uncertainty in:
  - the values of the physical properties for both the bed material and the air flowing through it, and
  - the amount of storage material in the bed.

5.4 Sensitivity tests

5.4.1 Effect of the convective heat transfer coefficient

In this section, the effect of varying h_c on how close the predicted and measured outlet fluid temperatures agree is investigated. Three different values of h_c are used to see whether agreement between predicted and measured results becomes better or worse by slightly changing the value of h_c. The fluid volume flow rates for the morning and afternoon units are as given in Figure (5.3) and the basic parameters are given in Table (5.1).

Figure (5.6) shows how sensitive the numerical model is to slight changes in h_c for the afternoon unit. A time period of 18 hours is chosen to get a closer look than for the whole of the fortnight. This period also covers the two cooling periods for this unit. These are 12 pm to 3:30 pm and 10 pm to 6 am as shown in the figure. The second week is chosen to make sure the numerical system has settled down. The shown data is from Tuesday but the trend is the same over the entire two week period, morning or afternoon.

It can be seen from Figure (5.6) that the effect of increasing h_c is to dampen the response of the fluid outlet temperature. The higher the h_c the higher the gain in the fluid temperature. This is clear for the period 12 mid-day to 3:30 pm when the air is blown through the unit by the pm fan. During this period, the heat transfer on the rock-air interface is driven by forced convection. For the period 3:30 pm to 10 pm both fans are off and the heat transfer on the rock-air interface is facilitated by free convection and during the last period 10 pm to 6 am it is back to forced convection. Similar behaviour is also exhibited by the morning unit.

The weakness of the model in its current form is that it assumes a constant h_c throughout the entire period. Generally, low h_c values (for example $6\,W/m^2\,^\circ C$) are valid for the free

convection and higher values for forced convection. In the period of free convection a flow rate of $0\,m/s$ is assumed. $\dot{V}_f = 0.6\,m/s$ is used for forced convection as recommended by the consulting engineer who was involved in the construction of the Harare International School. Several correlations between h_c and $\dot{V}_f$ have been published for example in [29] by Schmidt and Willmont and in [16] by Duffie and Beckman. However, some of these correlations have been indicated to be not entirely satisfactory. They apply for bed material with different physical properties and size and not for the granite used. An example is the following correlation between the volumetric heat transfer coefficient h_v and the mass flow rate $\dot{m}_f$ for a packed bed of pebbles by Duffie and Beckman. Contrary to this, the rocks at the Harare International School are much bigger, typically 20 cm in diameter.

$$h_v = 650 \left(\frac{\dot{m}_f}{2\,R\,S_{fr}} \right)^{0.7}$$

Expressed in terms of h_c, this is

$$h_c = 650 \left(\frac{\dot{m}_f}{2\,R\,S_{fr}} \right)^{0.7} \frac{S_{fr} L}{A}$$

where

$$h_v S_{fr} L = h_c A$$

and $\dot{m}_f$ is related to $\dot{V}_f$ by

$$\dot{m}_f = \rho_f \dot{V}_f$$

5.4.2 Effect of the fluid flow rate

Similar to the previous section, this section investigates the effect of $\dot{V}_f$ on the agreement between predicted and measured fluid outlet temperature. Figure (5.7) shows the transient response of the afternoon unit for different peak values of $\dot{V}_f$ denoted by V_f in the figure. h_c is assumed to be constant at $6\,W/m^2\,^\circ C$ and the other parameters are as given in Table (5.1). The temperatures shown in Figure (5.7) are for Tuesday of the second week but the trend is the same over the whole two week period for either the morning or afternoon unit.

From the figure it is clear that the effect of using a lower flow rate of $\dot{V}_f = 0.4\,m^3/s$ is to

dampen the fluid outlet temperature. It brings the predicted values closer to the measured values. The greater gain achieved with a lower flow rate may be because the air is given more time to be in contact with the rocks. Also, the measured average value of $\dot{V}_f = 0.6\,m^3/s$ recommended for use in the modelling is subject to error. Information about how this figure was arrived at and if it is likely to be above or below the true figure was not available. Furthermore, the fluid must be well mixed before taking a measurement otherwise the reading is not a true representative of the fluid flow rate.

5.5 Ground coupling

Considered here is the effect of thermal interaction between the packed bed unit and the surrounding ground for a bed that is subject to a step change in its fluid inlet temperature. The bed is initially at a uniform temperature $T_0 = 0°C$. Suddenly, the fluid inlet temperature experiences a step change to a constant value $T_{fi} = 20°C$ while the environment temperature is maintained at a constant temperature. The time scale of interest is 30 hours. The basic parameters are as given in Table (5.1) together with the following additional parameters. The value of 15° C used for the ground temperature is an estimate for the year.

U	$=$	2	$W/m^2\,°C$
P	$=$	26.8	m
T_{env}	$=$	15	$°C$

Figure (5.8) shows the effect of ground coupling on the fluid outlet temperature. The fluid outlet temperature is plotted for the case when there is no thermal interaction with the ground surrounding the packed unit. On the same graph, the fluid outlet temperature is plotted for the case when ground coupling is taken into account. The bottom half of the figure shows the difference in fluid outlet temperature with or without ground coupling.

The figure indicates that the fluid outlet temperature in the presence of ground coupling is higher initially because of the extra heat gained from the ground. The opposite is true when heat transfer between the ground and the bed reverses its direction of flow. The effect of adding ground coupling is to increase the thermal capacity of the bed and hence delay the time it takes for the fluid outlet temperature to reach its maximum possible value of 20° C.

The value of 15^oC for the ground temperature is the annual mean and hence gives an average effect. The effect may vary depending on the time of year. For example, during the

summer the supply air temperature comes in at relatively high temperatures and hence the ground contributes better in storing excess energy during hours of occupancy. This energy is extracted by the supply air to the building's exteriour after hours. Hence the supply air acts as an energy transporting medium.

5.6 Parametric study

5.6.1 Introduction

A parametric study can be used to optimise the design of a packed bed and to come up with optimal operational parameters for example an optimal fluid volume flow rate. In this section one such study is carried out by investigating the effect of

- length of bed L,
- fluid volume flow rate $\dot{V}_f$, and
- type of bed material,

on the amount of heat stored in the bed after a fixed time of operation. A similar analysis is carried out on the fraction of maximum possible heat stored in the bed. A packed bed operating in single-blow mode is considered with three different types of bed material. These are granite, concrete rubble and brick rubble and their physical properties are shown in Table (5.2).

Brick rubble	c_m	=	800	$J/kg\,^o$C
	ρ_m	=	1700	kg/m^3
	k_m	=	0.73	$W/m\,^o$C
Concrete rubble	c_m	=	878	$J/kg\,^o$C
	ρ_m	=	2100	kg/m^3
	k_m	=	1.1	$W/m\,^o$C
Granite rocks	c_m	=	800	$J/kg\,^o$C
	ρ_m	=	2700	kg/m^3
	k_m	=	2.1	$W/m\,^o$C

Table 5.2: Physical properties for three different materials

Additional information required for the analyses is as follows:

- The duration of heat storage is chosen to be $t = 8$ hours. Note that the same analysis as carried out here can be applied to heat recovery (storage of coolth). The duration used here was chosen to match the duration of storage of coolth for the Harare International School. This begins at 10 pm and ends at 6 am the following morning.
- The inlet fluid temperature $T_{fi} = 20°C$.
- The initial temperature throughout the bed $T_0 = 0°C$.

The values for the other basic parameters are given in Table (5.1). The solid particles for all the three types of material are spheres of radius 10 cm.

As for the heat resulting from the power absorded by the fan, a corresponding term should ideally be incorperated in the energy equations. However, it is assumed that the effect is negliglible.

5.6.2 On the absolute amount of energy stored

The absolute amount of energy stored in the bed, Q after time t is given by

$$Q(t) = \dot{m}_f c_f \int_0^t (T_{fi} - T_{fo}(\tau))\, d\tau \tag{5.1}$$

Similar to the explanation given in section (3.5.2), since no big changes in temperature between neighbouring data points are expected, the Trapezoidal rule is used for the numerical evaluation of the integral in equation (5.1). No significant gain in accuracy is expected by using the Simpson's rule instead. Tables (5.3) through (5.5) show the effect of L and $\dot{V}_f$ on the absolute amount of energy stored in the bed after 8 hours for the three different types of storage material. The results indicate that:

- Much less absolute heat energy is stored by increasing $\dot{V}_f$ than by increasing L.
- The amount of absolute energy stored is higher in the order: brick rubble, concrete rubble and granite rocks. This suggests that of the three different types of material, granite is the best storage material.

It is worth noting that a higher thermal capacity of the energy storage material results in increased reduction of the diurnal swing of the supply air temperature.

$L \backslash \dot{V}_f$	0.2	0.4	0.6	0.8	1.0	1.2
0.5	32.8	34.3	34.8	35.1	35.4	35.6
1.0	59.8	65.7	67.6	68.6	69.2	69.6
1.5	80.7	94.2	98.5	100.7	102.0	102.9
2.0	96.1	119.6	127.5	131.4	133.7	135.2
2.5	107.0	141.9	154.5	160.6	164.2	166.6
3.0	114.6	161.4	179.4	188.3	193.6	197.1

Table 5.3: absolute heat stored (MJ): brick rubble

$L \backslash \dot{V}_f$	0.2	0.4	0.6	0.8	1.0	1.2
0.5	40.6	43.4	44.4	45.0	45.3	45.6
1.0	70.7	81.3	84.9	86.8	88.0	88.8
1.5	91.7	113.9	121.9	126.0	128.5	130.2
2.0	105.7	141.5	155.4	162.6	166.9	169.9
2.5	114.7	164.5	185.4	196.5	203.2	207.8
3.0	120.2	183.5	212.2	227.8	237.4	243.9

Table 5.4: absolute heat stored (MJ): concrete rubble

$L \backslash \dot{V}_f$	0.2	0.4	0.6	0.8	1.0	1.2
0.5	45.1	48.8	50.2	50.9	51.4	51.8
1.0	76.6	90.2	95.1	97.7	99.2	100.3
1.5	97.2	124.8	135.3	140.8	144.2	146.5
2.0	110.1	153.2	171.0	180.4	186.3	190.3
2.5	117.9	176.1	202.4	216.7	225.6	231.6
3.0	122.5	194.5	229.8	249.6	262.1	270.7

Table 5.5: absolute heat stored (MJ): granite

5.6.3 On the relative amount of energy stored

The fraction of maximum possible heat stored in the bed after time t is defined in terms of the outlet fluid temperature $T_{fo}(t)$ by equation (5.2).

$$Q^+(t) = \frac{Q}{Q_{max}} = \frac{\dot{m}_f c_f \int_0^t (T_{fi} - T_{fo}(\tau))\, d\tau}{\rho_m S_{fr} L(1-\epsilon) c_m (T_{fi} - T_0)} \tag{5.2}$$

Tables (5.6) through (5.8) show the effect of L and $\dot{V}_f$ on the relative amount of energy stored in the bed after 8 hours for the three different types of storage material.

The results indicate that:

- The relative heat stored increases with flow rate for each bed material. However, increasing volume flow rate is subject to the constraint of a maximum allowable pressure

$L \backslash \dot{V}_f$	0.2	0.4	0.6	0.8	1.0	1.2
0.5	0.894	0.933	0.948	0.957	0.964	0.969
1.0	0.814	0.894	0.920	0.934	0.942	0.948
1.5	0.732	0.855	0.894	0.914	0.926	0.934
2.0	0.654	0.814	0.868	0.895	0.910	0.920
2.5	0.583	0.773	0.841	0.875	0.895	0.908
3.0	0.520	0.732	0.814	0.855	0.879	0.895

Table 5.6: relative heat stored: brick rubble

$L \backslash \dot{V}_f$	0.2	0.4	0.6	0.8	1.0	1.2
0.5	0.816	0.872	0.892	0.903	0.911	0.917
1.0	0.710	0.816	0.853	0.872	0.884	0.892
1.5	0.614	0.763	0.816	0.844	0.861	0.872
2.0	0.531	0.711	0.780	0.816	0.838	0.853
2.5	0.461	0.661	0.745	0.789	0.816	0.835
3.0	0.403	0.614	0.711	0.763	0.795	0.816

Table 5.7: relative heat stored: concrete rubble

$L \backslash \dot{V}_f$	0.2	0.4	0.6	0.8	1.0	1.2
0.5	0.773	0.837	0.860	0.873	0.881	0.888
1.0	0.656	0.773	0.815	0.837	0.851	0.860
1.5	0.556	0.713	0.773	0.805	0.824	0.837
2.0	0.472	0.657	0.733	0.774	0.799	0.816
2.5	0.404	0.604	0.694	0.743	0.774	0.794
3.0	0.350	0.556	0.657	0.713	0.749	0.774

Table 5.8: relative heat stored: granite

drop for the fans. More fan power is required to blow air through the bed at higher flow rates.

- The relative energy stored decreases with length of bed. The longer the bed the less efficient it is as not all storage material is utilised. The heat can only penetrate to a certain depth of storage material.

- Higher relative heat is stored for granite, concrete rubble and brick rubble in that order.

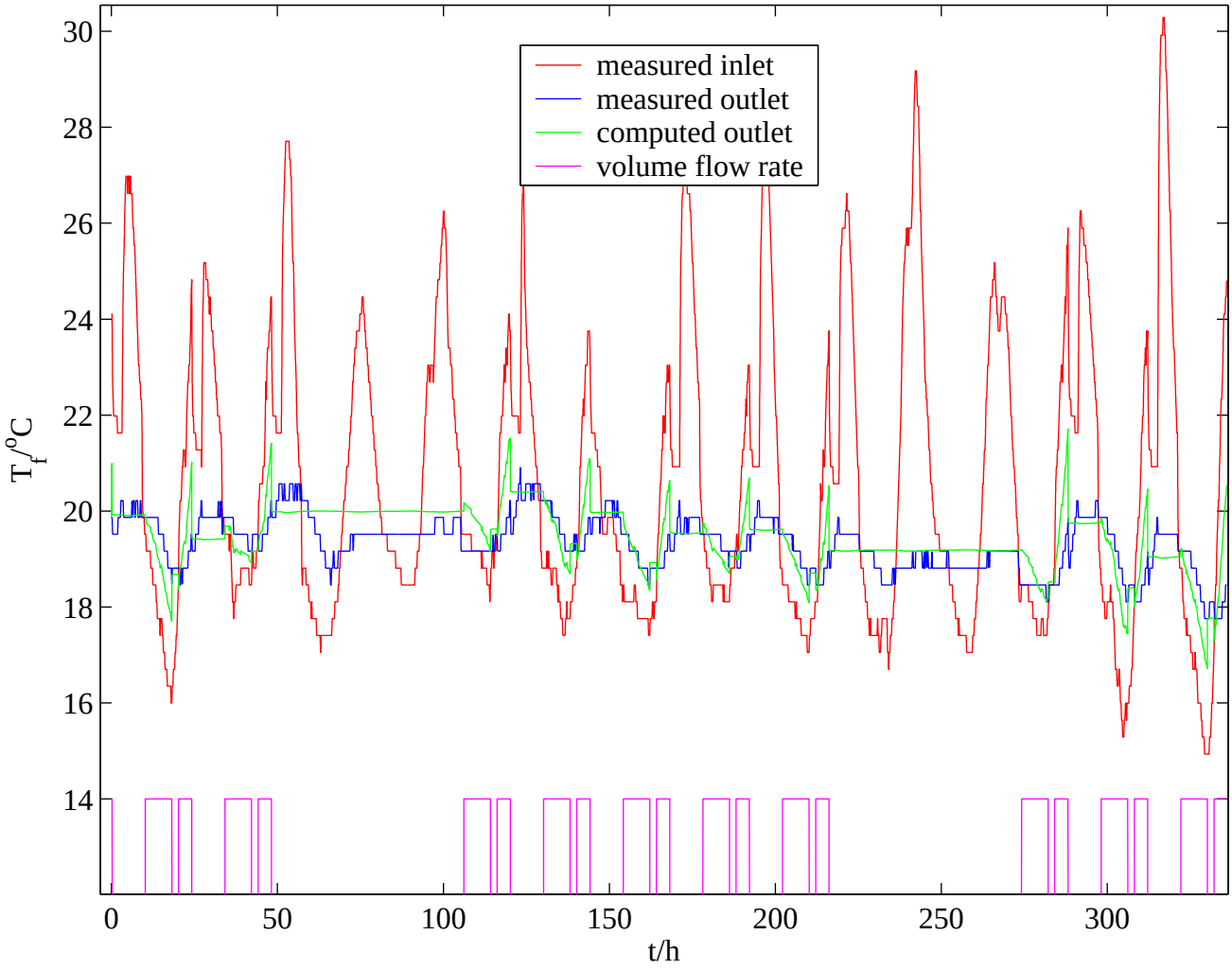

Figure 5.4: Transient response of the morning unit to ambient air temperature with night and morning cooling only

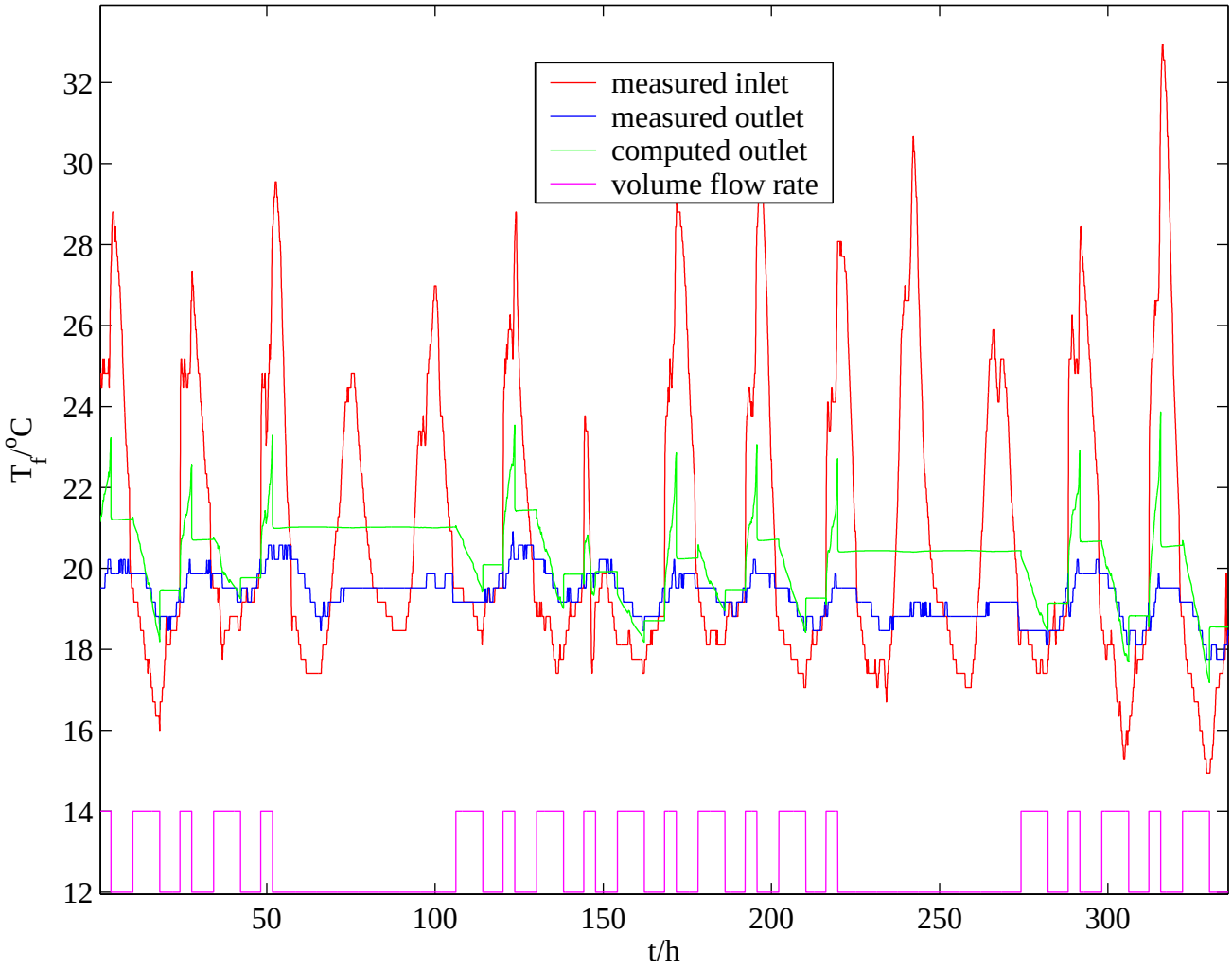

Figure 5.5: Transient response of the afternoon unit to ambient air temperature with night and afternoon cooling only

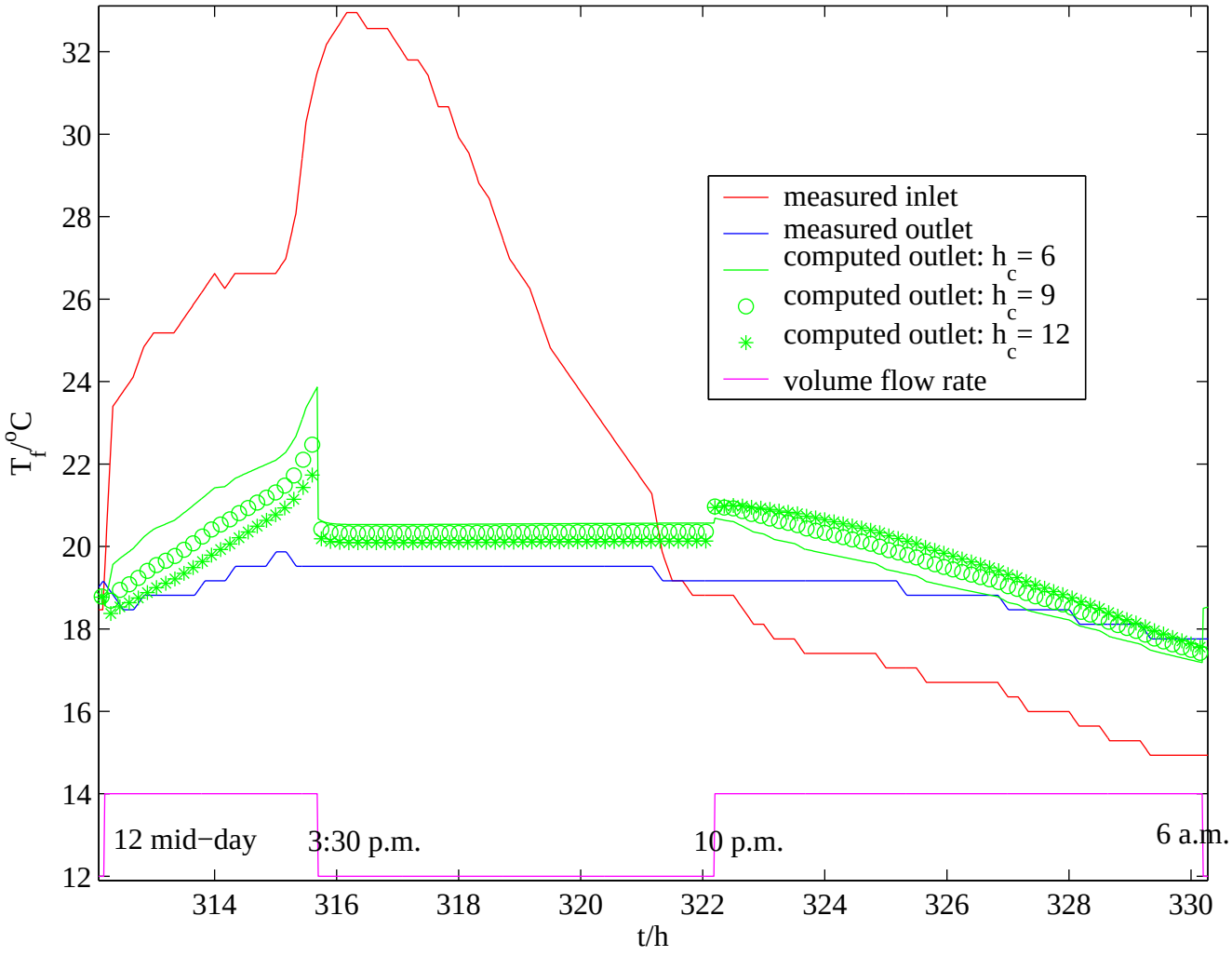

Figure 5.6: Effect of h_c on the performance of the afternoon unit over 18 hours

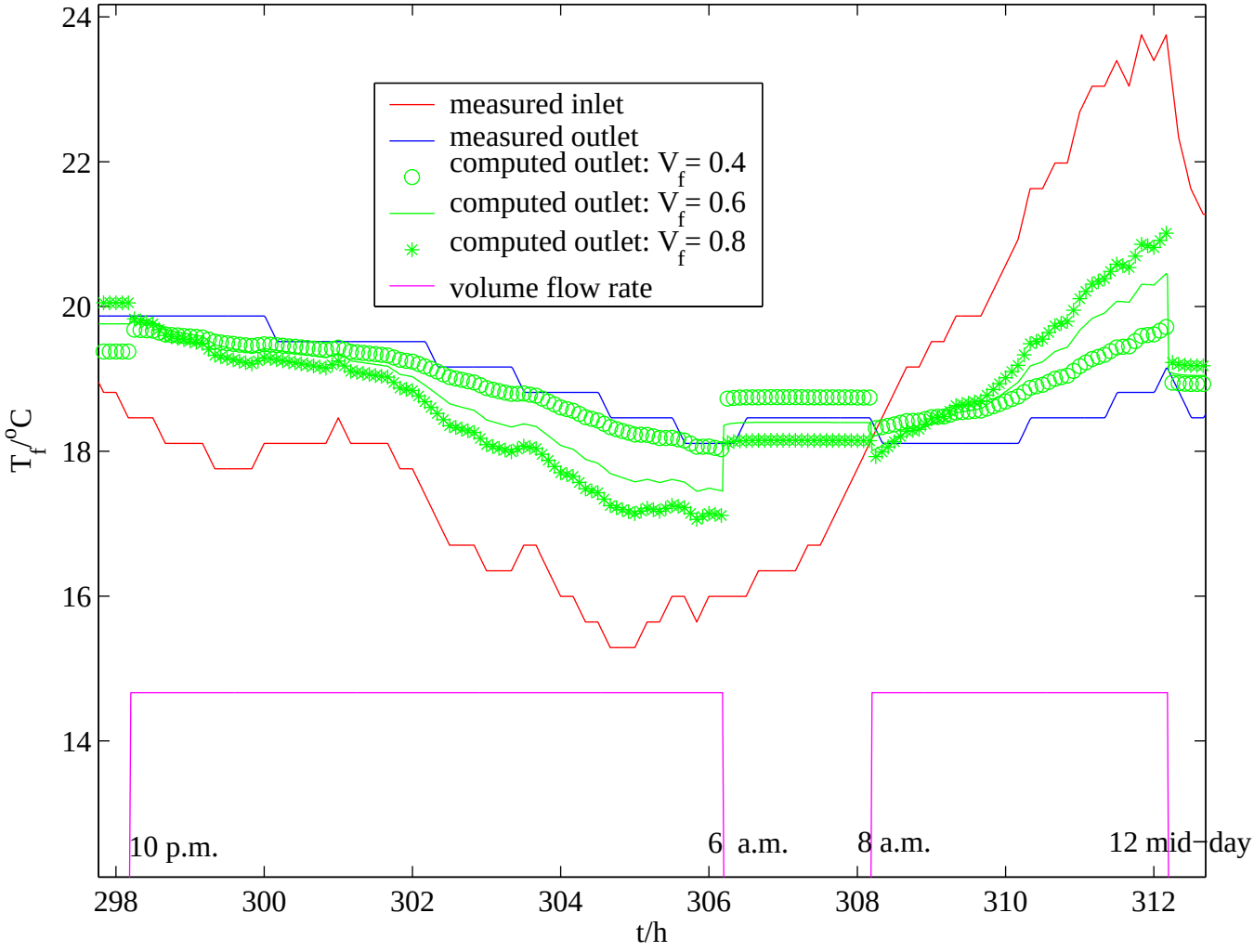

Figure 5.7: Effect of $\dot{V}_f$ on the performance of the afternoon unit over 14 hours

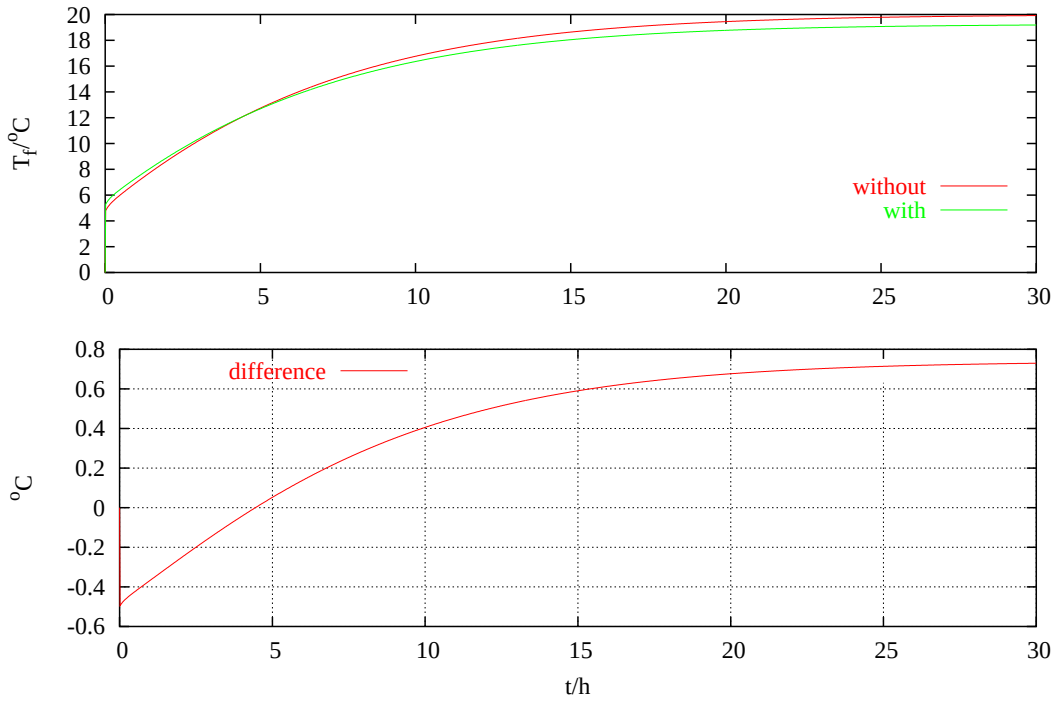

Figure 5.8: Effect of ground coupling on the fluid outlet temperature

Chapter 6

Conclusions and further work

6.1 Eastgate building

A general understanding of the cooling system has been gained through discussion with the project engineer and through interpreting measured data from the data logger.

The integrity of the measured data was established through testing the equipment and examining its position in the building.

A mathematical model was coded for heat transfer in a ventilated slab driven by a measured air inlet temperature. In order to solve the mathematical mode three numerical methods were compared. Two were forms of the electrical analogue of heat flow and the third was finite elements. The numerical methods were tested on simplified forms of the ventilated slab thermal storage problem in order to obtain experience of accuracy and mesh refinement. All three were suitable with finite elements having a slight advantage.

- A comparison was made of predicted with measured air outlet temperatures. There is good agreement in trend but there are differences, the main one being the predicted underestimate the measured temperatures. Possible ways of improving the modelling include the following.
  - Replacing the insulation boundary condition on the interface between the slab and the room above, with a convection boundary condition and using the available measured room air temperature. This requires a modification to the code.

  - The assumption of constant air velocity could be relaxed to account for the complex fluid flow in the passage. This may require thorough fluid flow analysis.
  - Revising the parameter values, especially the the convective heat transfer coefficient h_c.

- Sensitivity tests were carried out and they indicate how the parameters can be modified to move the predicted air outlet temperatures closer to the measured values.

Further work includes better estimation of the parameters, and optimising the design and operational parameters. An experimental approach could be used to determine h_c, and a statistical analysis done to determine the uncertainty of values for h_c.

6.2 Harare International School

Research on packed beds was studied and the implementation of this form of cooling was discussed with the project engineer at the Harare International School.

A mathematical model was coded for the transient response of a packed bed unit to measured air inlet temperature and validated by comparing with similar but distinct numerical methods.

- The model was tested against measured data and there is a good agreement.
- Sensitivity tests were carried out and they show how parameters affect the prediction of the model.
- A parametric study giving heat stored for bed size and different storage materials was reported. This showed the potential of the code in designing more energy efficient buildings. Through contact with Prof Mike Holmes of Ove Arup and Partners Ltd in London the packed bed thermal storage code is being tested with a view to it being incorporated into the company's design software.

Further work

- More work needs to be done to come up with a suitable correlation for h_c.

- Another aspect of the modelling that requires a more detailed study is the effect of ground coupling on the thermal performance of the bed.
- An optimisation study could be made to aid the future design of buildings using packed beds for cooling or heating. Since packed beds are generally more efficient and easier to vary in size and the materials used than ventilated slabs, they are more likely to be used in future building designs.

Appendix A

Simplified problems for Eastgate

A.1 Analytical solution for test problem A

$$\frac{T(y,t)-T_0}{T^\infty-T_0} = 1 - 2\sum_{j=1}^{\infty} \frac{\sin m_j}{\sin m_j \cos m_j + m_j} \exp[-(m_j\alpha)^2 t] \cos\left[m_j \frac{B-y}{B}\right], \qquad \text{(A.1)}$$

where $m_j, j = 1, 2, \ldots \infty$ are the roots of

$$m_j \tan m_j = Bi = h_c \frac{B}{k}$$

Note that because of symmetry in the problem the solution is independent of the x co-ordinate.

A.2 A derivation of the energy equation for the air

Consider heat transfer in a fixed control volume of length Δx, depth g and unit thickness. The energy balance is

$$\left\{\begin{array}{l}\text{net rate of}\\ \text{heat flow into}\\ \text{the control}\\ \text{volume}\end{array}\right\} = \left\{\begin{array}{l}\text{rate of heat}\\ \text{flow through}\\ \text{the control volume}\\ \text{along the air void}\end{array}\right\} + \left\{\begin{array}{l}\text{convective heat}\\ \text{flow rate}\\ \text{into the}\\ \text{control volume}\end{array}\right\}$$

which can be written in mathematical form as

$$\begin{aligned}\rho_f c_f \Delta x \cdot 1 \cdot g \frac{\partial T^\infty}{\partial t} &= \{\dot{m}_f c_f T^\infty \mid_x - \dot{m}_f c_f T^\infty \mid_{x+\Delta x}\} \\ &\quad + \{h_c \Delta x \cdot 1 \left(T \mid_x - T^\infty \mid_x\right) + h_c \Delta x \cdot 1 \left(T^* \mid_x - T^\infty \mid_x\right)\} \quad \text{(A.2)}\end{aligned}$$

Upon dividing equation (A.2) throughout by Δx and taking the limit as $\Delta x \to 0$ the following is obtained as the governing equation for the heat transfer in the air void.

$$\rho_f c_f g \frac{\partial T^\infty}{\partial t} + \dot{m}_f c_f \frac{\partial T^\infty}{\partial x} = h_c \left(T - T^\infty\right) + h_c \left(T^* - T^\infty\right). \quad \text{(A.3)}$$

Appendix B

Nomenclature

A	=	Area of convective heat transfer	m^2
c	=	specific heat capacity	$J/Kg\,^\circ C$
D	=	solid particle diameter	m
d_i	=	internal diameter of cylindrical bed	m
h	=	heat transfer coefficient	$W/m^2\,^\circ C$
k	=	thermal conductivity	$W/m\,^\circ C$
L	=	length of bed	m
P	=	perimeter of bed	m
Q	=	energy stored in bed	J
r	=	radial distance	m
R	=	radius of solid particle	m
S_{fr}	=	surface frontal area	m^2
T	=	temperature	$^\circ C$
t	=	time	s
U	=	heat loss coefficient	$W/m^2\,^\circ C$
v_f	=	fluid velocity	m/s

x	=	distance in the direction of flow	m
z	=	axial distance (cylindrical bed)	m
ρ	=	density	Kg/m^3
σ	=	Stefan's constant	$W/m^2\ ^\circ C^4$
		Dimensionless quantities	
Bi	=	Biot number	
ϵ	=	void fraction	
ϵ'	=	emmisivity	
η	=	radial distance	
NTU	=	number of transfer units	
NTU_c	=	modified number of transfer units	
Pe	=	Peclet number	
Q^+	=	heat stored	
θ	=	temperature	
$\bar{\theta}$	=	average temperature	
ξ	=	distance in the direction of fluid flow	
τ	=	time	
		Subscripts	
c	=	convective	
e	=	effective (overall)	
env	=	environment	
f	=	fluid	
fi	=	fluid inlet	
fo	=	fluid outlet	
m	=	bed material	
max	=	maximum	
o	=	initial instant	
r	=	radiative	
v	=	volumetric	
		Superscripts	
∞	=	fluid (ventilated slab analysis only)	
$\star$	=	ceiling slab	

References

[1] *Getting Started with Matlab*. The Mathworks Inc., 1998.

[2] G. A. Adebiyi. A second–law study on packed bed thermal storage systems utilizing phase–change materials. *ASME Journal of Solar Energy Engineering*, 113:146–156, 1991.

[3] G. A. Adebiyi and D. J. Chenevert. An appraisal of one–dimensional models for the packed bed thermal storage systems utilizing sensible heat storage materials. *Transactions of the ASME Journal of Energy Resources Techonolgy*, 118:45, 1996.

[4] G. A. Adebiyi, B. K. Hodge, W. G. Steele, A. Jalaalzadeh-Azar, and E. C. Nsofor. Computer simulation of a high–temperature thermal energy storage system employing multiple families of phase change storage materials. *Transactions of the ASME Journal of Energy Resources Techonolgy*, 118(2):102–111, 1996.

[5] G. A. Adebiyi, E. C. Nsofor, W. G. Steele, and A. Jalaalzadeh-Azar. Parametric study on the operating efficiencies of a packed bed for high–temperature sensible heat storage. *Transactions of the ASME Journal of Solar Energy Engineering*, 120(1):2–13, 1998.

[6] M. Al-Nimr, M. K. Abu-quadais, and M. D. Mashaqi. Dynamic behaviour of packed bed energy storage system. *Energy Convers. Mgmt*, 37:23–30, 1996.

[7] M. Al-Nimr, M. Tahat, and M. Al-Rashdan. A night cold storage system enhanced by radiative cooling – a modified australian cooling system. *Applied Thermal Engineering*, 19(1999):1013–1026.

[8] A. K. Athienitis. Investigation of thermal performance of a passive solar building with floor radiant heating. *Solar energy*, 61(5):337–345, 1997.

[9] C. A. Balaras. The role of thermal mass on the cooling load of buildings. an overview of computational methods. *Energy and Buildings*, 24(1996):1–10.

[10] P. Barton, C. B. Beggs, and P. A. Sleigh. A theoretical study on the thermal performance of the TermoDeck hollow core slab system. *Applied Thermal Engineering*, 22(2002):1488–1499.

[11] A. Bejan. *Heat transfer*. Wiley, 1993.

[12] S. J. Bhardwarj, S. C. Kaushik, and H. P. Garg. Sensible thermal storage in rock beds for space conditioning: a state of the art study. *International Journal of Ambient Energy*, 20(4):211, 1991.

[13] T. Y. Chen. Real-time predictive supervisory operation of building thermal systems with thermal mass. *Energy and Buildings*, 33(2001):141–150.

[14] W. Chen and W. Liu. Numerical and experimental analysis of convection heat transfer in passive solar heating room with greenhouse and heat storage. *Solar Energy*, 76(2004):623–633.

[15] D. J. Close. Design and performance of a thermal storage air conditioning system. *ASME Transactions Journal of Heat transfer*, 98:336, 1976.

[16] J. A. Duffie and W. A. Beckman. *Solar engineering of thermal processes*. Wiley, 1980.

[17] D. J. Henwood and J. Bonnet. *A gentle introduction to finite elements*. MacMillan, 1996.

[18] J. P. Holman. *Heat transfer*. McGraw–Hill, 1976.

[19] M. J. Holmes and A. Wilson. Assessment of the performance of ventilated floor thermal storage systems. *Building and Environment*, 102(1), 1996.

[20] G. T. Marewo. Mathematical modelling of the storage of coolth in a building strucure (the Eastgate building). Master's thesis, University of Zimbabwe, 1998.

[21] C. B. Moler and C. W. Stewart. An algorithm for generalized matrix eigenvalue problems. *SIAM Journal of Numerical Analysis*, 10(2), 1973.

[22] K. W. Morton and D. F. Mayers. *Numerical solution of partial differential equations*. Cambridge, 1993.

[23] D. E. Newland. *Mechanical vibration analysis and computation*. Longman Scientific & Technical, 1989.

[24] B. Paul and J. S. Saini. Optimization of bed parameters for packed bed solar energy collection system. *Renewable Energy*, 29(2004):1863–1876.

[25] M. Rainbow. School of hard rocks: lessons out of Africa. In *Third International Conference on Sustainable Energy Technologies*, School of Build Environment, University of Nottingham, U. K, 2004.

[26] M. J. Ren and J. A. Wright. A ventilated slab thermal storage system model. *Building and Environment*, 33(1), 1998.

[27] M. Riaz. Analytic solutions for single and two–plane models of packed bed thermal energy systems. *ASME Transactions Journal of Heat transfer*, 99:489, 1977.

[28] M. B. Russell and P. N. Surendan. Influence of active heat sinks on fabric thermal storage in building mass. *Applied Energy*, 70(2001):17–33.

[29] F. W. Schmidt and A. J. Willmont. *Thermal storage and regeneration.* McGraw Hill, 1981.

[30] T. E. W. Schumann. Heat transfer: A liquid flowing through a porous prism. *J. Franklin Inst*, 208:405, 1929.

[31] B. D. Shaw. Asymptotic analysis of the lumped capacitance approximation. *International journal of heat flow*, 36(4), 1992.

[32] R. Shukla, S. D. Dhole, R. P. Chhadra, and V. Eswaran. Convective heat transfer for power law fluids in packed and fluidised beds of spheres. *Chemical Engineering Science*, 59:645–659, 2004.

[33] G. D. Smith. *Numerical solution of partial differential equations.* Oxford, 1965.

[34] J. Yam, Y. Li, and Z. Zheng. Non-linear coupling between thermal mass and natural ventilation in buildings. *International Journal of Heat and Mass Transfer*, 46(2003):1251–1264.

[35] M. T. Zarrinehkafsh and S. M. Sadrameli. Simulation of fixed bed regenerative heat exchangers for flue gas heat recovery. *Applied Thermal Engineering*, 24(2–3):373–382, 2004.

[36] M. A. Ziada and Z. S. Abdel-Rehim. Thermal analysis of energy storage in packed beds of multilayer storing medium. *Energy sources*, 20:209–222, 1998.